Using Peptidomimetics to Dissect Activator-Coactivator Protein-Protein Interactions

by

Kevon Daniel Stanford

A dissertation submitted in partial fulfillment
of the requirements for the degree of
Doctor of Philosophy
(Chemistry)
in the University of Michigan
2021

Doctoral Committee:

Professor Anna K. Mapp, Chair
Assistant Professor Kristin Koutmou
Professor Neil Marsh
Associate Professor Patrick O'Brien

Kevon Daniel Stanford

sdkevon@umich.edu

ORCID iD: 0000-0002-3138-4399

Acknowledgments

This is perhaps the most challenging task I have faced thought my time in school. It was not done without great challenges; however, it has given me a unique experience that I do not believe I would have gained without graduate school. I have experienced struggles, but I learned from them, and they have been a part of the many elements that have helped me to develop as a scientist. This was not done without the support of many people in my life, so I would like to thank them for their support.

Firstly, I would like to acknowledge my advisor, Anna Mapp for her unwavering support throughout my time at the University of Michigan. There have been difficult times when I was mentally and emotionally devastated, and she would recognize my plight supported me in whatever way necessary. She has been very understanding and patient, which have allowed me to strive and become an independent problem solver. The culture she has created in the lab has been conducive to fostering success while having a work-life balance.

Other crucial people involved in this process are my committee members. They have been very valuable to the completion of my dissertation. They have challenged my thoughts and allowed me to formulate ideas from different perspectives through suggestions and questions that I had not asked myself.

Next, I would like to thank my lab mates and friends for their tremendous support and cooperation throughout my time, which was very difficult occasionally. There were great personal challenges sometimes where I thought that that would have been the end of my journey in graduate school,

however my lab mats were very supportive in lending assistance and support to get through the challenges. The many times that we have taken coffee breaks, talk about science and other topics have helped me to recharge.

Another important group in all this journey is my family. I could not have done this without their continued support. Their encouragement meant so much to me - it allowed me to push harder to complete my PhD throughout the trying times. The phone calls and little conversations we had, especially with my mom, dad, and grandmother were invaluable.

Finally, my wife, Shanice has been a very strong support throughout some of the most tumultuous times. Her support is expressed in everything I do and for that I am most grateful. She has listened to my frustrations and advised me so that I could recover and function optimally. I thank you and I love you!

Table of Contents

List of Figures:

List of Tables:

Abstract

Peptoids as Transcription Factor Mimics to Target the Coactivator Med25

Protein-protein interactions (PPIs) play significant roles in all cellular activities. The interactions are guided by cellular signals which direct how and where these proteins assemble. The information encoded by DNA is transcribed, for example, as a result of complex PPI networks formed by dynamic transcriptional proteins. If any of the PPIs malfunction, then the resulting dysregulation leads to human diseases such as cancer, neurodegenerative disorders, developmental disorders, and abnormal metabolic activities.

At the core of the transcriptional PPI network are proteins known as transcriptional activators that bind to specific sequences of DNA. The other basic component of activators is the transcriptional activator domain (TAD), which functions to recruit coactivators in the process of assembling the transcription machinery. Coactivators play a key role in transcriptional regulation as they serve to interact with multiple protein partners, including activators. The complexes formed between activators and coactivators have modest affinity and are often transient in nature, since they are formed as part of the assembly/disassembly part of the transcriptional machine. Additionally, coactivators use binding sites with large surface areas to form PPIs with activators and other binding partners. This aids the recruitment of the RNA polymerase following the interactions of these classes of proteins.

Typically, small molecules tend to be most potent when they act as ligand for proteins such as enzymes that have deeper grooves and small surface areas. However, coactivator proteins have

large surface areas and produce moderate affinities when interacting with binding partners. Because of these characteristics, it has been challenging using small molecules to target these interactions. In the case of the target coactivator for this study, Med25, the domain that interacts with activators has two 900 $Å^2$ binding surfaces that are intractable for small molecule ligands. Med25 is dysregulated in many human diseases and there is thus a strong need to identify synthetic modulators that would be useful for mechanistic studies.

Towards this end, we first identified minimal binding sequences from known transcriptional activators that interact with the Activator Interaction Domain (AcID). The information gleaned from these studies presented the opportunity to develop synthetic ligands of Med25 AcID using peptidomimetics based on those sequences. Peptoids were chosen as the scaffold due to their ability to resist proteolytic degradation, cover large surface areas and present diverse functional groups as sidechains. We demonstrated that we could design peptoids based on identified minimal peptides that interact with Med25 AcID to recapitulate binding to the Med25. After optimization, the best peptoid exhibited low micromolar affinity for Med25 AcID and good selectivity against a related coactivator.

The work yielded promising results leading us to improve the compounds so that that they have intercellular applications. Cell penetrating peptides were appended to the optimal peptoid and the cell permeability assessed by visualizing Vari-068 cells, a triple-negative breast cancer cell line, treated with fluorescently-labeled variants of the peptoid. One version could be seen throughout the cell, including the nucleus, after 6 hours. Taken together, this work demonstrates

that we can design mimics of native TADs to interact with larger surface areas with moderate affinities for the target proteins and eventually modify these for efficient intracellular delivery and inhibition.

Chapter 1

The Challenges and Opportunities of Targeting Transcriptional Activator•Coactivator Complexes

Abstract

Protein-protein interactions play a significant role in maintaining cellular processes in cells. These are complex networks involving numerous proteins interacting with each other in a transient fashion. One of the essential functions of cellular systems is transcription, which is a process in which genetic information is regulated. This involves key proteins such as transcriptional activators, which at a minimum comprise a DNA binding domain (DBD), that binds to a specific DNA sequence and transcriptional activation domain (TAD) that recruits coactivators to the DNA transcription site. The coactivator interacts with the TAD with its Activator Binding Domain (ABD) as it helps to assemble the other components of the transcription machinery such as the RNA polymerase II enzyme. Misregulation of activator-coactivator complexes contributes to a wide range of human diseases. As a result, these complexes are attractive therapeutic targets. One of the most common techniques for targeting activator-coactivator PPIs is discovery of small molecule ligands. However, due to the large surface areas of the PPIs these molecules are often incapable of being effective modulators as they are incapable of covering large surface areas. Here, we propose using peptidomimetics as a strategy that could address the limitations of small molecules as they possess diverse chemical structures, can interact with large binding surfaces, and are resistant to proteolytic degradation.

1.2 Transcriptional Activator-Coactivator Complexes

Protein-protein interactions (PPIs) are essential for biological systems to function, and, as a result PPIs are tightly regulated by preprogrammed cellular signals.[1] An example of a functionally important class of PPIs are those formed between transcriptional activators and coactivators in the earliest step of gene transcription. Transcriptional activators recognize particular sequences in the promoter regions of genes in a signal-responsive fashion and then form short-lived PPIs with transcriptional coactivators to initiate formation of the transcriptional machinery.[2,3] At the core of this multiprotein network is the RNA polymerase II (Pol II), which is the central enzyme in the transcriptional machine.[2,4,5] The well-characterized protein family ETV/PEA3 includes examples of transcriptional activators that form PPIs with the coactivator protein Med25; ETV/PEAS-Med25 complexes lead to the recruitment of the Mediator complex to genes such as MMP-1, stimulating transcription.

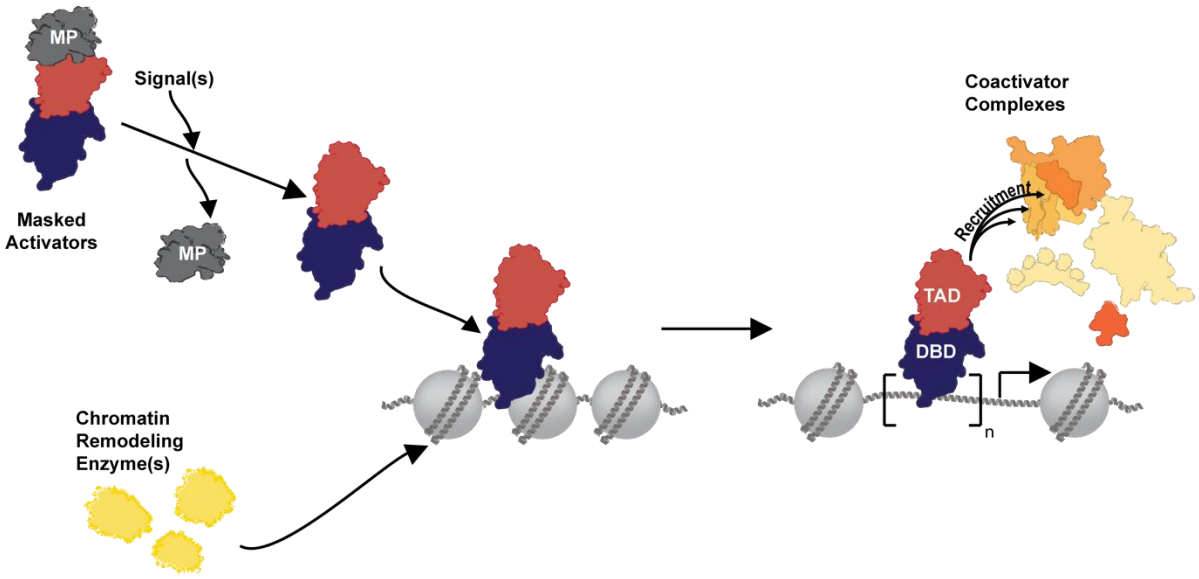

Figure 1.1 Transcriptional Machinery Assembly. Activator-coactivator complexes facilitate assembly of the transcriptional machinery in a signal-responsive fashion. Transcriptional activators are often held by masking proteins (MP) in inactive form until needed. A signal, often in the form of a post-translational modification, causes the masking protein-activator interaction to change. The DNA binding domain (DBD, deep blue) of the activator localizes the activator to particular sites in the genome. The transcriptional activation domain (TAD, red) then forms PPIs with coactivators to stimulate formation of the transcriptional machine.

Misregulation of activator-coactivator PPIs, not surprisingly, results in myriad diseases such as autoimmune diseases, cancers, neurological degenerative and cardiovascular diseases to name a few.[6–14] To ameliorate situations arising from misregulation of activator•coactivator complexes, it is important to understand the mechanism(s) through which these molecules function. Transcriptional activators are minimally composed of a DNA-binding domain that localizes the protein to particular sites within a genome and a transcriptional activation domain, or TAD, that forms complexes with coactivators.[15–18] Activators are often classified based upon the sequence of their TAD, falling into the category of amphipathic/acid-rich, glutamine-rich, or proline-rich. The largest class is that of the amphipathic group, in which the TAD sequences are (as the name suggests) comprised of hydrophobic residues that are interspersed with polar amino acids, often glutamic or aspartic acid.[3,19–22]

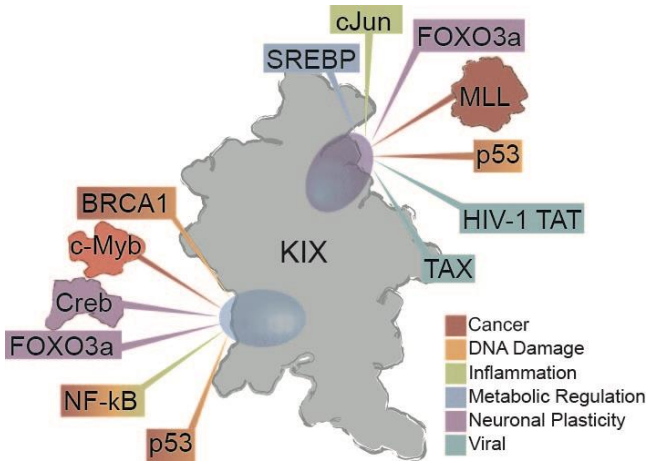

Figure 1.2. TADs interact with coactivator protein. The CBP/p300 KIX domain interacts with several TADs using both of its binding sites. The TADs represent examples of diseases in which they are implicated.

TADs commonly interact with two classes of proteins. One class comprises masking proteins, and the well-studied tumor suppressor and transcriptional activator p53 and its masking protein partner MDM2 are an excellent example.[23–26] Another example is the yeast transcription factor Gal4 and

its binding partner Gal80 masking protein-TAD PPI.[23,24] Typically, masking proteins bind with high affinity to activator partners, with dissociation constants in the low nanomolar range.[24] Conversely, TADs interact with coactivators, the second class of binding partners, with low to moderate affinities (micromolar to high nanomolar dissociation constants).[25] TADs are diverse in size as they range from a few amino acids to over 100 amino acids in length. Some activators such as VP16 and p53 have multiple TAD domains that allow them to interact independently with other proteins.[26–32]

A remarkable feature of transcriptional activators and their coactivator binding partners is that they are hub proteins, using a single domain to interact with many different binding partners. The TAD within the yeast activator Gal4, for example, interacts with more than 10 different

coactivators.[33–36] The hub domains within coactivators are called activator-binding domains or ABDs. Some coactivators such as cAMP-response element binding protein (CREB-binding protein – CBP) contain multiple ABDs. The CBP ABD KIX interacts with CREB, MLL, c-Jun, c-Myb and p53 along with other proteins (Figure 1.2).[37] A similar KIX domain in the Mediator subunit Med15 interacts with several unique proteins including Pdr1p, Pdr3p, Oaf1p, Gcn4p and Gal4p.[38–42]

As noted above, the complexes formed between transcriptional activators and their coactivator binding partners are implicated in a number of diseases. This can be due to up- or down-regulation of one or both binding partners, altered signaling pathways, or mutations/deletions/translocations of the transcription factor. For example, in a subset of AML, chromosomal translocation of the transcriptional activator MLL leads to loss of function, contributing to leukomogenesis.[43–45] In an example relevant to this dissertation, the ETV/PEA3 transcriptional activators are up-regulated in a number of cancers (Figure 1.3).[44,46–49] Table 1 illustrates further examples of misregulated transcription factors and cancer and other diseases are highlighted.

a)
ETV1/ER81(42-73) DSEELFQDLSQLQETWLAEAQVPDNDEQFVPD
ETV4/PEA3(49-80) DSEDLFQDLSHFQETWLAEAQVPDSDEQFVPD
ETV5/ERM(42-72) DSEELFQDLSQLQEAWLAEAQVPD-DEQFVPD

b)

		activation mechanism	phenotype
ETV1	early prostate cancer	chromosomal translocation and/or over-expression	invasion, migration
	triple negative breast cancer; Her2+ breast cancer	coactivation with Ras signaling and/or Her2 signaling	invasion, migration growth
	melanoma	amplification	invasion
ETV4	metastastic prostate cancer	coactivation with Ras, PI3 kinase signaling	invasion, migration
	triple negative or Her2+ breast cancer	coactivation with Ras and/or Her2 signaling	invasion, migration growth
	pancreatic cancer	coactivation with ERK signaling	invasion, migration
ETV5	head and neck cancer	top 1% of genes amplified	N/A

Figure 1.3 ETV/PEA3 activators. a) The three ETV family members have nearly identical transcriptional activation domains.[50] b) Although all three ETV family members are considered to be oncogenes, there is considerable evidence for activation of ETV1 and ETV4 inducing invasion and migration programs through several mechanisms. There is less data for ETV5 but The cancer Genome Atlas (TCGA) database analysis reveals that it is in the top 1% amplified genes in head and neck cancer.[50–53] ~~52-55~~

Transcriptional Activator	Result of Misregulation
TAL-1	T cell acute lymphoblastic leukemia
c-Myb	hematopoietic malignancies/breast cancer
ETV-1	Early prostate cancer
ETV-5	Head & Neck cancer
ETV-4	Prostate cancer
FoxO-3	Degenerative disorder
P53	Cancer, DNA damage
CREB	Degenerative disorder
IRF-5	Inflammation/immunodeficiency
STAT-1	immunodeficiency
STAT-2	immunodeficiency
STAT-3	immunodeficiency
XBP-1	Neurodegenerative disease
RUNX-2	Developmental disorder
MLL	Acute myelogenous leukemia
HIF1-a	Cancer (solid tumors)

Table 1: Examples of transcription and the consequences of misregulation. These transcriptional activators are involved in a complex network of protein-protein interactions with coactivators and other proteins. If there are any anomalies in the formation of the PPIs, the result can lead to diseases.[7]

As noted in Figure 1.3, a group of particularly exciting activator•coactivator complexes are those formed between the ETV/PEA3 activators and the coactivator Med25. The ETV activators regulate the transcriptional status of their cognate genes through a direct interaction between their transcriptional activation domains and the coactivator Med25.[54–56] More specifically, the Activator Interaction Domain (AcID) of Med25 is the target of the ETV activators, with a K_D of ~500 nM.[57] Med25 is anchored to the Mediator complex via its VWA domain and formation of the ETV-Med25 AcID complex leads to recruitment of Mediator to promoters, a critical step in assembly of the transcriptional pre-initiation complex.[58] Overexpression of the Med25 AcID or the VWA domain inhibits ETV-mediated transcription. In triple-negative breast cancer cells, for example,

overexpression of AcID led to down-regulation of metastasis-associated genes such as matrix metalloproteases, as did shRNA knockdown of ETV1, 4 and 5; importantly, the most effective

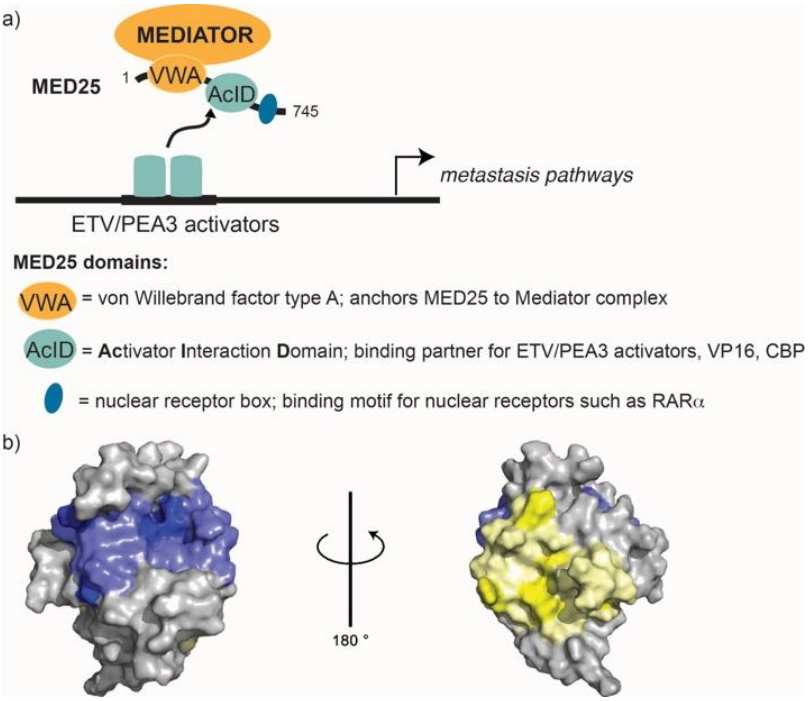

Figure 1.4 Med25 AcID is the critical binding partner for ETV/PEAs and other activators. a) The domains and function of Med25. b) Solution structure of Med25 AcID in complex with the transcriptional activation domain of VP16(413-490) (not shown). Highlighted residues indicate the predicted activator binding sites, with dark blue and maize colors indicating residues that shift significantly upon addition of VP16.(11) The blue site is termed the H1 binding surface as it interacts with the amino terminal residues of VP16 while the maize site is the H2 surface, targeted by the C-terminus of VP16. Figure derived from PDB 2L23.

inhibition was observed when all three ETV activators were knocked down.[54] Taken together, the hypothesis that emerges from these data is that a synthetic inhibitor of the Med25-ETV complex would block key metastasis pathway and, as a result, be effective mechanistic probes for defining the role(s) of the ETV/PEA3 transcription factors in the metastatic transformation. However, as described below, Med25 AcID presents a challenge for small-molecule modulator discovery.

1.3 Activator•Coactivator Complexes are Considered 'Undruggable'

Activator•coactivator complexes have long been deemed 'undruggable' because of their undesirable biophysical characteristics.[59–62] As noted above, they typically are modest in affinity and transient. Additionally, they typically occur over large surface areas, ranging from 700-2000 $Å^2$ unlike enzyme active sites with an average surface area between 300 and 500 $Å^2$ (Figure 1.5).

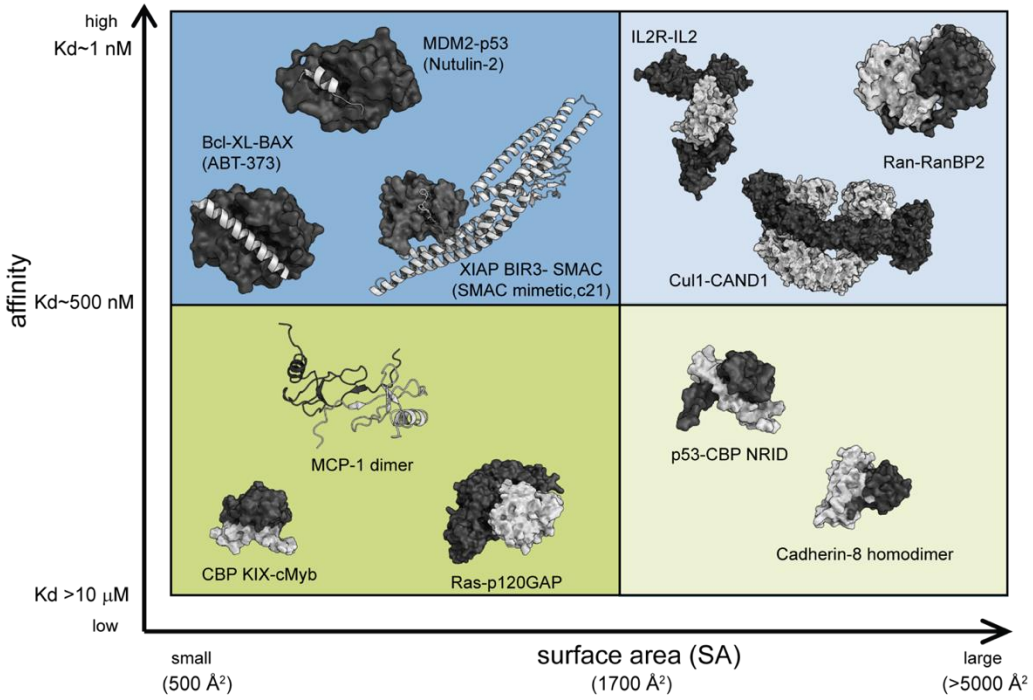

Figure 1.5: Chemical space of protein-protein interactions. Some PPIs exist in the high affinity-small surface area, low affinity small surface area, high affinity large surface area, or the low affinity-large surface area space. Examples of these proteins are shown in each of these spaces.

Previous work by former co-worker Dr. Steve Sturlis with the VP16(438-454) - Med25 AcID complex illustrates that the coactivator Med25 has a large binding surface, rather than one or more binding 'hot spots' (Figure 1.6). Replacement of each of the amino acids within the VP16 sequence with alanine and measurement of the binding affinity for Med25 revealed that the binding energy is spread over a large surface area, rather than localized to a few specific residues. As discussed in later sections, this is consistent with the challenge of identifying small molecule binders of

coactivators such as Med25 as small molecules typically do not have the array of functional groups needed for effective binding.[63]

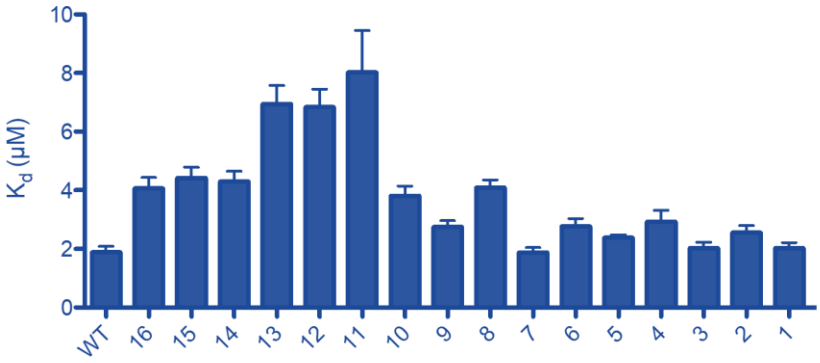

Figure 1.6: Alanine scan of VP16 (438-454). The Direct binding was measured for the peptide against Med25 Acid. This shows that binding is spread over a large surface area. Experiments were conducted by Dr. Steve Sturlis.

In addition to the large surface area and modest affinity of activator-coactivator complexes posing a challenge for inhibitor discovery, both the individual binding partners and the resulting complexes are structurally highly dynamic. Transcriptional activation domains are unstructured prior to binding and the activator-binding domains within coactivators exist in numerous conformations (Figure 1.7). There is little high resolution structural data of activator-coactivator complexes, and, as a result, structure-based design strategies are ineffective.

An additional challenge associated with 'drugging' activator•coactivator complexes is that with transcription taking place in the nucleus, inhibitors must be not just cell permeable but also traffic to the nucleus.[64] The cell membrane serves not just as a barrier to contain the components of the cell, but also poses a great challenge to efficiently delivering potent inhibitors of transcription. Native chemical elements of the cell membrane dictate what compounds it permits to pass through. The phospholipid bilayer would repel drug molecules that are negatively charged thus defeating

any hope for targeting transcription. Modulating the PPIs of activators and coactivators often mimics the amphipathic activators involved the in complex formation. In targeting the coactivators, the amphipathic molecule must successfully cross the membrane after introducing it to the biological system; however, this will be repelled upon interaction with the negatively charged phosphate heads of the membrane. For all of the reasons discussed in this section, activator-coactivator complexes have historically considered 'undruggable'.[59]

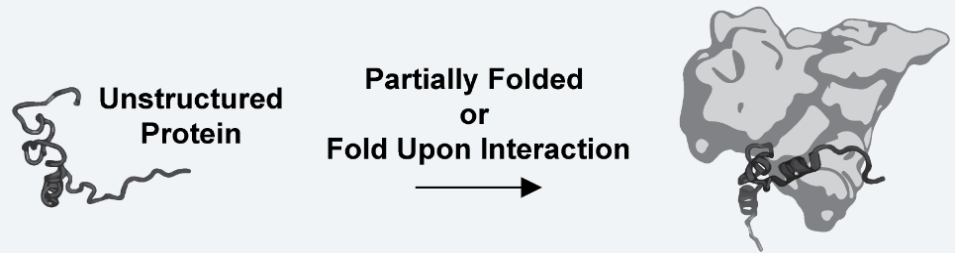

Figure 1.7. Protein adopts helical conformation upon interaction with target protein. PPIs are highly dynamic, thus posing as a great challenge for designing structure-based PPIs

.

1.4 Small Molecule Modulators of Activator•Coactivator PPIs

Despite the challenges outlined in the previous section, there has been a great deal of effort devoted to identifying small-molecule inhibitors of activator-coactivator targets as mechanistic probes and as therapeutics. In this section I describe some key examples and summarize the lessons learned.

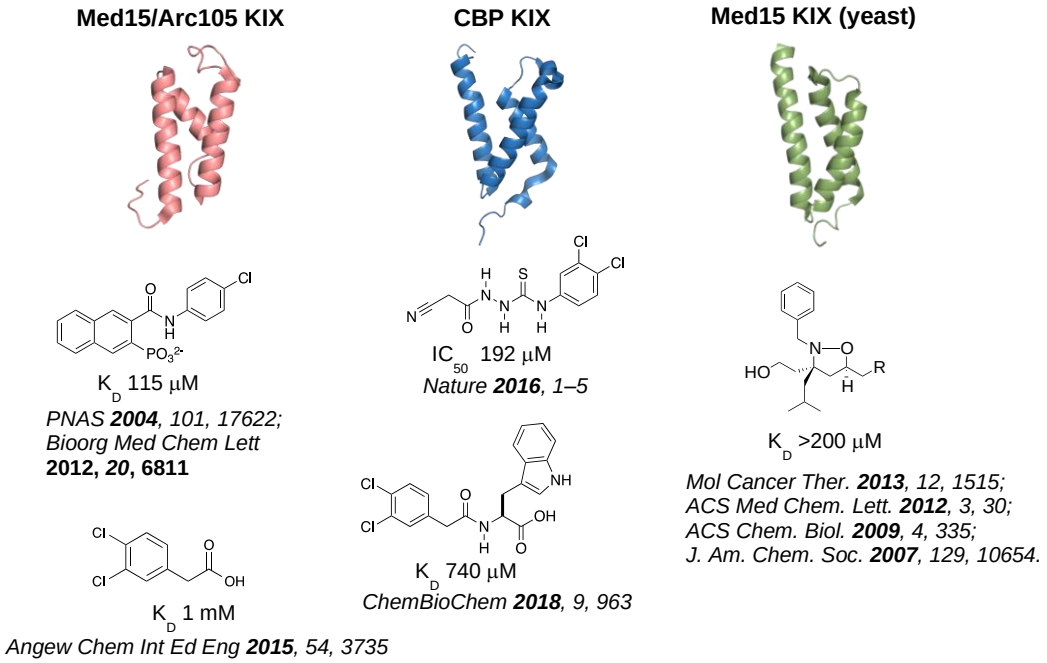

Figure 1.8: Examples of small molecules inhibitors of the KIX activator-binding domain found in CBP/p300, ARC105, SREBP and other coactivtors. KIX domains, like other coactivator motifs, are tough to target due to conformational dynamics. Thus, although a number of potential inhibitors have been identified they all have modest to poor affinity for the their target, KIX.

One of the most investigated coactivator targets is the master coactivator CPB/p300. Within that multi-domain coactivator is the KIX activator-binding domain (Figure 1.2, Figure 1.8) that through its interactions with the Myb and MLL transcriptional activators regulates hematopoiesis. The ternary Myb-KIX-MLL complexes is frequently dysregulated in acute myeloid leukemias (AML) and genetic and pharmacological studies have shown that disruption of KIX is sufficient to block leukemogenesis. Additionally, the PPI formed with the transcriptional activator CREB plays a prominent role in certain cancers as well as in neuropathic pain. For these reasons, multiple small molecule libraries have been screened against the KIX domain to identify inhibitors and design strategies have also been attempted.[65]

One of the earliest compounds to achieve success in targeting activator-coactivator interactions is the 2-naphthol-AS-E-phosphate (top left structure, Figure 1.8). This compound was identified from a drug discovery screen with over 700 compounds, and has been shown to bind specifically at a binding interface between CREB-CBP binding complex. Through a series of HSQC NMR experiments, the residues responsible for participating in the interaction were identified and further provided information for the most critical residue in the interaction. This surface that interacts with CREB also interacts with other proteins such Myb despite differing binding mechanisms, thus creating an opportunity to investigate whether the inhibitor has the ability to function specifically or broadly. Later results have illustrated that 2-naphthol-AS-Ephosphate is more a more potent inhibitor of Myb-CBP interaction compared to the CREB-CBP complex. Nonetheless, even after optimization, the K_D for KIX remains poor, 115 mM. Further, the selectivity of the molecule for CBP/p300 KIX over other coactivators (even other KIX domains) has not been established.[4,5,22]

Several synthetic KIX ligands demonstrated that they can inhibit transcriptional activators such as Myb and MLL, which bind to opposite faces of the KIX domain of CBP. For example, small molecule inhibitors for KIX identified from library screening include depsides (Sekikaic acid) and depsidones (lobaric acid) (Figure 1.9). These molecules successfully inhibited the MLL binding surface of KIX, thus underscoring the ability to use of the small molecules to target coactivators and show some specificity for a particular surface of the targeted protein despite the challenges. However, the structural complexity of the ligands has hampered further optimization.

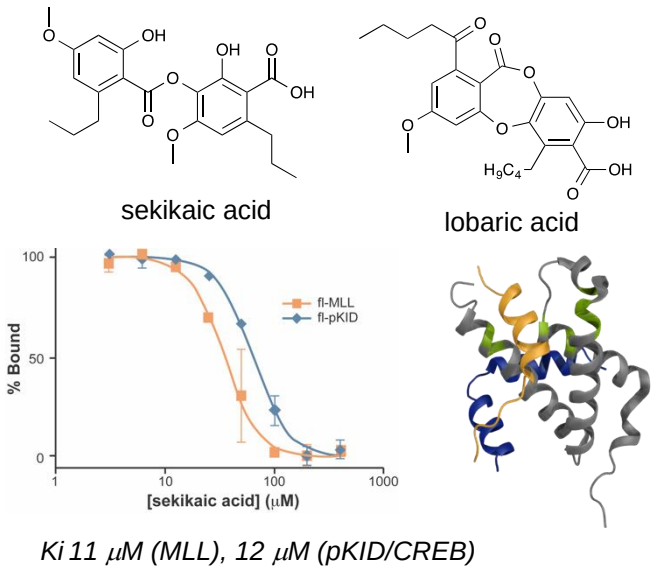

Ki 11 μM (MLL), 12 μM (pKID/CREB)

Figure 1.9: Library screening identified small molecule inhibitors of activator coactivator PPI. Sekikacic acid and Lobaric acid have been identified as two of the more potent inhibitors of activator-coactivator interactions**.**

The coactivator that is the focus of this thesis, Med25, has also been a target of interest. It was demonstrated that Med25 AcID-activator complexes are able to be disrupted, like KIX-activator complexes, using natural products. Norstictic acid, psoromic acid and garcinolic acid were identified as effective inhibitors of the PPIs of Med25 AcID, which could potentially be used to inhibit transcription activation of genes regulated by the Med25 protein network. Co-workers Dr. Steve Sturlis, Dr. Paul Bruno and Julie Garlick identified norstictic acid from two different screens of a complex between Med25 AcID and the activator ERM. It is a covalent inhibitor that binds to a loop on the H2 face of Med25 and in doing so inhibits complex formation at both the H1 and H2 face with low micromolar apparent IC_{50} values in vitro and in cells. A related structure, psoromic acid, shows similar activity. Norstictic acid also shows excellent selectivity (5-100-fold) for Med25 AcID over all coactivators tested. As in the KIX examples, however, due to the structural complexes of norstictic acid and psoromic acid, further optimization has not been possible.

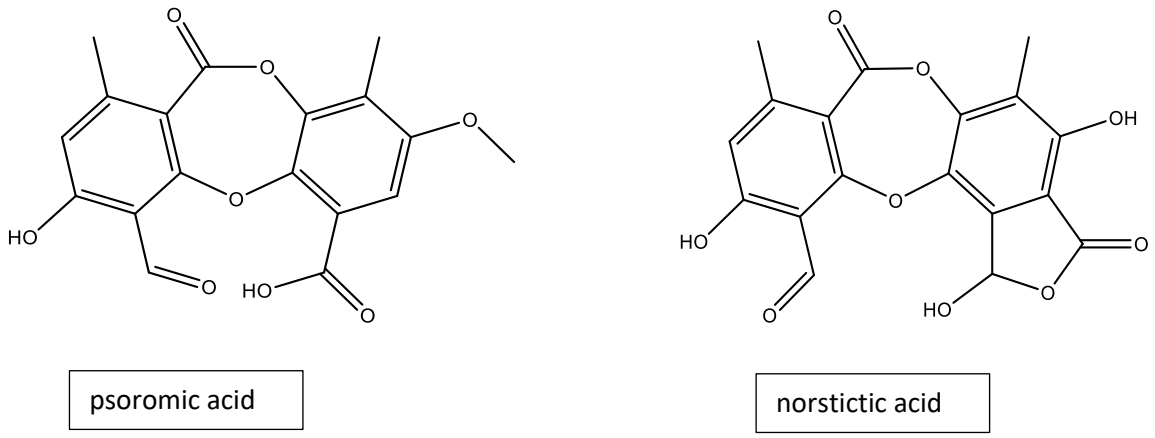

Figure 1.10: Natural products identified as inhibitors for activator-Med25 AcID complexes. These natural product inhibitors have shown to be potent inhibitors of TAD-Med25 AcID interactions.

The examples above show that it is possible to identify inhibitors, even selective inhibitors, of activator-coactivator complexes. However, the most successful inhibitors are natural products with structural complexities that prevent further optimization. Co-workers in the Mapp lab and other groups have attempted to identify more drug-like scaffolds for KIX, Med25, and other coactivators. In the case of Med25, for example, former co-workers Dr. Steve Sturlis and Dr. Paul Bruno screened all 150,000 small molecules in the Center for Chemical Genomics collection and obtained not a single hit. Co-worker Julie Garlick has screened focused libraries from the University of Illinois and from AtomWise, again with no success. Given these results, our focus shifted to developing peptidomimetics that could be based on the amino acid sequences of transcriptional activators. The advantage would be the synthetic ease with which the size and

complexity of peptidomimetics can be tailored and, specifically, we chose peptoids as the peptidomimetic scaffold on which to focus.

1.5 Peptoids as Protein Ligands and PPI Inhibitors

Peptoids were first reported in the 1980s as modular peptidomimetics. Like peptides, individual peptoid monomers are connected through amide bonds that can be formed via solid-phase synthesis. What distinguishes peptoids is that the side chain of each monomer is on the nitrogen, rather than on the a-carbon as in peptides, leading to a-chiral molecules and the ability to install a wide range of functional groups during the synthesis (Figure 1.11). By the early 1990s peptoid pioneer Ronald Zuckerman along with others had developed many peptoids with improved pharmacokinetics compared to their peptide counterparts and with a variety of applications.[66,67]

Because peptoids can be synthesized using automated strategies, the ease with which libraries can be prepared lead to screening approaches to identify protein-protein interaction inhibitors. An early example yielded one of the first peptoid ligands with a high affinity for 7-transmembrane G protein-coupled receptors. The identification of CHIR 2279 binding to α_1-adrenoreceptors with a low nanomolar K_i proved that it was possible to develop a peptidomimetic library and successfully select lead compounds that can be used in a biological system.[68]

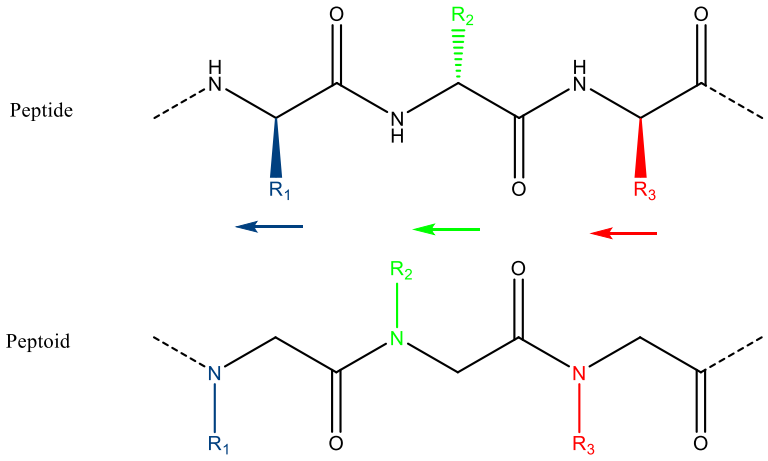

Figure 1.11: Comparison of peptide and peptoid structures. Peptoids mimic peptides with the substitution on the nitrogen atom instead of the alpha carbon.

The Src homology 3 domains are frequently found in eukaryotic signaling proteins and thus are important targets for PPI inhibitors. These proteins are attractive targets as they are implicated in diseases such as cancer and degenerative diseases. They make contact with their target proteins via proline-rich regions of the targets. Jack Nguyen and colleagues developed a hybrid peptide-peptoid library of molecules to improve selectivity. A library was developed with peptides and peptide-peptoid library and screened to identify potent binding ligands. The characteristics of peptoids were leveraged by substituting at least one amino acid in some sequences, which resulted in an improvement in affinity by 100-fold and specificity by 300-fold. These hybrids illustrate that incorporating peptoids in a canonical motif can remedy the challenge of designing potent inhibitors of protein-protein interactions.

A third example of peptoids working to modify PPI networks is in the realm of transcriptional PPIs. p53 is transcriptional activator that is regulated by associating with masking protein MDM2 in normal cells. However, upon abnormal cellular functioning such as cellular stress or genomic

damage, it performs its transcriptional tasks to regulate transcription by binding to many proteins including coactivator proteins such as CBP/p300 and PC4 to regulate the cell cycle.[69–72] Toshiaki Hara and colleagues demonstrated the successful design of a peptoid that inhibits the association of p53 with its binding partner MDM2. They were able to identify a peptoid with comparable affinity for the masking protein as the native p53 peptide. In another example, Kodadek and co-workers carried out a screen of a peptoid library against the transcriptional coactivator Med15 and in doing so identified a number of short (7-residue) peptoids with micromolar affinity for the coactivator. Also, peptoids stability exceeds that of peptides *In vivo* due to their ability to withstand proteolytic degradation, withstand denaturants have shown to not produce anti-immune response.[73–75] Taken together, these examples indicate that peptoids are a good scaffold for developing ligands of Med25 and, in the future, modulators of the Med25 PPI network.[76,77]

1.5. Dissertation Summary

The overall goal of this thesis is to develop peptidomimetics that can inhibit native protein-protein interactions between activators and coactivators. In these studies, we use Med25 AcID as our model to garner key insights into the engagement mechanism between Med25 AcID and its binding partners. Med25 AcID functions primarily as the key domain of coactivator Med25 subunit that allows the protein to interact with activators. Because a number of the activator proteins that interact with Med25 are implicated in multiple diseases, synthetic ligands would have high value as mechanistic probes. We hypothesize that we can leverage the characteristics of peptidomimetics to develop lead compounds to form inhibitors of activator coactivator interactions.

In Chapter Two we show that Med25 has two discrete binding faces that selectively bind to the activators ERM and ATF6a. Additionally, truncation studies of the Med25-dependent activator VP16 were used to identify minimal peptide sequences needed for Med25 binding. Through The work described in Chapter Three demonstrated that we could identify minimal sequences with good affinity for Med25 and optimize the peptoids to identify a structure with low micromolar affinity for Med25 and good cell permeability.

1.6 References

1. Ulrich Stelzl *et al.* A Human Protein-Protein Interaction Network: A Resource for Annotating the Proteome. *Cell* **122**, 957–968 (2005).
2. Ptashne, M. & Gann, A. *Genes and Signals*. (Cold Spring Harbor Laboratory Press, 2002).
3. Escher, D., Bodmer-Glavas, M. & Barberis, A. Conservation of Glutamine-Rich Transactivation Function between Yeast and Humans. *Molecular and Cellular Biology* **20**, 2774–2782 (2000).
4. Cosma, M. Ordered Recruitment: Gene-SpecificMechanism of Transcription Activation. *Molecular Cell* **10**, 227–236 (2002).
5. Wang, W., Carey, M. & Gralla, J. Polymerase II promoter activation: closed complex formation and ATP-driven start site opening. *Science* **255**, 450–453 (1992).
6. Thakur, J., Yadav, A. & Yadav, G. Molecular recognition by the KIX domain and its role in gene regulation. *Nucleic Acids Research* **42**, 2112–2125 (2014).
7. Lee, T. I. & Young, R. Transcriptional Regulation andIts Misregulation in Disease. *Cell* **152**, 1237–1251 (2013).
8. Arkin, M. Protein–protein interactions and cancer: small molecules going in for the kill. *Current Opinion in Chemical Biology* **9**, 317–324 (2005).
9. Zinzalla, G. & Thyrston, D. Targeting protein–protein interactions for therapeutic intervention: a challenge for the future. *Future Medicinal Chemistry* **1**, 65–93 (2009).
10. Lage, K. Protein-protein interactions and genetic diseases: The Interactome. *Biochimica et biophysica acta* **1842**, 1971–1980 (2014).
11. Arndt, H. Small molecule modulators of transcription. *Chem Int Edit* **45**, 4552–4560 (2006).

12. Triezenberg, S. Structure and function of transcriptional activation domains. *Current Opinion in Genetics & Development* **5**, 190–196 (1995).
13. Darner Jr, J., E. Transcription factors as targets for cancer therapy. *Nature Reviews Cancer* **2**, 740–749 (2002).
14. Duncan, S., A., Navas, A., M. & Dufort, D. Regulation of a Transcription Factor Network Required for Differentiation and Metabolism. *Science* **281**, 692–695 (1998).
15. Keegan, L., Gill, G. & Ptashne, M. Seperation of DNA binding from the transcription activating function of a eurkaryotic regulatory protein. *Science* **231**, 699–704.
16. Ansari, A. Z., Mapp, A. K. & Nguyen, D. H. Towards a minimal motif for artificial transcriptional activators. *Chem Biol* **8**, 583–592 (2001).
17. Ansari, A. Z. & Mapp, A. K. Modular design of artificial transcription factors. *Current Opinion in Chemical Biology* **6**, 765–772 (2002).
18. Mapp, A. K. & Ansari, A. Z. A TAD Further: Exogenous Control of Gene Activation. *Chem Biol* **2**, 62–75 (2007).
19. Johnson, P. F., Sterneck, E. & Williams, S. Activation domains of transcriptional regulatory proteins. *The Journal of Nutritional Biochemistry* **4**, 386–398 (1993).
20. Mitchell, P., J. & Tjian, R. Transcriptional Regulation in Mamnalian Cells by Sequence-Specific DNA Binding Proteins. *Science* **245**, 371–378 (1989).
21. Uesugi, M., Nyanguile, O. & Lu, H. Induced alpha helix in the VP16 activation domain upon binding to a human TAF. *Science* **277**, 1310–1313 (1997).
22. Ptashne, M. & Gann, A. *Genes and Signals*. (Cold Spring Harbor Laboratory Press, 2002).
23. Pilauri, V., Bewley, M. & Hopper, J. Gal80 Dimerization and the Yeast GAL Gene Switch. *Genetics* **169**, 1903–1914 (2005).

24. Melcher, K. & Xu, E. Gal80-Gal80 interaction on adjacent Gal4p binding sites is required for complete GAL gene repression. *EMBO J* **20**, 841–851 (2001).
25. Wu, Y., Reece, J. & Ptashne, M. Quantitation of putative activator-target affinities predicts transcriptional activating potentials. *EMBO J* **15**, 3951–3963 (1996).
26. Vojnic, E., Mourao, A., Seizl & Wenzeck, L. Structure and VP16 binding of the Mediator Med25 activator interaction domain. *Nature Structural & Molecular Biology* **18**, 404-U429 (2011).
27. Herbig, E., Warfield, L., Fishburn, J. & Knutson, B. Mechanism of Mediator recruitment by tandem Gcn4 activation domains and three Gal11 activator-binding domains. *Molecular and Cellular Biology* **30**, 2376–2390 (2010).
28. Langlois, C., Mas, C. & Di Lello, P. NMR structure of the complex between the Tfb1 subunit of TFIIH and the activation domain of VP16: Structural similarities between VP16 and p53. *Journal of the American Chemical Society* **130**, 10596–10604 (2008).
29. Drysdale, C., M., Duenas, E. & Jackson, B. The transcriptional activator GCN4 contains multiple activation domains that are critically dependent on hydrophobic amino acids. *Molecular and Cellular Biology* **15**, 1220–1233 (1995).
30. Hope, I. A. & Struhl, K. Functional dissection of a eukaryotic transcriptional activator protein, GCN4 of yeast. *Cell* **46**, 885–894 (1986).
31. Ma, J. & Ptashne, M. A new class of yeast transcriptional activators. *Cell* **51**, 113–119 (1987).
32. Ma, J. & Ptashne, M. Deletion analysis of GAL4 defines two transcriptional activating segments. *Cell* **48**, 847–853 (1987).

33. Malik, S. & Roeder, R. G. The metazoan Mediator co-activator complex as an integrative hub for transcriptional regulation. *Nature Reviews Genetics* **11**, 761–772 (2010).
34. Singh, G. P., Ganapathi, M. & Dash, D. Role of intrinsic disorder in transient interactions of hub proteins. *Protein* **66**, 761–765 (2007).
35. Vo, N. & Goodman, R. H. CREB-binding Protein and p300 in Transcriptional Regulation. *Journal of Biological Chemistry* **276**, 13505–13508 (2001).
36. Higurashi, M., Ishida, T. & Kinoshita, K. Identification of transient hub proteins and the possible structural basis for their multiple interactions. *Protein Science Publication* **17**, 72–78 (2008).
37. Dyson, H. J. & Wright, P. E. Role of intrinsic protein disorder in the function and interactions of the transcriptional coactivators CREB-binding protein (CBP) and p300. *J Biol Chem* **291**, 6714–6722 (2016).
38. Park, J., Kim, H.-S. & Han, S. In Vivo Requirement of Activator-Specific Binding Targets of Mediator. *Molecular and Cellular Biology* **20**, 8709–8719 (2000).
39. Lee, Y., Park, J. & Min, S. An Activator Binding Module of Yeast RNA Polymerase II Holoenzyme. *Molecular and Cellular Biology* **19**, 2967–2976 (1999).
40. Thakur, J., Arthanari, H. & Yang, F. Mediator Subunit Gal11p/MED15 Is Required for FattyAcid-dependent Gene Activation by Yeast TranscriptionFactor Oaf1p. *Journal of Biological Chemistry* **284**, 4422–4428 (2009).
41. Thakur, J., Arthanari, H. & Yang, F. A nuclear receptor-like pathway regulating multidrug resistance in fungi. *Nature* **452**, 604–609 (2008).

42. Jedidi, I., Zhang, F. & Qiu, H. Activator Gcn4 Employs Multiple Segments of Med15/Gal11,Including the KIX Domain, to Recruit Mediator to TargetGenesin Vivo. *Journal of Biological Chemistry* **285**, 2438–2455 (2010).
43. Crans, H. & Sakamoto, K. Transcription factors and translocations in lymphoid and myeloid leukemia. *Leukemia* **15**, 313–331 (2001).
44. Benz, C. C., O'Hagan, R. C. & Richter, B. HER2/Neu and the Ets transcription activator PEA3 are coordinately upregulated in human breast cancer. *Oncogene* **15**, 1513–1525 (1997).
45. Chandra, K. Genetic Abnormalities and Challenges in the Treatment of Acute Myeloid Leukemia. *Genes and Cancer* **2**, 95–197 (2011).
46. Aytes, A., Mitrofanova, A. & Kinkade, C., W. ETV4 promotes metastasis in response to activation of PI3-kinase and Ras signaling in a mouse model of advanced prostate cancer. *Proc. Natl. Acad. Sci.* **110**, 3506–3515 (2013).
47. Keld, R., Guo, B. & Downey, P. PEA3/ETV4-related transcription factors coupled with active ERK signalling are associated with poor prognosis in gastric adenocarcinoma. *Br J Cancer* **105**, 124–130 (2011).
48. Keld, R., Guo, B. & Downey, P. The ERK MAP kinase-PEA3/ETV4-MMP-1 axis is operative in oesophageal adenocarcinoma. *Molecular Cancer* **9**, 1476–4598 (2010).
49. de Launoit, Y., Baert, J.-L. & Chotteau-Lelievre, A. The Ets transcription factors of the PEA3 group: transcriptional regulators in metastasis. *Biochimica et Biophysica Acta* **1766**, 79–87 (2006).
50. Oh, S., Shin, S. & Janknecht, R. ETV1, 4 and 5: An oncogenic subfamily of ETS transcription factors. *Biochimica et Biophysica Acta* **1826**, 1–12 (2012).

51. Baena, E., Shao, Z. & Linn, D. ETV1 directs androgen metabolism and confers aggressive prostate cancer in targeted mice and patients. *Genes and Development* **27**, 683–698 (2013).
52. Yuan, Z.-Y., Dai, T. & Wang, S.-S. Overexpression of ETV4 protein in triple-negative breast cancer is associated with a higher risk of distant metastasis. *Onco Targets Ther* **7**, 1733–1742 (2014).
53. Pallecchia, A., Pescucci, C. & De Lorenzo, E. Overexpression of ETV4 is oncogenic in prostate cells through promotion of both cell proliferation and epithelial to mesenchymal transition. *Oncogenesis* 1–11 (2012).
54. Johnson, K. Rapid Kinetic Analysis of Mechanochemical Adenosinetriphosphatases. *Methods in Enzymology* **134**, 677–705 (1986).
55. Erlanson, D., Wells, J., A. & Brainsted, A., C. Tethering: fragment-based drug discovery. *Annu REv Biophys Biomol Struct.* **33**, 199–223 (2004).
56. Hilser, V., J. & Thompson, E. Intrinsic disorder as a mechanism to optimize allosteric coupling in proteins. *Proc. Natl. Acad. Sci.* **104**, 8311–8315 (2007).
57. Henderson, A., Henley, M. & Foster, N. Conservation of coactivator engagement mechanism enables small-molecule allosteric modulators. **115**, 8960–8965 (2018).
58. Verger, A., Baert, J.-L. & Verreman, K. The Mediator complex subunit MED25 is targeted by the N-terminal transactivation domain of the PEA3 group member. *Nucleic Acids Research* **41**, 4847–4859 (2013).
59. Hopkins, A. L. & Groom, C. R. The druggable genome. *Nature Review Drug Discovery* **1**, 727–730 (2002).
60. Overington, J. P., Al-Lazikani, B. & Hopkins, A. L. How many drug targets are there? *Nature Review Drug Discovery* **5**, 993–996 (2006).

61. Drews, J. Drug discovery: a historical perspective. *Science* **287**, 1960–1964 (2000).
62. Stumpf, M., Thorne, T. & de Silva, E. Estimating the size of the human interactome. *National Academy of Sciences* **105**, 6959–6964.
63. Lipinski, C. Drug-like properties and the causes of poor solubility and poor permeability. J Pharmacol Toxicol Methods. *J Pharmacol Toxicol Methods* **44**, 235–249 (2000).
64. Ptashne, M. & Gann, A. Transcriptional activation by recruitment. *Nature* **386**, 569–577 (1997).
65. Gee, C., Arnston, K. & Koleski, E. Dual Labeling of the CBP/p300 KIX Domain for 19 F NMR Leads to Identification of a New Small-Molecule Binding Site. *Chembiochem* **19**, 963–969 (2018).
66. Zuckermann, R. Peptoid Origins. *Peptide Science* **96**,.
67. Dohm, M., Kapoor, R. & Barron, A. Peptoids: Bio-Inspired Polymers as Potential Pharmaceuticals. *Current Pharmaceutical Design* **17**, 2732–2747 (2011).
68. Gibbons, J., Hancock, A. & Vitt, C. Pharmacologic Characterization of CHIR 2279, an NSubstituted Glycine Peptoid with High-Affinity Binding for alpha1- Adrenoceptors. *The Journal of Pharmacology an Experimental Therapeutics* **277**, (996).
69. Fernandez-Fernandez, M. & Sot, B. The relevance of protein-protein interactions for p53 function: the CPE contribution. *Protein Engineering, Design and Selection* **24**, 41–51 (2010).
70. Banerjee, S., Kumar, B. & Kundu, T. General Transcriptional Coactivator PC4 Activates p53 Function. *Molecular and Cellular Biology* **24**, 2052–2062 (2004).

71. Fabbro, M., Savage, K. & Hobson, K. BRCA1-BARD1 complexes are required for p53Ser-15 phosphorylation and a G1/S arrest following ionizing radiation-induced DNA damage. *Journal of Biological Chemistry* **279**, 1251–1258 (2004).
72. Beckerman, R. & Prives, C. Transcriptional Regulation by p53. *Cold Spring Harbor Perspectives in Biology* **2**, 1–19 (2010).
73. Sandborn, T., Wu, C. & Zuckermann, R. Extreme stability of helices formed by water-soluble poly-N-substituted glycines (polypeptoids) with alpha-chiral side chains. *Biopolymers* **63**, 12–20 (2002).
74. Miller, S., Simon, R. & Ng, S. Comparison of the Proteolytic Susceptibilities of Homologous L-Amino Acid, D-Amino Acid, and N-Substituted Clycine Peptide and Peptoid Oligomers. *Drug Development Research* **35**, 20–32 (1995).
75. Astle, J., Udugamasooriya, D. & Smallshaw, J. A VEGFR2 Antagonist and Other Peptoids Evade Immune Recognition. *International Journal of Peptide Research and Therapeutics* **14**, 223–227 (2008).
76. Reddy, M., Bachhawat-Sikder, K. & Kodadek, T. Transformation of Low-Affinity Lead Compounds into High-Affinity Protein Capture Agents. *Chemistry & Biology* **11**, 1127–1137.
77. Hara, T., Durell, S. & Myers, M. Probing the Structural Requirements of Peptoids That Inhibit HDM2-p53 Interactions. *J. Am. Chem. Soc.2* **128**, 1995–2004 (06).

Chapter Two

Coactivator Med25 Contains Two Binding Surfaces Targetable by Minimal Activator Sequences[1]

2.1 Abstract

Transcriptional coactivators are a molecular recognition marvel because a single domain within these proteins, the activator binding domain or ABD, interacts with multiple compositionally diverse transcriptional activators to regulate transcription. Also remarkable is the structural diversity among ABDs, which range from conformationally dynamic helical motifs to those with a stable core such as a □-barrel. A significant objective is to define properties of ABD•activator complexes that allow them to be targeted by inhibitors. The ABD of the coactivator Med25 (Activator Interaction Domain or AcID) is unique in that it contains secondary structural elements that are on both ends of the spectrum: helices and loops that display significant conformational mobility and a seven-stranded □-barrel core that is structurally rigid. Here, we use protein NMR and mutational analysis to identify the binding surfaces used by the natural activators ERM and ATF6α for complex formation. We further find that a minimal 8-residue sequence from the transcriptional activator binding partners is sufficient for binding. Taken together, these data indicate that modulating the Med25 PPI network should be possible using mimetics of the core transcriptional activation domain sequences.

[1] Portions of this chapter are taken from "Conservation of coactivator engagement mechanism enables small-molecule allosteric modulators" A. R. Henderson, M.J. Henley, N. J. Foster, A.L. Peiffer, M.S. Beyersdorf, **K.D. Stanford**, S. M. Sturlis, B. M. Linhares, Z.B. Hill, J. A. Wells, T. Cierpicki, C. L. Brooks III, C.A. Fierke, A. K. Mapp. *Proc. Natl. Acad. Sci. USA* **2018** *115*, 8960-65.

2.2 Introduction

Modulating the protein-protein interactions (PPIs) formed between activator binding domains (ABDs) of transcriptional coactivators and their cognate activator binding partners is a formidable task and the reasons are revealed by biophysical studies of these functionally critical complexes.[1] An excellent example of this is the ABD of the Mediator protein Med25, termed AcID (Activator Interaction Domain; Figure 1A).[2–4] As is standard for ABDs, AcID is a binding partner of a diverse array of transcriptional activators, including VP16, ATF6α,[5] and the ETV/PEA3 activators.[6,7] Through these interactions, Med25 plays significant roles in the unfolded protein response and in oncogenesis, generating significant interest in small molecule modulators. However, data from NMR studies of AcID in complex with VP16 and ETV/PEA3 activators suggest that modulating these PPIs would not be trivial.[2–4] The VP16 transcriptional activation domain contacts a surface of approximately 1800 Å^2 of AcID, wrapping around the topologically challenging β-barrel while also contacting two flanking helices. The transcriptional activation domain of the ETV/PEA3 member ERM interacts with one face of the β-barrel, a binding surface referred to as H1 that is ~900 Å^2 in area.[6,7] The β-barrel core of AcID is highly unusual among ABDs, with helices more commonly observed, and raises the question of the role that the barrel might play in the molecular recognition of activators relative to the other substructures within AcID.

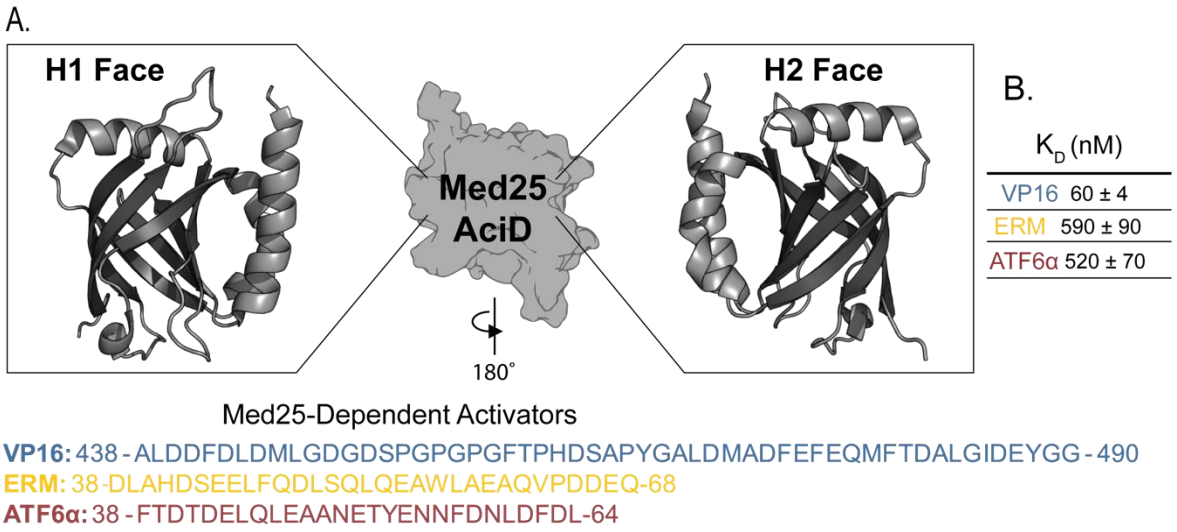

Figure 2.1: Med25 AcID with transcriptional activators (A) The AcID is the binding partner of a growing number of transcriptional activators and contains at least two binding surfaces, termed H1 and H2. The sequences of the transcriptional activation domains of the three Med25-dependent activators used in this study are shown below the protein structure (PDB ID code 2XNF) (B) Equilibrium dissociation constants for each of. Med25 AcID–activator complexes, measured through fluorescence anisotropy experiments using fluorescein-labeled peptides. These values are the average of at least three independent measurements with the error indicated (standard deviation of the mean). Binding measurements were completed by Dr. Andrew Henderson and Dr. Matthew Henley.

The observation that a portion of VP16 and ERM utilize the same H1 binding surface in AcID despite their distinct sequences suggests that conformational plasticity within the ABD could play a role in its molecular recognition capabilities and ultimately function, similar to helical coactivators. Indeed, computational, and biophysical studies of Med25 and its complexes by our group demonstrate that Med25 recognizes its partners via a mechanism analogous to that of helical coactivators, in which the loops and helices flanking the β-barrel play a role in molecular recognition.[8] Remaining questions about Med25-activator complexes included identifying the binding site for the native partner ATF6α and the determination of the minimal binding sequences. Through mutational analysis I find that, analogous to helical coactivators, a minimal 8-residue sequence from activators is sufficient for interaction with Med25. Taken together, these results indicate that, despite its structural uniqueness, Med25 uses a similar molecular recognition

mechanism to complex with transcriptional activators. This sets the stage for inhibitor development based upon the native transcriptional activation domains.

Figure 2.2: VP16 TAD has two coactivator binding domains: the N-terminal half of the VP16 transcriptional activation domain (red; H1 domain) and the C- terminal region (green; H2 domain) are capable of independently stimulating transcription when associated with DNA.[9,10 11]

2.3 Results and Discussion

Separate NMR studies of AcID in complex with the transcriptional activation domains of VP16 and ERM suggest that the two activators both contact the H1 binding surface, with the significantly larger VP16 also interacting with the H2 surface.[2–4] While several lines of evidence indicate that ATF6α interacts with Med25 AcID as part of its function,[5] the binding site within the protein had not been established. We first measured the dissociation constants for each of the activators by fluorescence anisotropy experiments using fluorescein-tagged variants of VP16(438-490), ERM(38-68) and ATF6α(40-66) and this revealed that ERM and ATF6α interact with comparable affinities (Figure 1.1B).[2–6] To provide a direct comparison of the binding modes of the three activators and identify the binding site of ATF6α, we measured the chemical shift changes in each activator-AcID complex via ^{1}H, ^{15}N-HSQC NMR titration experiments, with VP16(438-490), ERM(38-68) and ATF6α(40-66) in the presence of ^{15}N-labeled Med25 AcID.

The amide proton perturbation patterns measured for the activator•AcID complexes suggest a different binding mode for each of the three activators. VP16 induced changes at both AcID binding surfaces and throughout the Med25 AcID structure, consistent with the tandem transcriptional activation domains within its sequence (Figure 2.3)

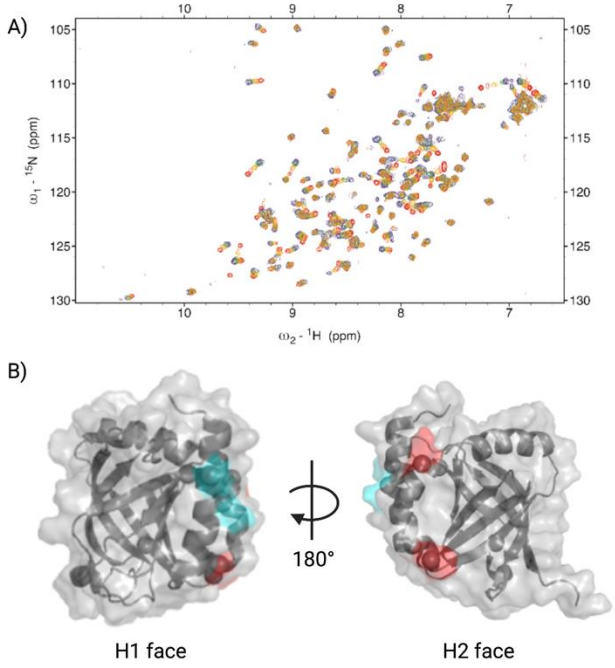

Figure 2.3 A: ^{1}H, ^{15}N-HSQC spectra of chemical shifts of Med25 AcID residues. ^{1}H,^{15}N-HSQC spectra of Med25 AcID show widespread chemical shifts changes upon titration with VP16(438-490). Med25 AcID apo (red), in solution with 0.2 (red orange), 0.5 (orange), 0.8 (gold) 1.1 (green), 2 (blue) and 3 (purple) equivalents of VP16. B) VP16 binding induces significant (>2 standard deviations above the average chemical shift change) chemical shift perturbations in the dynamic regions of Med25 AcID. This includes residues on the H1 binding surface (blue-green, residues I453, Q539 and T54) and the H2 binding surface (red, residues Q456, V471, L464 and R466). HSQC experiments carried out in collaboration with Dr. Matthew Beyersdorf.

ERM binding predominantly lead to perturbations at residues on the H1 surface of the AcID β-barrel, in agreement with the model in which it preferentially interacts at that site (Figure 2.4A;).[4,6,7] Key changes at residues K411, E538, and Q451, for example, were seen with both VP16 and ERM. In contrast, interaction with ATF6α led to significant chemical shifts changes on the H2 binding surface (Figure 2.4B). ATF6α induced shifts of residues Q456, M470, and H474 which were also affected to varying degrees by VP16 and largely unaltered by ERM. This is illustrated in Figure 2.4C, which highlights the distinct patterns of overlap of the chemical shift patterns of ATF6a and ERM with VP16. Additionally, while the chemical shift perturbations indicate that residues in the β-barrel play a role in binding, the extensive shift changes in the flanking dynamic regions suggest that those dynamic substructures are also integral for binding.

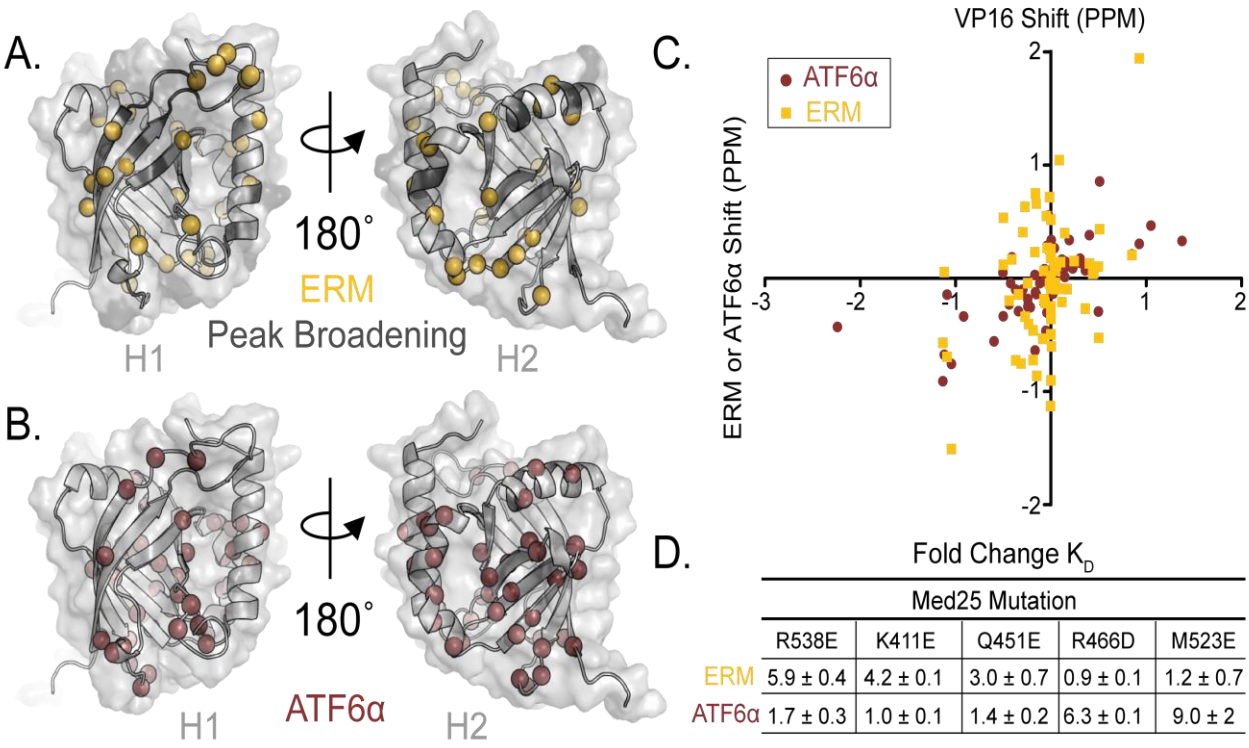

Figure 2.4: ATF6α binds to the H2 surface of Med25 AcID. (A) Results of chemical shift perturbation experiments superimposed upon the Med25 AcID structure (PDB ID code 2XNF). Residues displaying chemical shift perturbation greater than 2 SD upon ERM binding are depicted in maize squares. (B) Results displaying chemical shift perturbation greater than 2 SD upon ATF6α binding depicted in rust spheres. (C) Scatter plot illustrating correlations between the chemical shift perturbations (CSPs) of individual Med25 AcID residues from HSQC experiments with ERM, ATF6α, and VP16. The position of each maize square represents the CSP of an individual residue in Med25 AcID upon binding to ERM (y axis) and VP16 (x axis). Thus, squares along the dotted diagonal are residues that shift similarly in both ERM–AcID and VP16–AcID complexes. The same analysis for ATF6α is shown in rust circles. (D) Results of direct binding experiments with fluorescein-labeled activators and the indicated mutants of Med25 AcID as measured by fluorescence polarization expressed the fold change relative to the dissociation constant of each activator for the WT AcID. The indicated error is propagated from three independent dissociation constant measurements. (HSQC experiments completed by Dr. Matthew Henley, Dr. Andrew Henderson, and Dr. Brian Linhares; mutant generation and binding studies carried out in collaboration with Dr. Nick Foster and Dr. Steve Sturlis)

Consistent with ATF6α and ERM interacting on opposing sides of AcID, mutations introduced on one or the other of the binding surfaces produced distinct effects (Figure 2.4D). H1 mutations R538E, K411E, and Q451E inhibit ERM binding while ATF6α is largely unaffected. In contrast, H2 mutations R466D and M523E significantly inhibit ATF6α with minimal impact on ERM binding. Taken together these data indicate that ATF6α binds on the H2 binding surface of Med25 AcID, opposite the site of ERM. Further,

the distinct but overlapping chemical shift patterns observed upon binding of each of the activators to Med25 suggest several unique binding modes accommodated within AcID. This is analogous to helical activator binding domains such as GACKIX of CBP/p300, a three-helix bundle that contains at least two activator binding sites.[12]

Since a number of charged residues within Med25 exhibited chemical shift changes by ATF6α binding, we sought to test if altering the charge could be used to further enhance binding. Within the H2 binding surface, M523 was a candidate for mutation as it appears directly adjacent to the ATF6α binding site but not directly engaged. Given the overall negative charge of ATF6a, we hypothesized that mutation of M523 to glutamic acid would inhibit binding but that mutation to arginine would enhance binding. Consistent with this hypothesis, the M523E mutant attenuated binding of ATF6α approximately 9-fold. Surprisingly, the M523R mutation did not alter ATF6α binding. One explanation is that there is a sufficient array of positively charged residues already in the vicinity of the binding surface such that an energetic gain is minimal. The loop flanking the binding surface, for example, contains three lysine residues (K518, K519, K520). A more detailed mutational analysis will be required to define the roles of the various residues.

2.3A: Minimal 8-Residue Sequences from Activators Are Sufficient for Binding to Med25

To better understand the important features of activator-coactivator PPIs, it has been a long-standing strategy to develop synthetic activators, either de novo or by modifying existing activator sequences. One of the earliest synthetic designed activators is the 20 amino acid amphipathic helix (AH) peptide that has shown that it is possible to create minimal sequences that can function as transcriptional activation domains.[13–15] Subsequent studies identified shorter sequences (8-10 residues) from phage display selections that are capable of low micromolar binding to coactivator

protein such as CBP/p300.[16] Similarly, truncation studies of natural transcriptional activators indicate that sequences of 8-11 amino acids can be sufficient to interact with coactivators and stimulate transcription.[1718]

Using the reporter gene chloramphenicol acetyl transferase (CAT) driven by a DNA binding domain fused to various activator sequences, truncations of activators have identified minimal sequences that are capable of interacting with coactivators and the transcriptional machinery for transcriptional initiation to occur. Oaf1 is one of many activators that interact with the TAF9 coactivator. Using the one-hybrid assay, the transactivation ability of a variety of truncated Oaf1 TADs was tested in a mammalian cell line and even a 7-residue sequence demonstrated some level of activity, with a 10 residue sequence providing robust activation (Table 2.1).[17] Truncation studies of artificial KIX TADs model from CREB and c-Myb produced 8-residue sequences that interact with the cognate coactivator CBP with micromolar affinities.[19] Given the structural uniqueness of Med25, an open question at the outset of this work was if similar minimal activator sequences of transcriptional activators were sufficient to recognize Med25.

Construct	**TAD Sequence**	**Fold Induction (CAT)**
Gal4-DBD		1
Gal4-DBD- Oaf1(1035-1042)	LFDYDFLF	4
Gal4-DBD-Oaf1(1035-1047)	LFDYDFLFGNDFA	29
Gal4-DBD-Oaf1(1021-1047)	ANNTPFPGYFGGLDLFDYDFLFGNDFA	38

Table 2.1: Truncated TAD has transactivation activity in mammalian cells. Oaf1 TAD minimal sequence was identified, and transactivation activity was determined. CAT fold-induction is determined by normalizing CAT to β-galactosidase activity of cotransfected β-galactosidase plasmid [17] Truncation studies of the Med25 binding

partner VP16 carried out in our laboratory revealed that $VP16_{438\text{-}490}$ interacts with a sub-micromolar affinity of 60 nM (Figure 2.1).[20] Such tight binding arises in part from the ability of the nearly full-length transcriptional activation domain to contact both binding surfaces of Med25 AcID, in contrast to smaller activation domains such as those from ERM and ATF6α. Former colleague Dr. Steve Sturlis demonstrated that, consistent with these results, the amino terminus of the sequence (residues 413-437) retains little detectable affinity for Med25 AcID (Figure 2.5). This set the precedent for further truncation to identify shorter sequences that retained at least micromolar affinity for the coactivator and could be used as starting points for peptidomimetic design. As illustrated in Figure 2.5, initial studies carried out by Dr. Sturlis revealed that relatively short sequences 15-20 amino acids in length retained micromolar affinity for Med25.

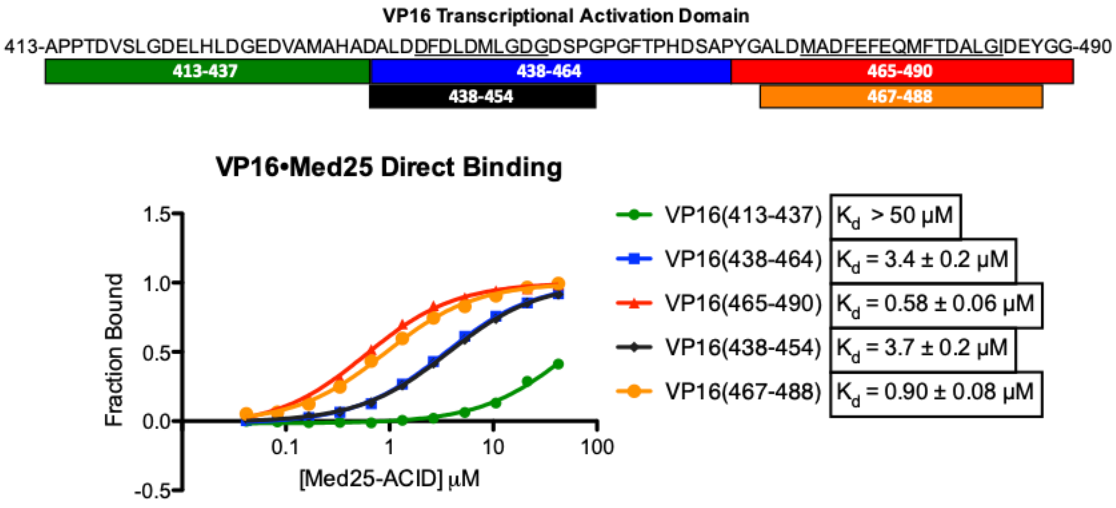

Figure 2.5 VP16 TAD Truncation. The VP16 TAD was truncated into three peptides of approximately equally length and an additional two peptides were synthesized based on purported α-helices within the TAD (underlined sequences within the TAD). The peptides were conjugated to fluorescein and the K_d of each peptide was determined for AcID using fluorescence polarization. Curves represent the means of three independent experiments with error bars representing the standard deviation of the fraction bound at the indicated concentration of AcID protein (Data adapted from the published dissertation of Dr. Steve Sturlis).[21]

Within the C-terminal sequence of 465-490 is a region predicted to become helical upon binding to Med25, amino acids 470-485, and an 8-residue sequence (472-479) that has been reported in the literature to function as a transcriptional activation domain when fused to a DNA binding domain (Table 2.1).[15,22] Because VP16(472-479) must interact with coactivators such as Med25 in order to active transcription, we chose this 8-residue sequence to further investigate. VP16(472-479) as well as mutant in which Q477 was replaced with an additional glutamic acid were synthesized and labeled with fluorescein for direct binding studies (Figure 2.6). The latter was initially prepared as a negative control, as prior studies have shown that increasing negative charge in a transcriptional activator sequence typically decreases binding.[23,24]

Name	Sequence
VP16 (465-490)	YGALDMADFEFEQMFTDALGIDEYGG
VP16 (470-485)	MADFEFEQMFTDALGI
VP16 (472-479)	DFEFEQMF
VP16 (472-479) Q477E	DFEFEEMF

Table 2.2 Sequences of the helical region of the C-terminus of the VP16 TAD. The 8-amino acid sequence is contained within the longer helical sequences.

As can be seen in Figure 2.6C, VP16(472-479) shows good binding to Med25 AcID, despite its considerably smaller size. Additionally, this short peptide preferentially binds to Med25 compared to the related activator binding domain of CBP, KIX (Figure 2.6D). However, the negative control, the Q477E mutant, showed greater than 2-fold increase in binding (Figure 2.6E). In retrospect, this was not an unexpected result; Med25 AcID has an unusually high percentage of positively-charged residues relative to other coactivators. Since these experiments were done, Dr. Nick Foster in the Mapp lab has carried out studies of Med25 in the presence of salts of different composition and

concentrations and found that indeed, activator binding to Med25 is substantively dependent upon electrostatic interactions.

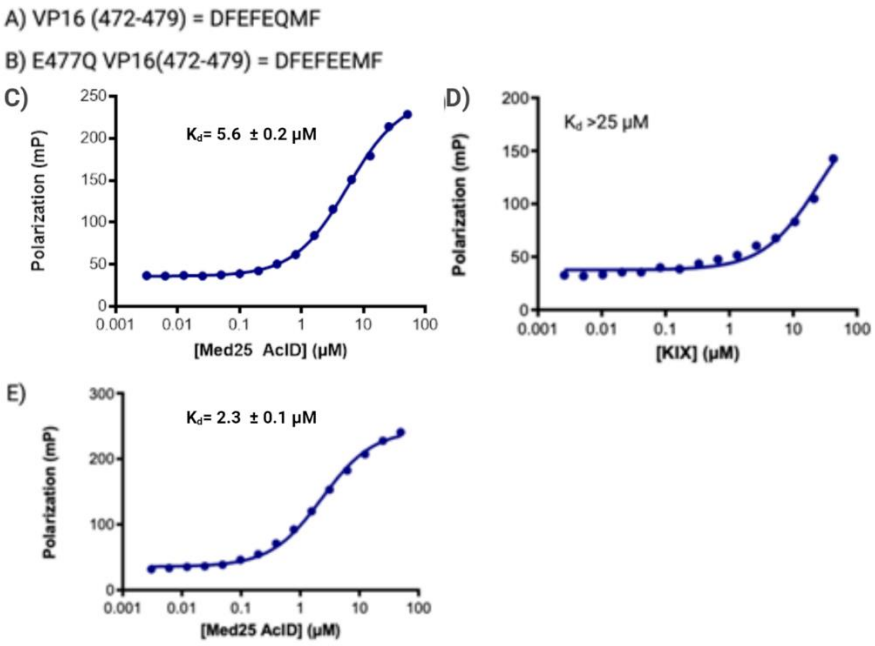

Figure 2.6: Direct binding assays of VP16 ligands to coactivator proteins. A. WT 8- amino acid sequence (VP16 472-479 bind to Med25 AcID with low micromolar affinity. B. Replacing the glutamine with glutamic acid retains low micromolar affinity for Med25 AcID. C. The WT ligand was tested for binding to CBP KIX and the KD could not be determined under the conditions used. The curves were obtained from plotting three the mean of three independently run experiments. The errors represent the standard deviations (Some error bars are smaller than data point symbols).

Further examination of the sequence of VP16 revealed a second 8 residue sequence (441-448) with a very similar sequence to VP16(472-479), termed VN8 in the literature.[22] Additionally, a nearly identical sequence is observed in the activator ATF6α, residues 61-68. We hypothesized that the ATF6α VN8 sequence would function similar to the VP16 sequence and interact with Med25 AcID. To test this, the sequence was synthesized by standard methods and direct binding experiments revealed an affinity of 6.1

± 0.5 µM for Med25 AcID (Figure 2.7). This peptide also showed good selectivity for Med25, with little binding to a coactivator with a similar set of binding partners, the KIX motif of CBP/p300. Thus, this octameric peptide similar seemed like a good starting point for peptidomimetic design.

ATF6α VN8 = DFDLDLMP

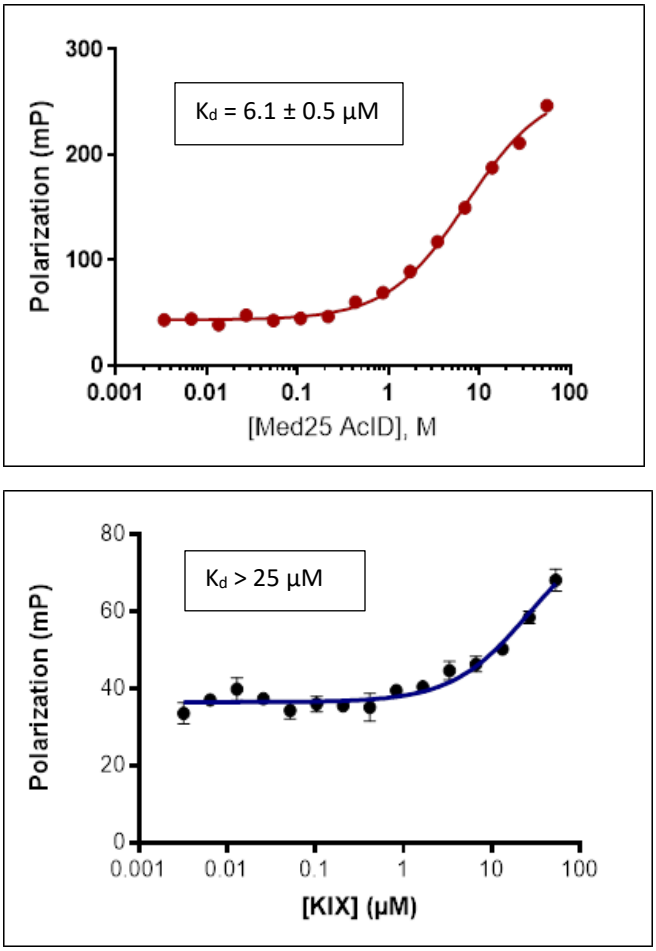

Figure 2.7: ATF6α VN8 Peptide shows selectivity for Med25 AcID. The curves were obtained from plotting the mean of three independently run experiments. The errors represent the standard deviations.

2.4 Conclusions

Med25 AcID is a transcriptional coactivator with a unique structure that nonetheless interacts with its transcriptional activator binding partners through a mechanism similar to that of other coactivators. Prior work and the results in this chapter illustrate that Med25 AcID uses two distinct binding surfaces located on opposite sides of its central β-barrel to interact specifically with different TAD sequences. More specifically, structural and biophysical experiments illustrated that the activators ERM and ATF6α interact with opposing binding surfaces on the β-barrel, the H1 and H2 sites, respectively. Med25 is a potential therapeutic target for breast and prostate cancer and as such, it would be especially useful to be able to target those two sites with synthetic ligands.

Building on previous work done in the Mapp lab, we sought to identify minimal peptide sequences capable of interacting with Med25 that could then be used to design peptidomimetic inhibitors. By truncating the VP16 TAD we identified two different octamer sequences that retain single digit micromolar KDs. And, preliminary data suggests that these sequences have at least modest selectivity for Med25 relative to other coactivators. A similar octamer sequence was found in another Med25 binding partner, ATF6α. Taken together these studies suggest that short peptides are an excellent starting point for the development of Med25 inhibitors, a strategy that is investigated in Chapter 3.

2.5 Materials and Methods

The pET21b-Med25 (394-543)-His_6 plasmid was a generous gift from the Patrick Cramer lab. The mutations were carried out through standard site-directed mutagenesis protocols.

Protein Expression and purifications

Med25 AcID(394-543) was purified by following standard expression protocols. The pET21b-Med25 (394-543)-His6 plasmid was transformed into heat-shock competent Rosetta pLys cells (Novagen) and plated onto LB plates containing ampicillin and chloramphenicol antibiotics then placed in the incubator inverted at 37 °C overnight for approximately 15-16 hours. The plates were then placed at 4 °C until needed. Starter cultures were prepared by pipetting 5 ml of Luria Broth into two disposable culture tubes each followed by 0.1 mg/ml ampicillin and 0.034mg/mL chloramphenicol. Using a sterile pipette tip, a single isolated colony was selected from the transformed plate and placed in each of the culture tubes after which the tubes were placed in an incubator at 37 °C with a rotation speed of 250RPM overnight. The following morning 1-2 mL of the starter culture was placed in 1L autoclaved Terrific Broth along with 0.1mg/mL of ampicillin, then placed in an incubator at 37 °C at 250 RPM and grown to an OD_{600} of 0.8-1.0. The culture was placed in an incubator at 18 °C for at least 30 minutes before the cells were induced with 0.2 mM Isopropylβ-d-1-thiogalactopyranoside (IPTG) and shaken at 200 RPM overnight. The following morning the cells were collected and centrifuged at 6000 x g RPM for 20 minutes at 4 °C. The pellets were collected and placed in 50 mL centrifuge tubes, centrifuged at 2000 RPM for 2 minutes to concentrate the pellet to the tube bottom then stored at -80 °C for later purification.

Med25 AcID was purified using manual protocol involving Ni-NTA resins and an automated protocol Ni-NTA 5mL HiTrap FPLC columns. The collected pellet was suspended in 35 mL lysis

buffer (50 mM phosphate, 300 mM sodium chloride, 10 mM imidazole, pH 7.2) with 35 µL β-mercaptoethanol (1:1000 dilution)and one cOmplete, Mini, EDTA-free Protease Inhibitor tablet (Sigma-Aldrich). The cells were then lysed via sonication on ice for a total of 6 minutes with pulse on for 3 seconds and off for 10 seconds. After the cells were fully lysed, the solution was placed in a 50 mL centrifuge tube and placed in a fixed angle centrifuge rotor to centrifuge at 9500 RPM for 30 minutes at 4 °C. At the completion of the spin cycle, the supernatant was poured into a new 50 mL centrifuge tube then placed back in the centrifuge and spun at 9500 RPM for 10 minutes at 4 °C to further separate large particulates. The supernatant from the second centrifugation was filtered into a clean 50 mL centrifuge tube using 0.45 µm syringe filters and placed on ice.

The supernatant was loaded onto a 5 mL Ni-NTA HiTrap equilibrated with Buffer A/Lysis Buffer (50 mM phosphate, 300 mM sodium chloride, 10 mM imidazole, pH 7.2) on an AKTA pure FPLC chromatography system. The sample was loaded onto the column at a rate of 2.5 mL per minute. The method was created to follow the following sequence: the loaded column was washed with 5 column volumes of Buffer A, then with 5 column volumes of 10% Buffer B (50 mM phosphate, 300 mM sodium chloride, 400 mM imidazole, pH 7.2), followed by a wash with 5 column volumes of 15% Buffer B: 85% Buffer A and finally, elution with a gradient from 15-100% Buffer B. The column was subsequently washed with 5 column volumes of 100% Buffer B.

Following the collection of the fractions, those containing the Med25 AcID protein were collected and combined into a chilled 50 mL centrifuge tube then diluted to 50 mL using chilled (4 °C) Source S buffer A (50 mM phosphate, pH 7.2).

The Med25 AcID protein was further purified using 5 mL Source S HiTrap column using the AKTA pure FPLC chromatography system. The column was equilibrated with Source S buffer A (50mM phosphate, pH 7.2) then the diluted sample was loaded onto the column. Next, the column

was washed with 5 column volumes of Buffer A. Next, the protein was eluted with high concentration of sodium ions as the column was washed with 10 column volumes over a concentration gradient of 0-100% Buffer B (50 mM phosphate, 1M sodium chloride, pH 7.2). The fractions were collected and analyzed via SDS-PAGE using a 12% acrylamide gel. The pure fractions were then combined and 1 mM DTT was added then buffer exchanged in storage buffer (10mM phosphate, 100mM sodium chloride, 10% glycerol, 1 mM DTT, pH 6.8) overnight. The protein was concentrated and stored in 150 µL aliquots at 100-200 µM concentrations at -80 °C. Protein concentrations were determined using UV-Vis spectroscopy with the extinction coefficient, ε = 22550 $M^{-1}cm^{-1}$ and mass confirmation was carried out by electrospray mass spectrometry.

Site-Directed Mutagenesis

Primers used for site-directed mutagenesis

Plasmid	Primer Sequence
pET21b-Med25(394-543)K411E-His6	F: CTGGAGTGGCAAGAGGAGCCCAAACCTGCCTCA R: TGAGGCAGGTTTGGGCTCCTCTTGCCACTCCAG
pET21b-Med25(394-543)R538E-His6	F:GGCTTCGTCAACGGCATCGAACAGGTCATCACCAACCTC R:GAGGTTGGTGATGACCTGTTCGATGCCGTTGACGAAGCC
pET21b-Med25(394-543)Q451E-His6	F: CCAGAAGCTGATCATGGAACTCATCCCCCAGCAG R: CTGCTGGGGGATGAGTTCCATGATCAGCTTCTGG
pET21b-Med25(394-543)R466D-His6	F: CTGGACCATCCTTGAGTTATCGAACAAAGGGCCCAG R: CTGGGCCCTTTGTTCGATAACTCAAGGATGGTCCAG

pET21b-Med25(394-543)M523E-His6	F: AAGAAGAAGATCTTCGAAGGCCTCATCCCCTA R: TAGGGGATGAGGCCTTCGAAGATCTTCTTCTT
pET21b-Med25(394-543)M523R-His6	F:TCGTCCAAGAAGAAGATCTTCCGGGGCCTCATCCCCTACGACCAG R:CTGGTCGTAGGG GATGAGGCCCCGGAAGATCTTCTTCTTGGACGA

Peptide Synthesis

Peptide synthesis was carried out using conventional solid phase peptide synthesis and microwave assisted peptide synthesis (CEM Liberty Blue).

Peptides were synthesized on 50 µmole scale using CEM rink-amide resin (0.19-0.21 meq). The synthesis was carried out with dimethylformamide as the main solvent. Fmoc-amino acid concentrations were made to be 0.2M, deprotection solution was made up containing 20% piperidine, 0.2M Oxyma Pure. Diisopropylcarbodiimide (DIC) was the activator acid and Oxyma Pure was the activator base. The amino acids were coupled using 4-minute single coupling for peptide sequences shorter than 20 amino acids. The peptides were cleaved with 95% TFA:2.5% TIPS: 2.5% H_2O. Excess cleavage cocktail was evaporated using nitrogen gas flow. The resulting solution was treated with cold diethyl ether then centrifuged to collect the peptide precipitate. The ether was decanted, and the pellet was redissolved in 30% 0.1% TFA/H_2O and acetonitrile and lyophilized before purification. Peptides were redissolved in minimal acetonitrile (25%) and 0.1% TFA/H_2O solution and purified using reverse-phase HPLC (Agilent) with C-18 columns and 0.1%TFA/H_2O-acetonitrile solvent system. The purified fractions were collected and analyzed using mass spectrometry. These pure fractions were combined after identifying through mass spectrometry and lyophilized until a dry powder was left.

Manual Peptide Synthesis

Peptides were synthesized using CLEAR amide resin (Peptide International) or rink amide resin (CEM). Manual synthesis reagents for CLEAR rink amide resin were HOBT, HBTU and DIPEA and that for CEM rink amide was DIC and HOBT. The first amino acids were coupled for a minimum of six hours followed by 2 hours of amino acid coupling up to the 10^{th} residue and subsequently 2.5 hours beyond 10 residues. After the completion of the sequence, the N-terminus was deprotected. For fluorescein labeling, beta alanine was coupled to the N-terminus and then 2 eq fluorescein isothiocyanate was coupled in the presence of 4 eq DIPEA. The N-terminus was acetylated for unlabeled peptide using 50 eq acetic anhydride and 50 eq DIPEA.

The peptides were cleaved with 95% TFA:2.5% TIPS: 2.5% H_2O. Excess cleavage cocktail was evaporated using nitrogen gas flow. The resulting solution was treated with cold diethyl ether then centrifuged to collect the peptide precipitate. The ether was decanted, and the pellet was redissolved in 30% 0.1% TFA/H_2O and acetonitrile and lyophilized before purification. Peptides were redissolved in minimal acetonitrile (25%) and 0.1% TFA/H_2O solution and purified using reverse-phase HPLC (Agilent) with C-18 columns and 0.1%TFA/H_2O-acetonitrile solvent system. The purified fractions were collected and analyzed using mass spectrometry. These pure fractions were combined after identifying through mass spectrometry and lyophilized until a dry powder was left.

The peptide was dissolved in DMSO. A sample of the DMSO was diluted 1:1000 in storage buffer to ascertain the concentration. Using UV-Vis, the concentration was measured at λ=495 nm for the FITC and an extinction coefficient, ε=72,000 $M^{-1}cm^{-1}$. Unlabeled peptides were weighed, and concentration determined.

Fluorescence Polarization

Fluorescence polarization direct binding assays were done in triplicate with a final volume of 20 µL in a low volume, non-binding, 384-well black plate (Corning). Fluorescein-labeled DMSO peptide stocks were diluted to 50 nM using assay buffer (5 mM HNa_2PO_4, 5 mM NaH_2PO_4, 100 mM sodium chloride, 10 % glycerol, pH 6.8). 10 µL of Med25 AcID was serially diluted two-fold going down the column of the 384-well plate using the assay buffer (10 µL assay buffer was placed in each well). No protein was added to the last row as it was a negative control with peptide only. Finally, 10 µL of peptide was added to each well to provide a final peptide concentration of 25 nM and the resulting mixtures left to incubate at room temperature for 30 minutes. After 30 minutes, the fluorescence polarization was measured using Tecan Genios Pro or PHERAstar plate reader (polarized excitation at 485 nm and emission intensity measured through a parallel and perpendicularly polarized 535 nm filter). Data was analyzed by binding isotherm that accounts for liganddepletion (assuming a 1:1 binding model of peptide to ACID) was fit to the observed

polarization values as a function of AcID to obtain the equilibrium dissociation,

Kd. Each data point is an average of the triplicate experiments from each peptide with Med25 AcID and the error for standard deviation. “a” and “x” are the total concentrations of fluorescent peptide and Acid, respectively, “y” is the observed anisotropy at a given AcID concentration, “b” is the maximum observed anisotropy value, and “c” is the minimum observed anisotropy value.

$$y = c + (b - c)\, X\, \frac{(K_D + a + x) - [\sqrt{(K_D + a + x)^2 - 4ax}]}{2a}$$

Fold change = $\frac{K_D \text{ for Mutant Med25 AcID}-\text{peptide interaction}}{K_{D\ for\ WT\ Med25\ AcID-peptide\ interaction}}$

$$\text{Fold Change} = \frac{K_D \text{ for Med25 AcID}-\text{minimal peptide interaction}}{\text{K}_{\text{D for Med25 AcID}-\text{full}-\text{length peptide interaction}}}$$

^{1}H, ^{15}N-HSQC NMR analysis of Med25 AcID-peptide

Purified ^{15}N- labeled Med25 AcID protein was complexed with purified N-acetylated peptides at varying equivalents. The experiments were carried out using a Bruker Advanced III 600 MHz spectrophotometer equipped with a cryogeneic probe at 30 °C. The varying titrations were done using Med25 AcID stored in ^{15}N-Med25 storage buffer (20 mM sodium phosphate, 150 mM sodium chloride, 5% D_2O, pH 6.5) with a final concentration of 73 µM. Acetylated peptides were added at 0, 0.2, 0.5, 0.8, 1.1, 2 and 3 equivalents and 2% final DMSO concentration. Our control sample was with Med25 and DMSO only. Two stocks of each peptides were prepared at concentrations of 2.5 and 25 mM. To keep the DMSO concentration at 2%, the 2.5 mM stock was used for 0.2, 0.5 and 0.8 equivalents samples and the 25 mM stock was used for the 1.1, 2 and 3 equivalents. Data processing and visualization was performed using NMR pipe and Sparky.

Circular Dichroism

Circular Dichroism (CD) spectra of Med25 was obtained using J-715 spectropolarimeter (Jasco Inc) using a 1mm path length quartz cuvette. The Med25 protien was dialyzed overnight into CD buffer (5mM NaH_2PO_4, 5mM Na_2HPO_4, 100 mM NaF, pH 6.8). The spectra was measured from 260-180 nm at 1 nm increments at 200 nm/minute. A baseline spectra was obtained using CD buffer only followed by measurement of Med25 AcID at 25 µM. The background spectra was subtracted from that of the protein before converting to mean residue ellipticity, θ using the following equation, where ψ = is the cd signal in degrees, n is the number of residues, l is the path length on centimeters and c is the concentration of the protein/peptide decimoles per cm^3.

$$[\theta] = \frac{\psi}{1000 * n * l * c}$$

Circular Dichroism-Observed Thermal Melt

After the CD spectra were collected, a CD-observed thermal melt spectrum was collected using without changing the buffer mentioned above. This was done using the variable temperature module. The protein was heated from 20- 100 °C by increasing the temperature at 1°C per minute. The spectrum was monitored at 222 and 208 nm. The data was collected using every two degrees throughout the interval. The data was then converted to Fraction unfolded and Tm was determined using the Prism's log '(inhibitor vs response – variable slope)' equation.

2.6 References

1. Mapp, A. K., Pricer, R. & Sturlis, S. Targeting transcription is no longer a quixotic quest. *Nature Chemical Biology* **11**, 891–894 (2015).
2. Vojnic, E., Mourao, A., Seizl & Wenzeck, L. Structure and VP16 binding of the Mediator Med25 activator interaction domain. *Nature Structural & Molecular Biology* **18**, 404-U429 (2011).
3. Milbradt, A. G., Kulkarni, M. & Yi, T. Structure of the VP16 transactivator target in the Mediator. *Nature Structural & Molecular Biology* **18**, 410–415 (2011).
4. Bontems, F., Verger, A. & Dewitte, F. NMR structure of the human mediator MED25 ACID domain. *J Struct Biol* **174**, 245–251 (2011).
5. Sela, D., Conkright, J. & Chen, L. Role for human mediator subunit MED25 in recruitment of mediator to promoters by endoplasmic reticulum stress-responsive transcription factor ATF6α. *J Biol Chem* **288**, 26179–26187 (2013).
6. Verger, A., Baert, J.-L. & Verreman, K. The Mediator complex subunit MED25 is targeted by the N-terminal transactivation domain of the PEA3 group member. *Nucleic Acids Research* **41**, 4847–4859 (2013).
7. Landrieu, I., Verger, A. & Baert, J.-L. Characterization of ERM transactivation domain binding to the ACID/PTOV domain of the Mediator subunit MED25. *Nucleic Acids Research* **43**, 7110–7121 (2015).
8. Henley, M., Linhares, B. & Morgan, B. Unexpected specificity within dynamic transcriptional protein–protein complexes. *Proc. Natl. Acad. Sci.* **44**, 27346–27353 (2020).
9. Cress, W. D. & Triezenberg, S. Critical structural elements of the VP16 transcriptional activation domain. *Science* **251**, 87–90 (1991).

10. Ikeda, K., Stuehler, T. & Meisterenst, M. The H1 and H2 regions of the activation domain of herpes simplex virion protein 16 stimulate transcription through distinct molecular mechanisms. Genes Cells 7, 49–58 (2002). *Genes Cells* **7**, 49–58 (2002).
11. Hirai, H., Tani, T. & Kikyo, N. Structure and functions of powerful transactivators: VP16, MyoD and FoxA. *Int J Dev Biol* **54**, 1589–1596 (2010).
12. Dyson, H. J. & Wright, P. E. Role of intrinsic protein disorder in the function and interactions of the transcriptional coactivators CREB-binding protein (CBP) and p300. *J Biol Chem* **291**, 6714–6722 (2016).
13. Ansari, A. Z., Mapp, A. K. & Nguyen, D. H. Towards a minimal motif for artificial transcriptional activators. *Chem Biol* **8**, 583–592 (2001).
14. Mapp, A. K., Ansari, A. Z. & Ptashne, M. Activation of gene expression by small molecule transcription factors. *Proc. Natl. Acad. Sci.* **97**, 3930–3935 (2000).
15. Seipel, K., Georgiev, O. & Schaffner, W. A Minimal Transcription Activation Domain Consisting of a Specific Array of Aspartic Acid and Leucine Residues. *Biol. Chem.* **375**, 463–470 (1994).
16. Frangioni, J., LaRiccia, L. & Cantley, L. Minimal activators that bind to the KIX domain of p300/CBP identified by phage display screening. *Nature Biotechnology* **18**, 1080–1085 (2000).
17. Piskacek, S., Gregor, M. & Nemethova, M. Nine-amino-acid transactivation domain:Establishment and prediction utilities. *Genomics* **89**, 756–768 (2007).
18. Rowe, S. & Mapp, A. K. Assessing the Permissiveness of Transcriptional Activator Binding Sites. *Biopolymers* **89**, 578–581 (2008).

19. Parker, D., Rivera, M. & Zor, T. Role of Secondary Structure in Discrimination between Constitutive and Inducible Activators. *Molecular and Cellular Biology* **19**, 5601–5607 (1999).
20. Henderson, A., Henley, M. & Foster, N. Conservation of coactivator engagement mechanism enables small-molecule allosteric modulators. **115**, 8960–8965 (2018).
21. Sturlis, S. Targeting the Activator Interaction Domain of Mediator Subunit Med25. (Univeristy of Michigan, 2016).
22. Tanaka, M. Modulation of promoter occupancy by cooperative DNA/binding and activation-domain function is a major determinant of transcriptional regulation by activators in vivo. *Proc. Natl. Acad. Sci.* **93**, 4311–4315 (1996).
23. Wu, Y., Reece, J. & Ptashne, M. Quantitation of putative activator-target affinities predicts transcriptional activating potentials. *EMBO J* **15**, 3951–3963 (1996).
24. Piskacek, M., Havelka, M. & Rezacova, M. The 9aaTAD Is Exclusive Activation Domain in Gal4. *PLos One* **12**, (2007).

Chapter 3

Peptoid Transcription Factor Mimics Interact with Med25 and Are Cell Penetrant

3.1 Abstract

Targeting activator-coactivator interfaces has been a challenge in part due to the structurally dynamic nature of the complexes. Additionally, the binding interface is typically large and thus small molecules ligands have shown little success. Alternatively, peptoids have been used as an effective synthetic tool to mimic and modulate protein-protein interactions. Most notable is their ability to mimic peptides and capability of covering larger surface areas. In this Chapter, we demonstrate that peptoids based upon the minimal activator sequences identified in Chapter 2 have similar affinity for Med25 as do the native binding partners. The affinity can be enhanced by incorporating additional activator sequences. We tested the hypothesis that a helical peptoid would exhibit further affinity enhancement and, unexpectedly, found that this did not increase the potency. Additionally, we were also able to modify the peptoids to improve the efficiency of transportation across the plasma membrane. Thus, the peptoids Med25 ligands developed here will be useful tools for mechanistic studies of the Med25 PPI network.

3.2 Introduction

It has been established that transcription regulation is essential for the successful conversion of genetic information to proteins, and that dysregulation of this process can result in disease.[1–5]

Although the protein-protein interactions (PPIs) involved in the assembly of the transcriptional machine are thus attractive therapeutic targets, the characteristics of these proteins render them difficult to target with ligands; these characteristics include the large surface areas of the proteins, the transient nature of these interactions, the weak to moderate affinities for binding to partners, and the lack of high resolution structural information due to the disordered nature of the binding partners. All these characteristics have led to many activator-coactivator interactions being labeled as "undruggable." Consistent with the above characterization, multiple strategies have been employed in targeting activator-coactivator interactions with small-molecules and yet have not yielded much success. Coactivator complex formation requires more points of contact than can easily be recapitulated with small molecules.

An excellent example of an important yet challenging coactivator is the focus of this work, Med25 (Figure 1.1). Within Med25 is the Activator-Interaction Domain (AcID) that forms protein-protein interactions with several activators, including VP16, the ETV/PEA3 activators, and ATF6α. The AcID PPI network is dysregulated in a number of cancers either through upregulation of Med25 or through upregulation of the binding partners. For example, the Merajver lab at the University of Michigan has found several examples of triple-negative breast cancers with significant upregulation of Med25 and in our group's collaborative work with them, genetic or pharmacological inhibition of Med25 decreases cell motility as well as markers of metastasis.[6–8] There has thus been great interest in identifying small molecule ligands of Med25 but the 900 $Å^2$ binding surfaces have been a nearly insurmountable barrier.

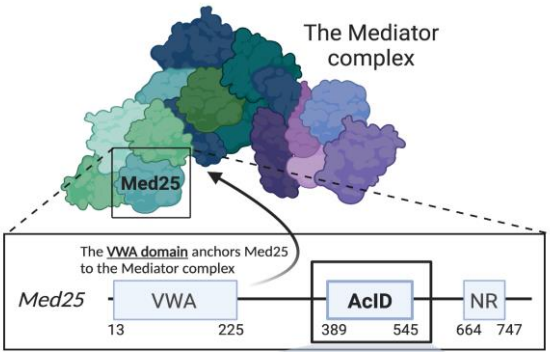

Figure 3.1 The coactivator Med25 has three domains: a VWA domain that interacts with the Mediator complex, the Activator Interaction Domain (AcID) that forms PPIs with transcriptional activators and coactivators, and the Nuclear Receptor (NR) motif that is an interaction site for several nuclear receptors. Figure adapted from doi: https://doi.org/10.1101/2021.03.26.437253 and created by Amanda Peiffer.

An alternative to small molecules is the use of peptidomimetics. In particular, N-substituted glycine oligomers or peptoids have been proven to be potent ligands of a number of different challenging PPI interfaces.[9–11] Peptoids are suitable for interacting with larger surface areas because structures as long as 48 monomers can be synthesized in a machine-assisted fashion, with each monomer containing a functional group that can potentially interact with the target. Another key property of peptoids is the ease with which diverse side chains can be introduced into the structures. Thus, functional groups that are identified in fragment screenings or other target studies can be readily incorporated into the larger structure of a peptoid.[12–14] Further, incorporation of chiral side chains into the oligomer induces helicity to the structure, thus enhancing affinity in cases where the preferred binding conformation is a helix.[15] Finally, this class of peptidomimetic is resistant to proteolytic degradation due its non-native amide backbone.[16]

Consistent with the above description, there are examples of successful targeting of coactivators and other transcriptional proteins with peptoids. For example, our group has successfully identified peptoids based upon the sequence of synthetic peptides discovered by Montminy that demonstrated improved binding to the GACKIX domain of CBP by ~6-fold (Figure 3.2).[17–19] This

suggests that the conformational flexibility of peptoids could be advantageous for interacting with dynamic protein surfaces.

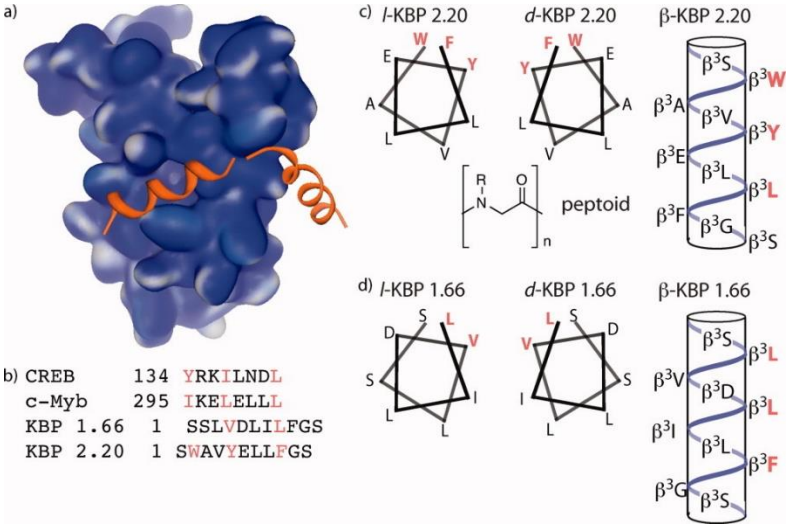

Figure 3.2 Peptoid improve binding to KIX. Previous work from the Mapp lab showed that peptoid variants of peptide ligands for the KIX motif of CBP/p300 showed improved binding. a) Illustration of KIX bound to a native partner, CREB. b) Sequences of natural transcriptional activators (CREB, cMyb) and non-natural ligands (KBP 1.66, 2.20) that bind to KIX. c,d) Schematic of peptidomimetic variants of the KBP 1.66 and KBP 2.20. Figure adapted from *Biopolymers*, Volume: 89, Issue: 7, Pages: 578-581, DOI: (10.1002/bip.20946)

In Chapter 2 I demonstrated that peptides as short as 8 residues derived from native transcriptional activators were sufficient to complex to Med25. In this Chapter, I test the hypothesis that peptoid variants of these sequences will interact with Med25 AcID and in doing so serve as ligands for future mechanistic studies. I identify an effective and stable Med25 ligand that will be an important tool for dissecting the Med25 PPI network in future studies.

3.3 Results and Discussion

As shown in the data of Chapter 2, I identified two octamer peptides derived from the Med25-dependent activators VP16 and ATF6a that retain low micromolar affinity for Med25 (Table 1). These octamers thus served as the starting point for peptoid ligand design.

Peptide name	**Sequence**	**K_D for Med25**
VP16(472-479)	DFEFEQMF	8 ± 1 μM
ATF6α VN8	DFDLDLMP	6.1 ± 0.5 μM

Table 3.1: Octamer peptides interact with Med25 AcID with low micromolar affinity

The sequence of VP16(472-479) can be mapped onto a peptoid backbone in a straightforward fashion (Figure 3.2), as it simply requires moving the amino acid side chain in the peptide to the adjacent amine. This produces an achiral amide polymer that can be readily synthesized by solid phase synthesis. Each monomer is constructed on the resin, via coupling of bromoacetic acid to the growing peptoid chain followed by addition of a primary amine bearing the relevant side chain that is suitably protected. There are constraints presented by this synthetic strategy, however, as some functional groups are incompatible with the synthetic procedure, either due to reactivity issues (methionine, asparagine/glutamine) or due to solubility challenges.[20] To address this in my peptoid design methionine was replaced with a simple hydrophobic side chain and the glutamine residue was replaced with glutamic acid. In the latter case, this particular change was found to enhance binding affinity of the peptide (Chapter 2, Figure 2.6). Peptoid **1** was synthesized on an

automated peptide synthesizer and was purified by HPLC. The identity and purity were verified by mass spectrometry and by analytical HPLC analysis.

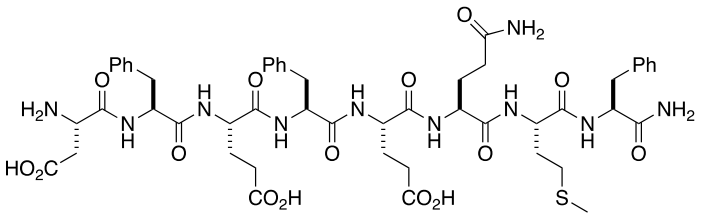

VP16(472-479)

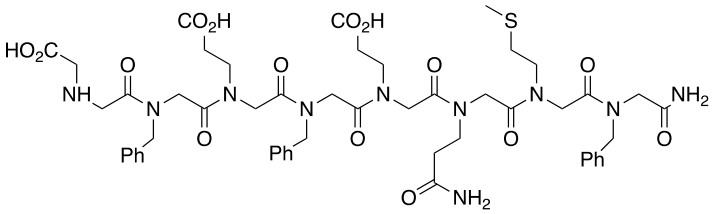

Peptoid VP16(472-479)

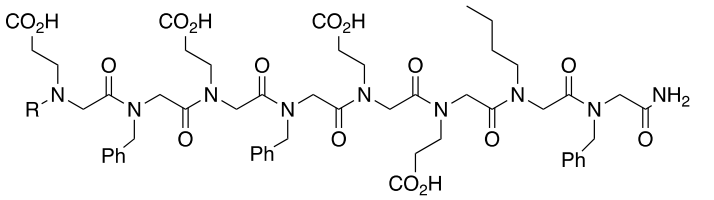

Peptoid **1**

Figure 3.3: VP16(472-479) minimal peptide sequence. The peptoids were designed by substituting amines that mimic the side chains of the corresponding amino acids. Methionine replaced by norleucine mimic (norleucine commonly replaces methionine to avoid oxidation).

Following synthesis and isolation of peptoid **1**, the structure of the peptoid in solution was assessed using circular dichroism at 25 °C. The molar residual ellipticity was measured from 260-185 nm with 5 scans that were averaged and mean residual ellipticity was calculated from the measured ellipticity observed in millidegrees. As expected with an achiral peptoid, a net mean residual ellipticity of zero was observed.

The affinity of peptoid **1** for Med25 AcID was measured using fluorescence polarization. To accomplish this, peptoid **1** was labeled at the amino terminus with fluorescein isothiocyanate for use in binding assays. Following standard protocols, the K_D was determined to be 6.7 ± 0.2 μM (Figure 3.3). This demonstrates peptoid peptidomimetics can successfully recapitulate binding of even a minimal transcriptional activator, despite lacking the backbone hydrogen bonding network that even in short peptides facilitates secondary structure formation upon binding. The data further suggest that this is a lead compound that can be modified improve affinity for Med25 and ultimately inhibitor potency.

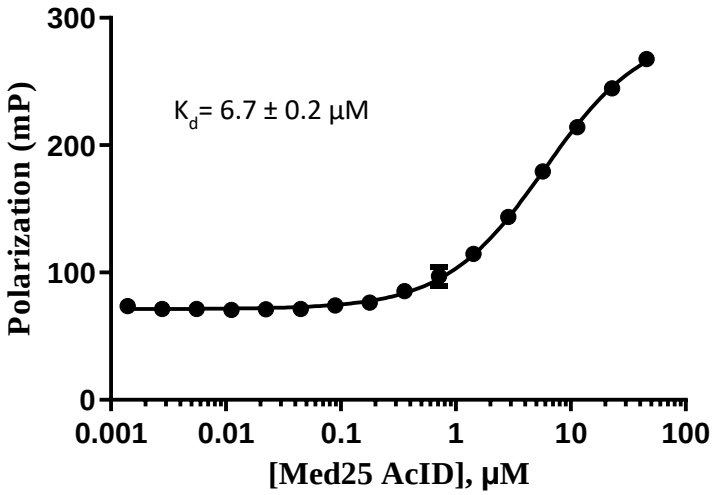

Figure 3.4 Results from a fluorescence polarization assay of peptoid **1** in the presence of increasing concentrations of Med25 AcID. The curve represents the mean of three independent experiments ran in triplicate with the error representing the standard deviation.

3.3A Inducing Secondary Structure by Introducing Chirality

Next, I tested the hypothesis that a helical peptoid would have improved affinity for Med25. We sought to induce helical structure of the peptoid by incorporating structural elements that have

induced helical conformation in peptoids.[21,22] It has been established that TADs remain largely unstructured in free solution; however, upon binding to their coactivators they adopt an α-helical conformation.[15,23] By extension, amines with aromatic α-chiral side chains have been demonstrated to successfully induce helical conformations in peptoids by forming polyproline-like helices. As a result of this, we substituted the aromatic achiral side chain, benzylamine, with (S)-(-)-α-methylbenzylamine to mimic an L-amino acid. To mimic a peptide constructed of D-amino acids, we introduced (R)-(+)-α-methylbenzylamine (Figure 3.4). The secondary structure of both peptoids was measured using circular dichroism and the mean residual ellipticity confirms a secondary structure profile that matches that of the enantiomer of the L-peptidomimetic, which would be the mimic of the D-peptide (Figure 3.5).

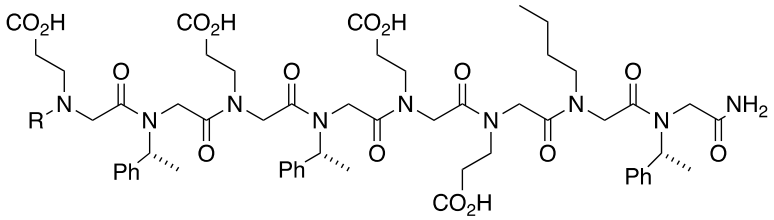

Peptoid **2a**

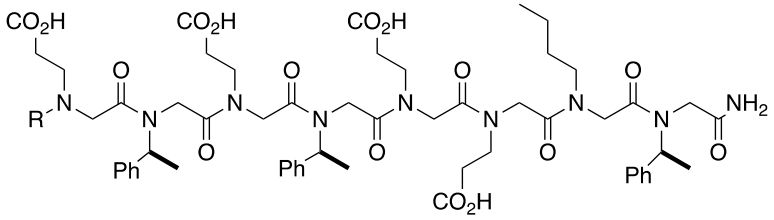

Peptoid **2b**

Figure 3.5: Structures of chiral versions of peptoid **1**. (S)- (-)-α-methylbenzylamine (Nspe) and (R)- (+)-α-methylbenzylamine (Nrpe) replaced the achiral benzylamine.

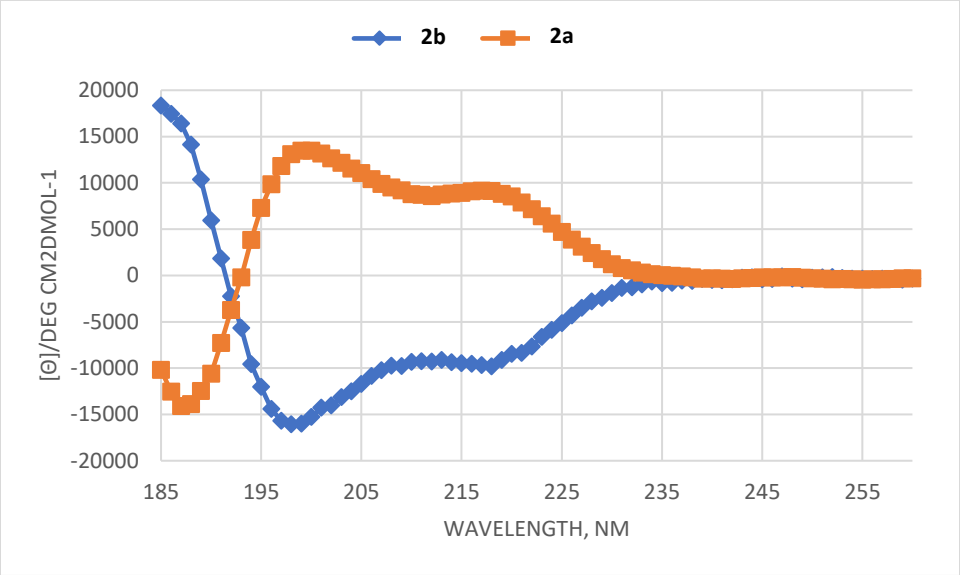

Figure 3.6: CD spectra of peptoids. Induced secondary peptoid structure for peptoids **2a** (orange) and **2b** (blue**)**. Mean residue ellipticity measured using circular dichroism of peptoids with (R)- or (S)- monomers**.**

The affinities of the chiral peptoids were measured using fluorescence polarization assays. The conditions mentioned above were used to set up the experiments using these modified compounds. Peptoids **2a** and **2b** were shown to be 10 ± 1 μM for both, indicating that the stereochemistry of peptoids does not strongly affect the interaction with Med25. It is not surprising that the enantiomers show similar binding, as this has been shown with transcriptional activator peptides in several cases. It is, however, the first demonstration with a peptoid. It was somewhat unexpected that the helical peptoids bound essentially identically to the parent, unstructured peptoid, since the parent peptide is predicted to become helical upon binding to Med25.

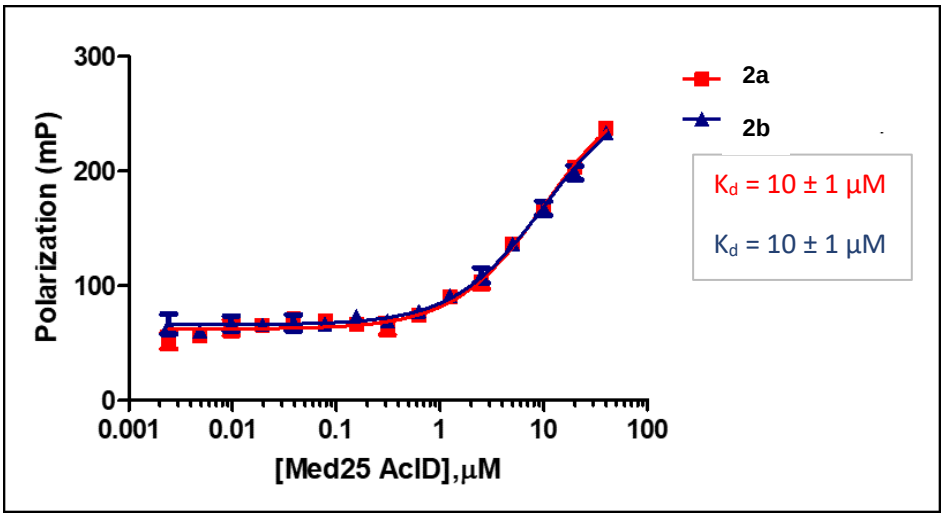

Figure 3.7: Fluorescence polarization assay. Enantiomeric peptoids containing chiral aromatic monomers show identical affinity for Med25 AcID.

From the information garnered from the VP16(472-479)-derived peptoids, I concluded that octamer peptoids are sufficient for moderate binding to Med25 and began to investigate if other octamer sequences such as ATF6α VN8 (Table 1), would show similar or even better affinity. I designed a peptoid based upon the ATF6α VN8 peptide, illustrated in Figure 3.8.

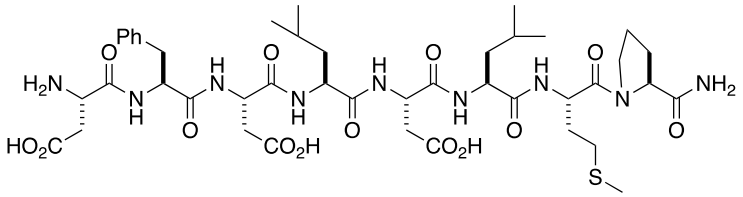

ATF6α VN8

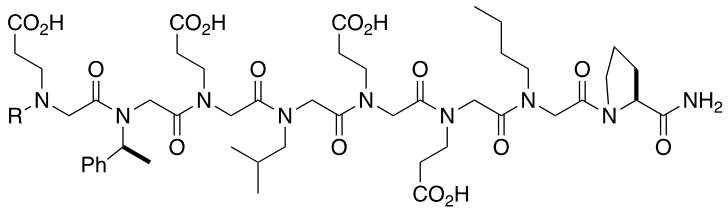

Peptoid **3**

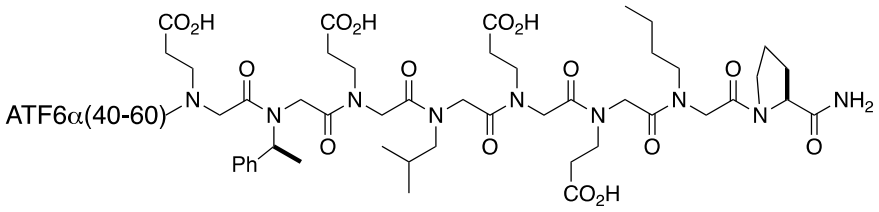

Peptoid **4**

Figure 3.8 Structures of ATF6α (61-68), also known as VN8 as well as two peptoids derived from that sequence. Note that peptoid **4** is a peptide-peptoid hybrid.

The peptide ATF6α VN8 was synthesized and tested against Med25 AcID for affinity and, as originally shown in Chapter 2, the resulting dissociation constant is 6 μM (Figure 3.9). Following this, the peptoid **3** was synthesized using (S)-(-)-α-methylbenzylamine as the mimic for the monomer phenylalanine. Upon completion and assessment of the net mean residual ellipticity, the peptoid were labeled at the amino terminus with fluorescein and the affinity for Med25 AcID was measured using fluorescent polarization. As shown in Figure 3.9, peptoid **3** had significantly attenuated affinity relative to the parent peptide (>10-fold decrease). However, the peptoid did

retain selectivity for Med25 AcID, (2-fold). For this reason, the focus on ATF6α-derived peptoids continued, with the goal of increasing the affinity while retaining or improving the selectivity.

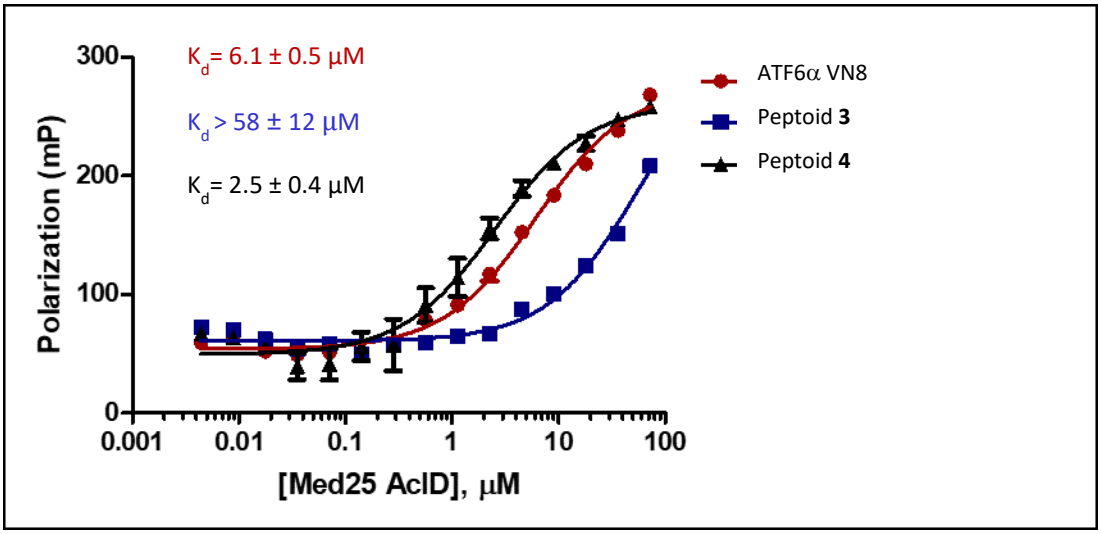

Figure 3.9: VN8-Med25 AcID direct binding. Results of direct binding experiments with fluorescein-tagged variants of ATF6α VN8, peptoid **3,** and ATF6α (40-60). Three independent experiments were done in triplicate with curves representing the mean. The errors represent the standard deviation.

3.3B Increasing the Peptoid length Improves the Binding Affinity for Med25 AcID

As shown above, octamer peptoids can display good (<10 µM) affinity for Med25. However, peptoid **3** displayed modest affinity for the target and it was necessary to improve this, particularly for cellular studies. One established strategy for increasing affinity of peptoids is the appendage of short peptide sequences to the peptoid core. In our case, ATF6α (40-60) was added to peptoid **3** to create peptoid **4** (Figure 3.8). The resulting peptoid-peptide hybrid showed a much-improved binding to Med25 AcID (K_d of 3 µM). This is not solely due to the intrinsic affinity of the peptide portion of the hybrid, as ATF6α(40-60) peptide (Figure 3.11) has a 12 mM affinity for Med25 AcID.

Given the results of the peptide-peptoid hybrid **4**, I synthesized and tested a wide range of peptoids and peptoid-peptide hybrids that incorporated additional components of the ATF6α transcriptional activation domain (Figure 3.10).

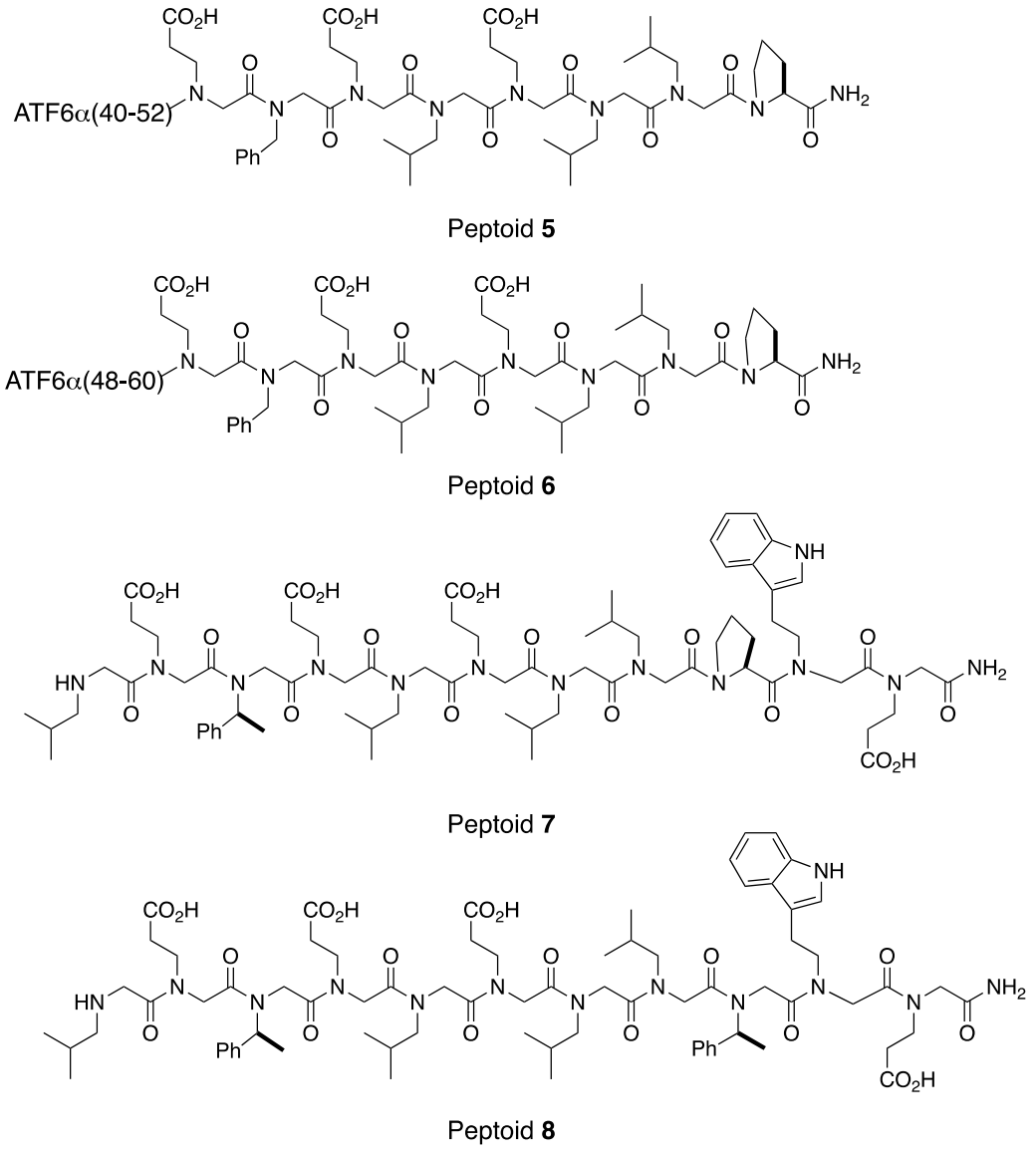

Figure 3.10. Peptoids and peptide-peptoid hybrids. ATF6α-derived peptoids and peptide-peptoid hybrids designed to increase the affinity and maintain selectivity for the target Med25.

All of the peptide-peptoid hybrids and peptoids were labelled with fluorescein and assessed in direct binding assays with Med25 AcID. Hybrids **5** and **6** differed in affinity two-fold. A third hybrid tested was the ATF6α(40-60) sequence in which the alanine residues at positions 48 and 48 were replaced with N-methyl glycine (labeled ATF6α(40-60)* in the figure). However, the affinity was unchanged from the peptide alone.

Most interesting were the results from peptoids **7** and **8**, which show improved binding compared to peptoids **5**, **6** and ATF6α 40-60* (alanine replaced with N-methyl glycine) despite being shorter sequences. The peptoid based upon ATF6α (60-70) (peptoid **7**) is shorter than the hybrid and peptide sequences but showed a significantly improved affinity of 7.7 μM. Replacement of the proline with a chiral phenylalanine mimic in peptoid **8** further increased the affinity to 3.6 μM.

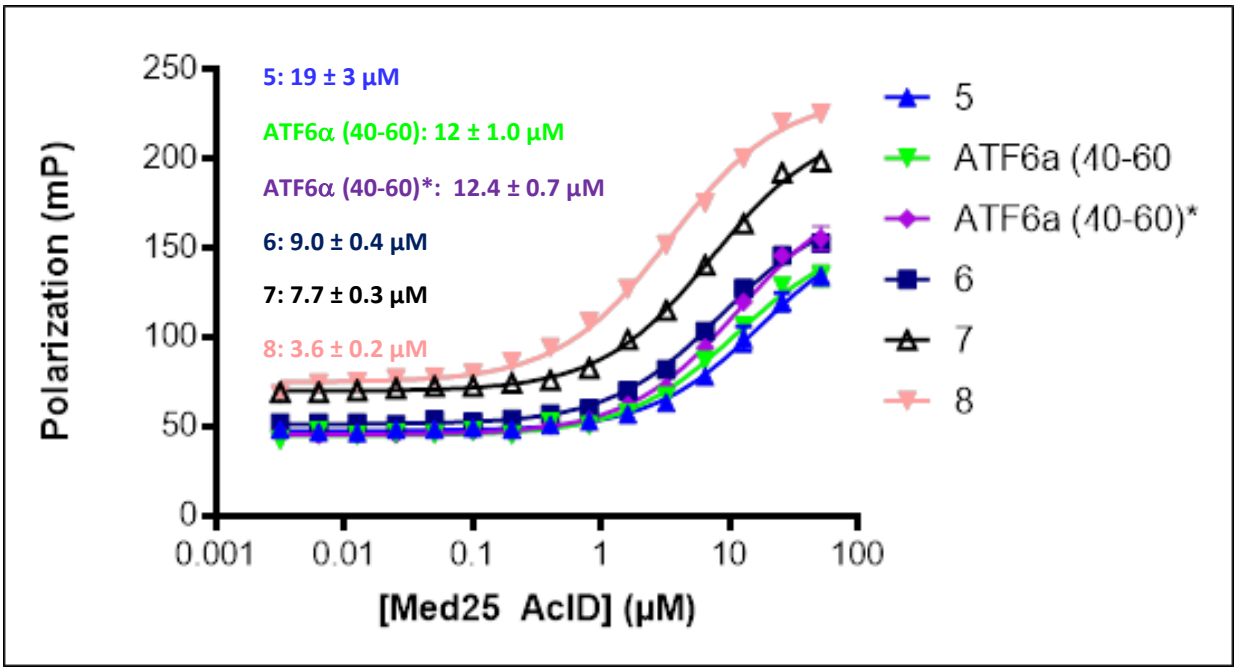

Figure 3.11: Results of direct binding experiments with fluorescein-tagged variants of ATF6α with Med25 AcID. Three independent experiments were done in triplicate with curves representing the mean. The errors represent the standard deviation.

As noted earlier, one of the key questions was if the peptoid ligands could maintain selectivity for Med25 AcID over other coactivators. To test this, the affinity of each were measured for a coactivator with a similar binding profile, the KIX domain of CBP/p300 (Figure 3.12). These experiments revealed that lead peptoid **8** shows nearly five-fold selectivity for Med25 AcID, an excellent selectivity window.

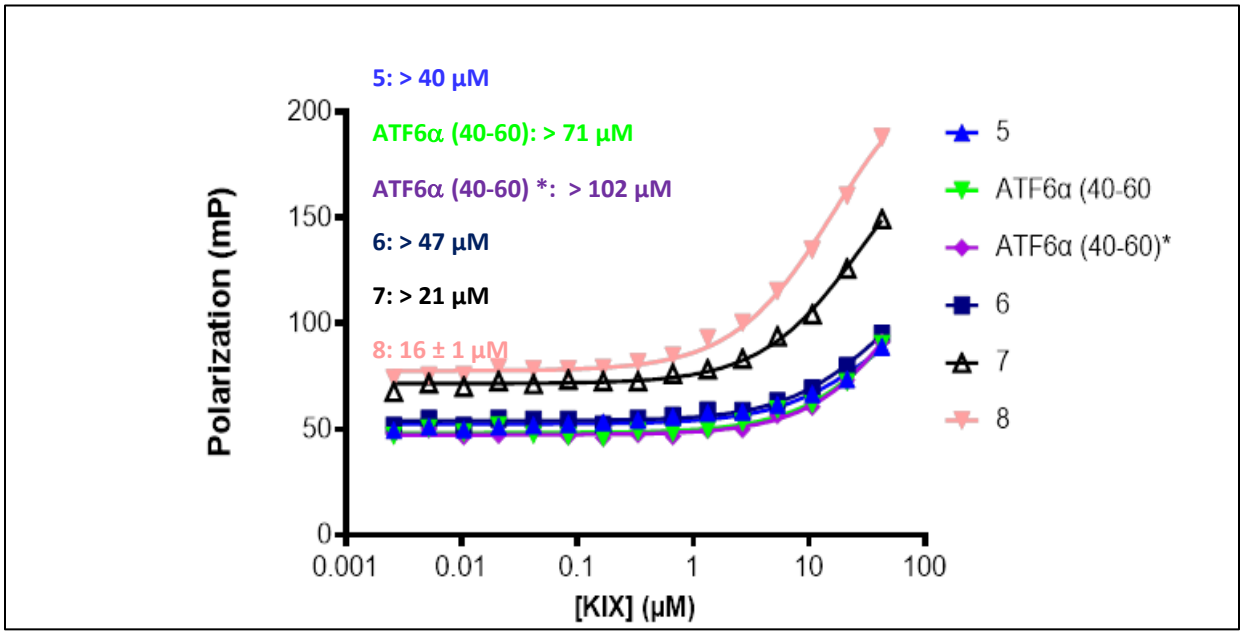

Figure 3.12 Results of direct binding experiments with fluorescein-tagged variants of ATF6α with CBP KIX. Three independent experiments were done in triplicate with curves representing the mean. The errors represent the standard deviation.

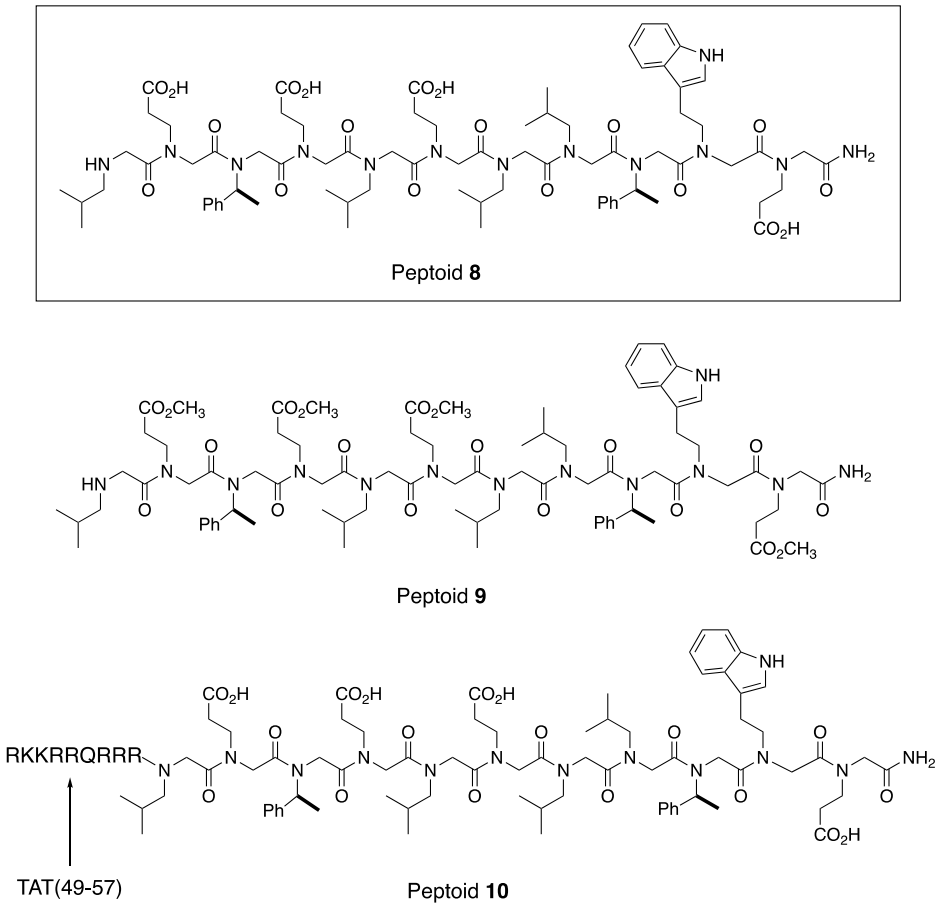

Figure 3.13: Peptoids modified to improve permeability.

3.3C Permeability

From the direct binding studies above, peptoid **8** was shown to have a good affinity for Med25 AcID and good selectivity relative to CBP KIX. With this promising result, we sought to modify the structure so that it would be transported across the plasma membrane for delivery. Earlier studies have identified the HIV-TAT sequence as an effective cell penetrating peptide (CPP) and has been used to delivery cargo to cells.[24–28] CPPs are generally short to moderately long sequences with positively charged amino acid repeats. This aids in their ability to travel across the plasma membrane with little to no resistance. HIV-1 $TAT_{49\text{-}57}$ has shown to aid in cell penetration by

keeping the structure to a minimum of 9 residues.[29] Appending the TAT to a net negatively charged sequence converts the structure to a net positively charged molecule, increasing the probability of transportation across the negatively charged membrane. For the TAT-containing peptoid **10**, fluorescein was added to the N-terminus of the TAT sequence to allow for visualization of the molecule in cell-penetration studies. In parallel a second strategy was explored with peptoid **9**, one in which the carboxylic acid side chains were masked as methyl esters expected to be hydrolyzed intracellularly.[30] To complete the design of the molecule I selected TAMRA as the fluorophore due to its neutrally charged state.

In collaboration with colleague Yejun Liu, the permeability of peptoids **9** and **10** were assessed in the triple negative breast cancer cell line VARIO68.[8,31] Cells were treated with **9** or **10** with a final concentration of 115 μM then observed under a confocal microscope at 3- and 6-hour intervals. After three hours (top panel) peptoid **9** shows increased trafficking relative to **10**. This is also true at the 6-hour time point (bottom pane), with peptoid **9** appearing to show nuclear entry. In contrast, **10** appears to be largely trapped in endosomes (green punctae), a common issue.[32,33] Taken together, these modifications and derivatives of the compounds have suggested that the ester modification as the bioactive precursor would be more effective due to the passive diffusion across the cell membrane.[30] These initial studies have provided valuable information to guide design of more efficient cell penetrants peptoids. Peptoid **9** is a promising compound for further studies.

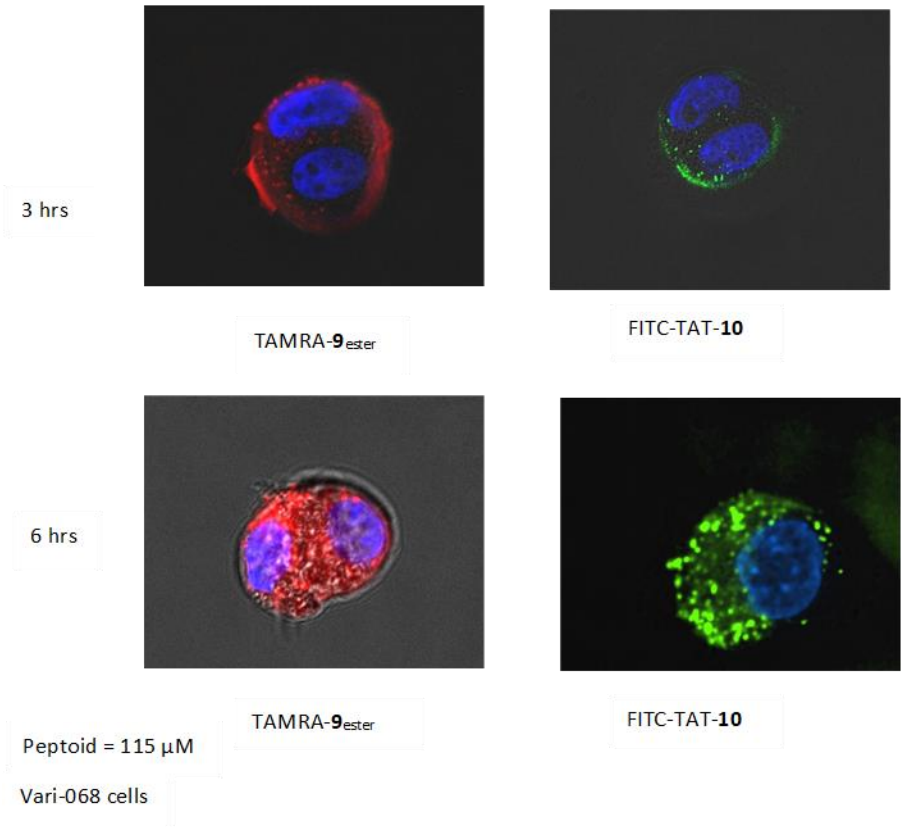

Figure 3.14 Peptoid permeability. Peptoid 8 was modified by appending the CPP TAT (left pane), modified acidic residues for ester (right pane). They were labeled with the fluorophore FITC or TAMRA. DAPI used to visualize nucleus. Some fluorophores enhance endosomal entrapment. Here, TAT seems to promote endosomal entrapment.

3.4 Conclusions and future Directions

Peptoids have long been used as one class of peptidomimetics for developing ligands for different classes of PPIs. In this Chapter I hypothesized that I could leverage the characteristics of peptoids to develop minimal sequence molecules that can bind to coactivators with low micromolar affinity. I showed that I could develop two peptoids with low micromolar affinities for the coactivator while maintaining specificity. This created the opportunity to further optimize the ATF6α peptoid since

it had an 8-fold weaker compared to the VP16. Amino acids flanking the core sequence allowed us to increase the length of the peptoid and improve binding. The resulting 11-residue sequence showed lower micromolar affinity and specificity for Med25 AcID. I demonstrated that we could deliver this sequence into cells by creating an ester derivative (peptoid **9**).

The results from these studies present questions to be answered in future studies. One such question to be addressed is how peptoid **9** affects the Med25 PPI network in vitro and in cell culture. My preliminary data suggests that the peptoid ligands *enhance* the binding of VP16-derived activators; the next question will be to test the full complement of Med25-dependent activators in such studies (ATF6α, the ETV/PEA3 activators). Additionally, a structural model of how peptoid **8** interacts with Med25 would be very useful for further optimizing the structure. Towards that end, ^{1}H, ^{15}N HSQC NMR experiments and analysis are ongoing.

3.5 Materials and Methods

The pET21b-Med25 (394-543)-His_6 plasmid was a generous gift from the Patrick Cramer lab. The mutations were carried out through standard site-directed mutagenesis protocols.

Protein Expression and Purifications

Med25 AcID(394-543) was purified by following standard expression protocols. The pET21b-Med25 (394-543)-His6 plasmid was transformed into heat-shock competent Rosetta pLys cells (Novagen) and plated onto LB plates containing ampicillin and chloramphenicol antibiotics then placed in the incubator inverted at 37 °C overnight for approximately 15-16 hours. The plates were then placed at 4 °C until needed. Starter cultures were prepared by pipetting 5 ml of Luria Broth into two disposable culture tubes each followed by 0.1 mg/ml ampicillin and 0.034mg/mL chloramphenicol. Using a sterile pipette tip, a single isolated colony was selected from the transformed plate and placed in each of the culture tubes after which the tubes were placed in an incubator at 37 °C with a rotation speed of 250 RPM overnight. The following morning 1-2 mL of the starter culture was placed in 1L autoclaved Terrific Broth along with 0.1mg/mL of ampicillin, then placed in an incubator at 37 °C at 250 RPM and grown to an OD_{600} of 0.8-1.0. The culture was placed in an incubator at 18 °C for at least 30 minutes before the cells were induced with 0.2 mM Isopropylβ-d-1-thiogalactopyranoside (IPTG) and shaken at 200 RPM overnight. The following morning the cells were collected and centrifuged at 6000 x g RPM for 20 minutes at 4 °C. The pellets were collected and placed in 50 mL centrifuge tubes, centrifuged at 2000 RPM for 2 minutes to concentrate the pellet to the tube bottom, then stored at -80 °C for later purification.

Med25 AcID was purified using manual protocol involving Ni-NTA resins and an automated protocol with Ni-NTA 5mL HiTrap FPLC columns. The collected pellet was suspended in 35 mL

lysis buffer (50 mM phosphate, 300 mM sodium chloride, 10 mM imidazole, pH 7.2) with 35 µL β-mercaptoethanol (1:1000 dilution)and one cOmplete, Mini, EDTA-free Protease Inhibitor tablet (Sigma-Aldrich). The cells were then lysed via sonication on ice for a total of 6 minutes with pulse on for 3 seconds and off for 10 seconds. After the cells were fully lysed, the solution was placed in a 50 mL centrifuge tube and placed in a fixed angle centrifuge rotor to centrifuge at 9500 RPM for 30 minutes at 4 °C. At the completion of the spin cycle, the supernatant was poured into a new 50 mL centrifuge tube then placed back in the centrifuge and spun at 9500 RPM for 10 minutes at 4 °C to further separate large particulates. The supernatant from the second centrifugation was filtered into a clean 50 mL centrifuge tube using 0.45 µm syringe filters and placed on ice.

The supernatant was loaded onto a 5 mL Ni-NTA HiTrap equilibrated with Buffer A/Lysis Buffer (50 mM phosphate, 300 mM sodium chloride, 10 mM imidazole, pH 7.2) on an AKTA pure FPLC chromatography system. The sample was loaded onto the column at a rate of 2.5 mL per minute. The method was created to follow the following sequence: the loaded column was washed with 5 column volumes of Buffer A, then with 5 column volumes of 10% Buffer B (50 mM phosphate, 300 mM sodium chloride, 400 mM imidazole, pH 7.2), followed by a wash with 5 column volumes of 15% Buffer B: 85% Buffer A and finally, elution with a gradient from 15-100% Buffer B. The column was subsequently washed with 5 column volumes of 100% Buffer B.

Following the collection of the fractions, those containing the Med25 AcID protein were collected and combined into a chilled 50 mL centrifuge tube then diluted to 50 mL using chilled (4 °C) Source S buffer A (50 mM phosphate, pH 7.2).

The Med25 AcID protein was further purified using 5 mL Source S HiTrap column using the AKTA pure FPLC chromatography system. The column was equilibrated with Source S buffer A (50mM phosphate, pH 7.2) then the diluted sample was loaded onto the column. Next, the column

was washed with 5 column volumes of Buffer A. Next, the protein was eluted with high concentration of sodium ions as the column was washed with 10 column volumes over a concentration gradient of 0-100% Buffer B (50 mM phosphate, 1M sodium chloride, pH 7.2). The fractions were collected and analyzed via SDS-PAGE using a 12% acrylamide gel. The pure fractions were then combined and 1 mM DTT was added then buffer exchanged in storage buffer (10mM phosphate, 100mM sodium chloride, 10% glycerol, 1 mM DTT, pH 6.8) overnight. The protein was concentrated and stored in 150 µL aliquots at 100-200 µM concentrations at -80 °C. Protein concentrations were determined using UV-Vis spectroscopy with the extinction coefficient, ε = 22550 $M^{-1}cm^{-1}$ and mass confirmation was carried out by electrospray mass spectrometry.

Peptide Synthesis

Peptide synthesis was carried out using conventional solid phase peptide synthesis and microwave assisted peptide synthesis (CEM Liberty Blue).

Peptides were synthesized on 50 µmole scale using CEM rink-amide resin (0.19-0.21 meq). The synthesis was carried out with dimethylformamide as the main solvent. Fmoc-amino acid concentrations were made to be 0.2M, deprotection solution was made up containing 20% piperidine, 0.2M Oxyma Pure. Diisopropylcarbodiimide (DIC) was the activator acid and Oxyma Pure was the activator base. The amino acids were coupled using 4-minute single coupling for peptide sequences shorter than 20 amino acids. The peptides were cleaved with 95% TFA:2.5% TIPS: 2.5% H_2O. Excess cleavage cocktail was evaporated using nitrogen gas flow. The resulting solution was treated with cold diethyl ether then centrifuged to collect the peptide precipitate. The ether was decanted, and the pellet was redissolved in 30% 0.1% TFA/H_2O and acetonitrile and lyophilized before purification. Peptides were redissolved in minimal acetonitrile (25%) and 0.1%

TFA/H_2O solution and purified using reverse-phase HPLC (Agilent) with C-18 columns and 0.1%TFA/H_2O-acetonitrile solvent system. The purified fractions were collected and analyzed using mass spectrometry. These pure fractions were combined after identifying through mass spectrometry and lyophilized until a dry powder was left.

The peptide was dissolved in DMSO. A sample of the DMSO was diluted 1:1000 in storage buffer to ascertain the concentration. Using UV-Vis, the concentration was measured at λ=495 nm for the FITC and an extinction coefficient, ε=72,000 $M^{-1}cm^{-1}$. Unlabeled peptides were weighed, and concentration determined.

Manual Peptide Synthesis

Peptides were synthesized using CLEAR amide resin (Peptide International) or rink amide resin (CEM). Manual synthesis reagents for CLEAR rink amide resin were HOBT, HBTU and DIPEA and that for CEM rink amide was DIC and HOBT. The first amino acids were coupled for a minimum of six hours followed by 2 hours of amino acid coupling up to the 10^{th} residue and subsequently 2.5 hours beyond 10 residues. After the completion of the sequence, the N-terminus was deprotected. For fluorescein labeling, beta alanine was coupled to the N-terminus and then 2 eq fluorescein isothiocyanate was coupled in the presence of 4 eq DIPEA. The N-terminus was acetylated for unlabeled peptide using 50 eq acetic anhydride and 50 eq DIPEA.

The peptides were cleaved with 95% TFA:2.5% TIPS: 2.5% H_2O. Excess cleavage cocktail was evaporated using nitrogen gas flow. The resulting solution was treated with cold diethyl ether then centrifuged to collect the peptide precipitate. The ether was decanted, and the pellet was redissolved in 30% 0.1% TFA/H_2O and acetonitrile and lyophilized before purification. Peptides were redissolved in minimal acetonitrile (25%) and 0.1% TFA/H_2O solution and purified using

reverse-phase HPLC (Agilent) with C-18 columns and 0.1%TFA/H_2O-acetonitrile solvent system. The purified fractions were collected and analyzed using mass spectrometry. These pure fractions were combined after identifying through mass spectrometry and lyophilized until a dry powder was left.

The peptide was dissolved in DMSO. A sample of the DMSO was diluted 1:1000 in storage buffer to ascertain the concentration. Using UV-Vis, the concentration was measured at λ=495 nm for the FITC and an extinction coefficient, ε=72,000 $M^{-1}cm^{-1}$. Unlabeled peptides were weighed, and concentration determined by what method?

Peptoid Synthesis

Peptoid synthesis was carried out using conventional solid phase peptide synthesis and microwave assisted peptide synthesis (CEM Liberty Blue).

Peptoids were synthesized on 50 µmole scale using CEM rink-amide resin (0.19-0.21 meq). The synthesis was carried out with dimethylformamide as the main solvent. Bromoacetic acid concentration was made to be 2M, deprotection solution was made up containing 20% piperidine, 0.2M Oxyma Pure to be used to deprotect Fmoc on amide resin and Fmoc-β-alanine. 2M Diisopropylcarbodiimide (DIC) was used as the coupling reagent for bromoacetic acid. The amines were made in 1M solutions and coupled using 4-minute single coupling. The peptoids were cleaved with 95% TFA:2.5% TIPS: 2.5% H_2O. Excess cleavage cocktail was evaporated using nitrogen gas flow. The resulting solution was treated with cold diethyl ether then centrifuged to collect the peptide precipitate. The ether was decanted, and the pellet was redissolved in 30% 0.1% TFA/H_2O and acetonitrile and lyophilized before purification. Peptides were redissolved in minimal acetonitrile (25%) and 0.1% TFA/H_2O solution and purified using reverse-phase HPLC (Agilent)

with C-18 columns and 0.1%TFA/H_2O-acetonitrile solvent system. The purified fractions were collected and analyzed using mass spectrometry. These pure fractions were combined after identifying through mass spectrometry and lyophilized until a dry powder was left.

The peptoid was dissolved in DMSO. A sample of the DMSO was diluted 1:1000 in storage buffer to ascertain the concentration. Using UV-Vis, the concentration was measured at λ=495 nm for the FITC and an extinction coefficient, ε=72,000 $M^{-1}cm^{-1}$. Unlabeled peptoids were weighed, and concentration determined by what method.

Fluorescence Polarization

Fluorescence polarization direct binding assays were done in triplicate with a final volume of 20 µL in a low volume, non-binding, 384-well black plate (Corning). Fluorescein-labeled DMSO peptide stocks were diluted to 50 nM using assay buffer (5 mM HNa_2PO_4, 5 mM NaH_2PO_4, 100 mM sodium chloride, 10 % glycerol, pH 6.8). 10 µL of Med25 AcID was serially diluted two-fold going down the column of the 384-well plate using the assay buffer (10 µL assay buffer was placed in each well). No protein was added to the last row as it was a negative control with peptide only. Finally, 10 µL of peptide was added to each well to provide a final peptide concentration of 25 nM and the resulting mixtures left to incubate at room temperature for 30 minutes. After 30 minutes, the fluorescence polarization was measured using Tecan Genios Pro or PHERAstar plate reader (polarized excitation at 485 nm and emission intensity measured through a parallel and perpendicularly polarized 535 nm filter). Data was analyzed by binding isotherm that accounts for liganddepletion (assuming a 1:1 binding model of peptide to ACID) was fit to the observed

polarization values as a function of AcID to obtain the equilibrium dissociation,

Kd. Each data point is an average of the triplicate experiments from each peptide with Med25 AcID and the error for standard deviation. “a” and “x” are the total concentrations of fluorescent peptide and Acid, respectively, “y” is the observed anisotropy at a given AcID concentration, “b” is the maximum observed anisotropy value, and “c” is the minimum observed anisotropy value.

$$y = c + (b - c)\, X\, \frac{(K_D + a + x) - [\sqrt{(K_D + a + x)^2 - 4ax}]}{2a}$$

Circular Dichroism

Circular Dichroism (CD) spectra of Med25 was obtained using J-715 spectropolarimeter (Jasco Inc) using a 1mm path length quartz cuvette. The peptoids were dissolved in acetonitrile (Toshiaki Hara *et al*) as they were insoluble in water. The spectra were measured from 260-180 nm at 1 nm increments at 200 nm/minute. A baseline spectrum was obtained using acetonitrile only followed by measurement of peptoids at 60 µM. The background spectra were subtracted from that of the peptoid before converting to mean residue ellipticity, θ using the following equation, where ψ = is the cd signal in degrees, n is the number of residues, l is the path length on centimeters and c is the concentration of the protein/peptide decimoles per cm^3.

$$[\theta] = \frac{\psi}{1000 * n * l * c}$$

Permeability Assay for CPP-Peptoids

Dishes were pre-equilibrated by incubating 15 mm CELL-NEST dishes with 10% FBS DMEM. 2 ml of medium were pipetted the dishes then placed in the incubator for 15 minutes. The VARI-068 cells were passaged, counted, and suspended in 10% FBS DMEM. The cell culture medium was aspirated from the dish and cells were plated on the glass surface. 500 µl of cell suspension

was pipetted into 15 mm microwells. The cells were suspended in 35 mm culture dishes at 3 X 10^5 cells per well. The dishes were subsequently incubated for 1 hour at 37 °C. After 1 hour the remainder of the dishes were filled with medium. 2 ml of medium was added to the 35 mm dishes then incubated for 24 Hours. The medium was aspirated after 24 hours then 500µL of 1% FBS/DMEM and 1 uL of peptoid for a final concentration of 5µM was added. The cells were incubated for 3 and 6 hours.

The medium was removed after 1 hour and dished were washed with PBS 3 times. Cells were then fixed with 4% paraformaldehyde solution in PBS for 15 minutes at 37 °C The dishes were washed three times with PBS to remove non-specific binding. The cells were then treated with DAPI for 15 minutes then washed with PBS three times. The cells were then observed under the confocal microscope.

3.6 References

1. Ptashne, M. & Gann, A. *Genes and Signals*. (Cold Spring Harbor Laboratory Press, 2002).
2. Cosma, M. Ordered Recruitment: Gene-SpecificMechanism of Transcription Activation. *Molecular Cell* **10**, 227–236 (2002).
3. Ulrich Stelzl *et al.* A Human Protein-Protein Interaction Network: A Resource for Annotating the Proteome. *Cell* **122**, 957–968 (2005).
4. Wang, W., Carey, M. & Gralla, J. Polymerase II promoter activation: closed complex formation and ATP-driven start site opening. *Science* **255**, 450–453 (1992).
5. Lee, T. I. & Young, R. Transcriptional Regulation andIts Misregulation in Disease. *Cell* **152**, 1237–1251 (2013).
6. Garlick, J., Sturlis, S. & Bruno, P. Norstictic Acid Is a Selective Allosteric Transcriptional Regulator. *Journal of the American Chemical Society* **143**, 9297–9302 (2021).
7. Yong, K., Ulintz, P. & Caceres, S. Heterogeneity at the invasion front of triple negative breast cancer cells. *Scientific Reports* **10**, 5781 (2020).
8. Liu, M., Liu, Y. & Deng, L. Transcriptional profiles of different states of cancer stem cells in tripple-negative breast cancer. *Molecular Cancer* **17**, 1–6 (2018).
9. Mojsoska, B., Carretero, G. & Larsen, S. Peptoids successfully inhibit the growth of gram negative E. coli causing substantial membrane damage. *Scientific Reports* **7**, (2017).
10. Schneider, J., Craven, T. & Kasper, A. Design of Peptoid-peptide Macrocycles to Inhibit the β-catenin TCF Interaction in Prostate Cancer. *Nature Communications* **9**, 1 (2018).
11. Lim, H.-S., Archer, C. & Kodadek, T. Identification of a Peptoid Inhibitor of the Proteasome 19S Regulatory Particle. *Journal of the American Chemical Society* **1292**, 7750–7751 (2007).

12. Gee, C., Koleski, E. & Pomerantz. Fragment Screening and Druggability Assessment for the CBP/p300 KIX Domain through Protein-Observed 19F NMR Spectroscopy. *Angew Chem Int Ed* **54**, 3735–3739 (2015).
13. Burkoth, T., Fafarman, A. & Charych, D. Incorporation of Unprotected Heterocyclic Side Chains into Peptoid Oligomers via Solid-Phase Submonomer Synthesis. *Journal of the American Chemical Society* **125**, 8841–8845 (2003).
14. Knight, A., Zhou, E. & Francis, M. Sequence Programmable Peptoid Polymers for Diverse Materials Applications. *Advanced Materials* 1–27 (2015).
15. Hirai, H., Tani, T. & Kikyo, N. Structure and functions of powerful transactivators: VP16, MyoD and FoxA. *Int J Dev Biol* **54**, 1589–1596 (2010).
16. Miller, S., Simon, R. & Zuckermann, R. Proteolytic studies of homologous peptide and N-substituted glycine peptoid oligomers. *Bioorg Med Chem Lett* **4**, 2657–2662 (1994).
17. Rowe, S. & Mapp, A. K. Assessing the Permissiveness of Transcriptional Activator Binding Sites. *Biopolymers* **89**, 578–581 (2008).
18. Frangioni, J., LaRiccia, L. & Cantley, L. Minimal activators that bind to the KIX domain of p300/CBP identified by phage. *Nature Biotechnology* **18**, 1060–1065 (2000).
19. Radhakrishnan, I., Perez-Alvarado, G. & Parker, D. Solution Structure of the KIX Domain of CBP Bound to the Transactivation Domain of CREB: A Model for Activator:Coactivator Interactions. *Cell* **91**, 741–752 (1997).
20. Cardenal, C., Vollrath, S., Schepers, U. & Brase, S. Synthesis of Functionalize GLutamine- and Asparagine-Type Peptoids - Scope and Limitations. *Helvetica Chimica Acta* **95**, 2237–2248 (2012).

21. Wu, C., Sanborn, T. & Huang, K. Peptoid Oligomers with R-Chiral, Aromatic Side Chains: Sequence Requirements for the Formation of Stable Peptoid Helices. *J. Am. Chem. Soc.* **123**, 6778–6784 (2001).
22. Stringer, J., Crapster, J. & Guzei, I. Extraordinarily Robust Polyproline Type I Peptoid Helices Generated via the Incorporation of α-Chiral Aromatic N-1-Naphthylethyl Side Chains. *J. Am. Chem. Soc.* **133**, 15559–15567 (2011).
23. Jonker, H., Wechselberger, R. & Boelens, R. Structural Properties of the Promiscuous VP16 Activation Domain. *Biochemistry* **44**, (2005).
24. Ocampo-Garcia, B., Santos-Cuevas, C. & Leon-Rodriguez. Design and biological evaluation of 99mTc-N2S2-Tat(49–57)-c(RGDyK): A hybrid radiopharmaceutical for tumors expressing α(v)β(3) integrins. *Nuclear Medicine and Biology* **40**, 481–487 (2013).
25. Gump, J. & Dowdy, S. TAT transduction: the molecular mechanism and therapeutic prospects. *Trends in Molecular Medicine* **131**, 443–448 (2007).
26. Santos-Cuevas, C., Ferro-Flores, G. & de Murphy, C. Design, preparation, in vitro and in vivo evaluation of 99mTc-N2S2-Tat(49–57)-bombesin: A target-specific hybrid radiopharmaceutical. *International Journal of Pharmaceuticals* **375**, 75–83 (2009).
27. Torchilin, V. Tat peptide-mediated intracellular delivery of pharmaceutical nanocarriers. *Adcanved Drug Delivery Reviews* **60**, 548–558 (2008).
28. Vives, E., Brodin, P. & Lebleu, B. A Truncated HIV-1 Tat Protein Basic Domain Rapidly Translocates through the Plasma Membrane and Accumulates in the Cell Nucleus. *Journal of Biological Chemistry* **272**, 16010–16017 (1997).
29. Debaisieux, S., Rayne, F. & Yezid, H. The Ins and Outs of HIV-1 Tat. *Traffic* 355–3631 (2012).

30. Zou, Y., Rojas-Pierce, M. & Raikhel, N. Preparation of methyl ester precursors of biologically active agents. *BioTechniques* **44**, 377–384 (2008).
31. Eckley, S., Buschhaus, J. & Humphries, B. Short-Term Environmental Conditioning Enhances Tumorigenic Potential of Triple-Negative Breast Cancer Cells. *Tomography* **5**, 346–357 (2019).
32. LeCher, J., Nowak, S. & McMurry, J. Breaking in and busting out: cell-penetrating peptides and the endosomal escape problem. *Biomol Concepts* **8**, 131–141 (2017).
33. Erazo-Oliveras, A., Muthukrishnan, N. & Baker, R. Improving the Endosomal Escape of Cell-Penetrating Peptides and Their Cargos: Strategies and Challenges. *Pharmaceuticals* **5**, 1177–1209 (2012).

Chapter 4

4.1 Conclusions

Protein-protein interactions (PPIs) are vital for the regular functioning of cellular systems. These interactions are the hallmarks of the transcription, which involves many proteins interacting in complex networks.[1] There are several areas where abnormalities can occur in the PPI network and can result in diseases. [2]Some of the most vital proteins involved in the transcription process are activators and coactivators. Activators have at minimum a DNA binding domain that binds to specific DNA sequences and a transcriptional activation domain (TAD) that recruits coactivators. The coactivators are large proteins that are often a part of larger coactivator hub complexes such as Mediator. Domains of the coactivators interacting with the TAD, activator-binding domains or ABDs, often bear large surface areas for PPIs without defined binding sites, thus making them challenging therapeutic targets.[3] Additionally, the transient interactions of these PPIs serve as a challenge to better understand the mechanisms. Nonetheless, some progress has been achieved by using kinetic tools to measure the time of interactions and provide data to predict conformations of the complexes formed.[4]

Despite the recent successes in the discovery of PPI-targeting small molecules, the same success has not been seen with activator-coactivator interactions due to the large surface area of the binding interfaces. As a result of these limitations, designing molecules for targeting these PPIs can be a daunting task. Hence, my strategy turned to designing molecules that can cover a larger surface

area by constructing mimics from the structure of the native TADs that can be more conformationally dynamic and more biologically robust.[5]

This work sought to identify the minimal binding sequences for the coactivator by identifying PPIs between identified TADs for the coactivators Med25 AcID. Previous work has proposed a structure for Med25 AcID that is structurally unique in comparison to other coactivators that are usually composed of the primarily a-helical structures.[6] Two distinct binding surfaces on Med25 AcID interact with specific TADs and the binding surfaces are denoted as H1 and H2. They are located on the opposite faces of the protein (Figure 4.1).

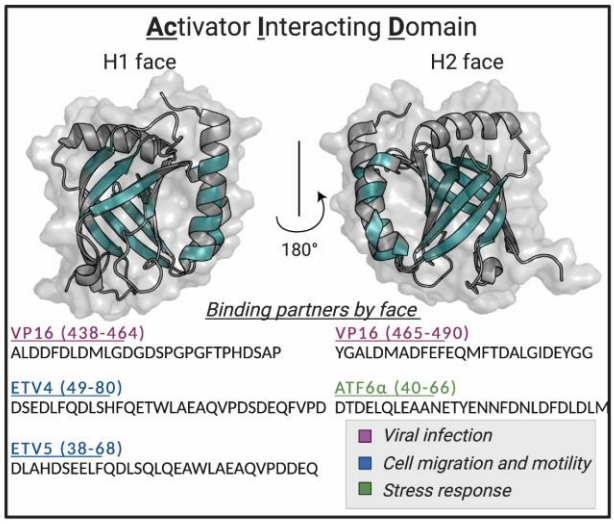

Figure 4.1 The AcID motif of the coactivator Med25 has two binding surfaces to interact with activators. These binding surfaces are denoted H1 and H2. This figure is adapted from and created by Amanda Peiffer.

The studies of Chapter Two confirmed that Med25 AcID interacts with three different activators despite the different sequences of each (Figure 4.1). Also, we confirmed that Med25 AcID binding surfaces show specificity for different TADs as demonstrated by mutations at the H1 and H2 surfaces that differentially affect the TADs.[7–9] Through experiments done by us and others, it was shown that ERM interacts with AcID in the H1 face. Mutations of three residues in the H1 face

affected binding of the ERM TAD by 3-6-fold. This did not affect the ATF6α TAD as it was known to interacts with H2 face of the coactivator.[4]

To identify the minimal sequences needed for binding to Med25, VP16 was truncated in three equal sections. Additionally, two sequences were synthesized based on the location of the putative α-helices. These sets of data, obtained by Dr. Steve Sturlis, suggest that we were able to design minimal sequences from the largest TAD to obtain low micromolar affinity. From this information, I demonstrated that we could reduce the sequences to even lower number VP16 472-479 has been shown to minimal activate transcription. This is an 8-residue peptide that is in the C-terminal domain of VP16 TAD. The direct binding was measured and produced a low micromolar affinity for Med25 AcID. The results of this suggest that we can use this to understand binding to Med25 AcID and to design peptidomimetics. Based on these results, I identified an octamer of similar sequence located in ATF6α that also binds to the H2 face Med25 with a sub-micromolar affinity.

In Chapter Three we showed that we synthesized peptoids mimicking minimal sequences identified in Chapter two. These were synthesized on solid support using amines mimicking the side chains of the parent peptides. We demonstrated that these can be mimicked and recapitulate binding to Med 25 AcID. We also addressed the question of specificity by comparing the binding to the CBP-KIX coactivator. The peptoids retained specificity for the target protein, thus allowing us to further address questions such as ability to improve the binding. These were done by extending the sequence with the surrounding residues.

We later sought to answer the question of cell permeability. We used the HIV-1 TAT_{49-57} as the cell penetrating peptide to append to the modified peptoid.[10–14] Some of the preliminary work illustrates that we can deliver mimicked TADs into cells. The ability for us to deliver these are

promising with the evidence we have garnered; we will seek to deliver peptoids of known TADs to create potent inhibitors.

4.2 Future Directions

The use of peptidomimetics for the development of effective activator•coactivator inhibitors hold great promise based on what has been established in this work and previous work of others. These peptoids hold great promise because they are comparable to small molecules inhibitors reported in previous studies. As can be gleaned from this dissertation, peptoids were developed with low micromolar affinities for the coactivator Med25 AcID. One example is the small molecule compound MS120/Ischemin, which has been an effective inhibitor of the CREB-p53 PPI despite having an affinity of 19 μM.[15,16] This is close to the affinities I have reported in the previous chapters. Therefore, this shows that these synthetic molecules reported earlier are promising synthetic molecules for successfully targeting coactivator-activator PPIs.

One other example of small molecule with affinity similar to peptoids reported in this dissertation is KG-501, which inhibits CBP-CREB interaction, and has an affinity for CBP of 50μM, a direct affinity up to 15-fold lower that what is described here. The third example is compound **2** (10074A4) with a Kd of ~5 μM, which is similarly a low micromolar affinity compound. Like the two small molecules mentioned earlier, this has successfully inhibited the c-Myc-Max interaction.[17]

With these similar numbers, these studies have established that despite not having a submicromolar affinity for their target proteins, they can successfully inhibit the PPI of coactivators and their binding partners.

Peptoids are dynamic mimetics that can be modified and synthesized with ease and are very cost-efficient. These allow for the testing and designing of diverse molecules that are capable of interacting with larger surface areas. By identifying the components of native TADs, these can be designed to create a lead compound that can be easily modified to improve potency. With the number of amines available, this allows for larger library creations with diverse functional groups.

Lead compounds can be identified using traditional library synthesis and screenings. In creating these large number of compounds this allows us to modify leads to improve the activities. As a result, this helps to better design these compounds and possible incorporate unnatural side chains to improve potency.

Following the identification of molecules, we can modify these and compare their activities by synthesizing both linear and cyclic versions of these molecules. Past studies have utilized cyclic versions of peptides to improve permeability as they are delivered to the sites. As recent as 2017, the Unites States Food and Drug Administration approved plecanatide, which is a cyclic peptide used to treat idiopathic constipation.[18] We will be able to develop the potent molecules with inspirations from various molecules that have successfully been developed.

As we understand more about the interactions, we hope to identify key components of other TADs that can help us to better understand how we can leverage the characteristics of peptoids to improve activities of the peptoids. We hope to use various mammalian systems and study the effect that these will have on toxicity as we improve the use of CPPs.[19]

By using many techniques to create a large toolbox and create a design consensus, we hope to better design peptidomimetics with improved activities. This can help us to better understand wider activator-coactivator interactions by obtaining information at a rapid rate and develop efficiency

of our designs. We will be able to produce more naturally occurring peptides and peptidomimetics that will help us to better understand PPIs and by extension develop therapeutics by design.

4.3 References

1. Ptashne, M. & Gann, A. *Genes and Signals*. (Cold Spring Harbor Laboratory Press, 2002).
2. Lee, T. I. & Young, R. Transcriptional Regulation andIts Misregulation in Disease. *Cell* **152**, 1237–1251 (2013).
3. Mapp, A. K., Pricer, R. & Sturlis, S. Targeting transcription is no longer a quixotic quest. *Nature Chemical Biology* **11**, 891–894 (2015).
4. Henderson, A., Henley, M. & Foster, N. Conservation of coactivator engagement mechanism enables small-molecule allosteric modulators. **115**, 8960–8965 (2018).
5. Zuckermann, R. Peptoid Origins. *Peptide Science* **96**,.
6. Bontems, F., Verger, A. & Dewitte, F. NMR structure of the human mediator MED25 ACID domain. *J Struct Biol* **174**, 245–251 (2011).
7. Landrieu, I., Verger, A. & Baert, J.-L. Characterization of ERM transactivation domain binding to the ACID/PTOV domain of the Mediator subunit MED25. *Nucleic Acids Research* **43**, 7110–7121 (2015).
8. Vojnic, E., Mourao, A., Seizl & Wenzeck, L. Structure and VP16 binding of the Mediator Med25 activator interaction domain. *Nature Structural & Molecular Biology* **18**, 404-U429 (2011).
9. Sela, D., Conkright, J. & Chen, L. Role for human mediator subunit MED25 in recruitment of mediator to promoters by endoplasmic reticulum stress-responsive transcription factor ATF6α. *J Biol Chem* **288**, 26179–26187 (2013).
10. Ocampo-Garcia, B., Santos-Cuevas, C. & Leon-Rodriguez. Design and biological evaluation of 99mTc-N2S2-Tat(49–57)-c(RGDyK): A hybrid radiopharmaceutical for tumors expressing α(v)β(3) integrins. *Nuclear Medicine and Biology* **40**, 481–487 (2013).

11. Futaki, S. Membrane-permeable arginine-rich peptides and the translocation mechanisms. *Advanced Drug Delivery Reviews* **57**, 547–558 (2005).

12. Torchilin, V. Tat peptide-mediated intracellular delivery of pharmaceutical nanocarriers. *Adcanved Drug Delivery Reviews* **60**, 548–558 (2008).

13. Gump, J. & Dowdy, S. TAT transduction: the molecular mechanism and therapeutic prospects. *Trends in Molecular Medicine* **131**, 443–448 (2007).

14. Santos-Cuevas, C., Ferro-Flores, G. & de Murphy, C. Design, preparation, in vitro and in vivo evaluation of 99mTc-N2S2-Tat(49–57)-bombesin: A target-specific hybrid radiopharmaceutical. *International Journal of Pharmaceuticals* **375**, 75–83 (2009).

15. Borah, J., Mujtaba, S. & Karakikes, I. A Small Molecule Binding tothe Coactivator CREB-Binding ProteinBlocks Apoptosis in Cardiomyocytes. *Chemistry & Biology* **18**, 531–541 (201AD).

16. Mujtaba, S., Zeng, L. & Zhoug, M.-M. Modulating Molecular Functions of p53 with Small Molecules. *Cell Cycle* **6**, 2575–2578 (2006).

17. Arndt, H. Small Molecule Modulators of Transcription. *Angew Chem Int Ed* **45**, 4552–4560 (2006).

18. Choi, J.-S. & Joo, S. Recent Trends in Cyclic Peptides as Therapeutic Agents and Biochemical Tools. *Biomol Ther* **28**, 18–24 (2020).

19. Miller, S. & Schneider, J. The effect of turn residues on the folding and cell-penetrating activity of β-hairpin peptides and applications toward protein delivery. *Peptide Science* **112**, (2020).

Appendix

Characterization of synthesized peptides and peptoids

The appendix contains the analytical chromatograms and mass spectrometry of the peptide and peptoids used in the fluorescence polarization assays and cell-penetrations studies throughout this thesis.

Analytical chromatogram of VP16 (472-479)

Sig= 214

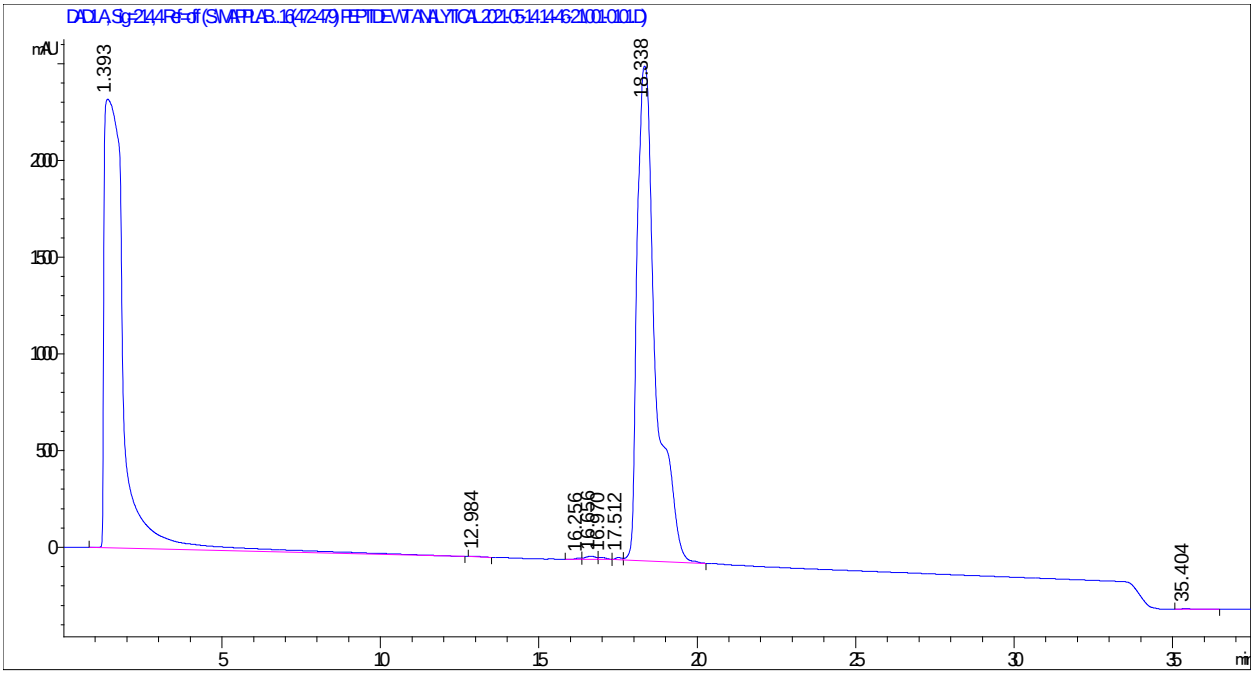

Sig= 280

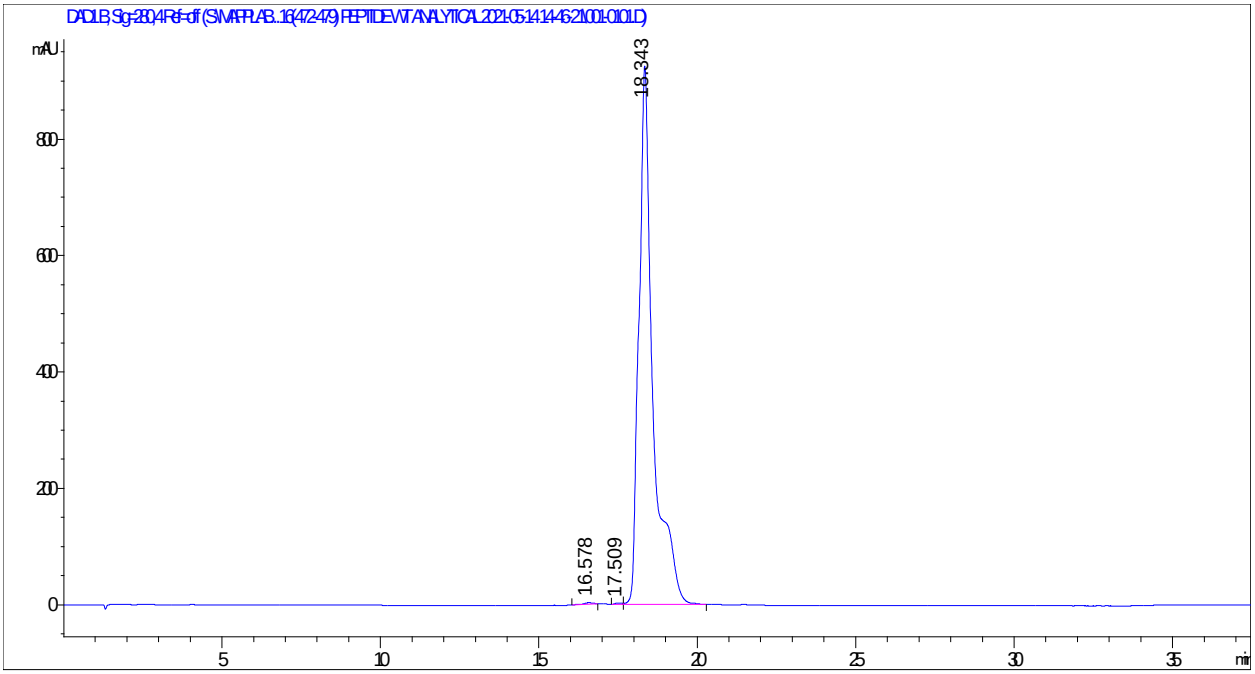

Sig= 495

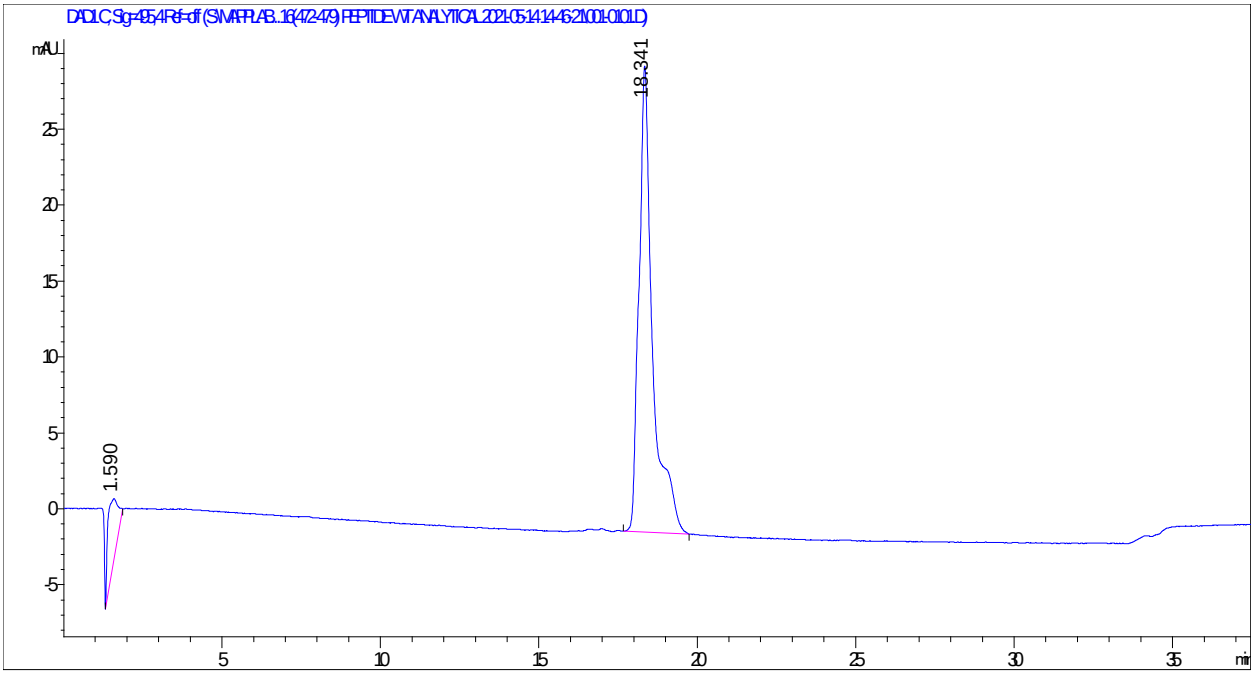

Analytical chromatogram of VP16 (472-479) Q→E

Sig=214

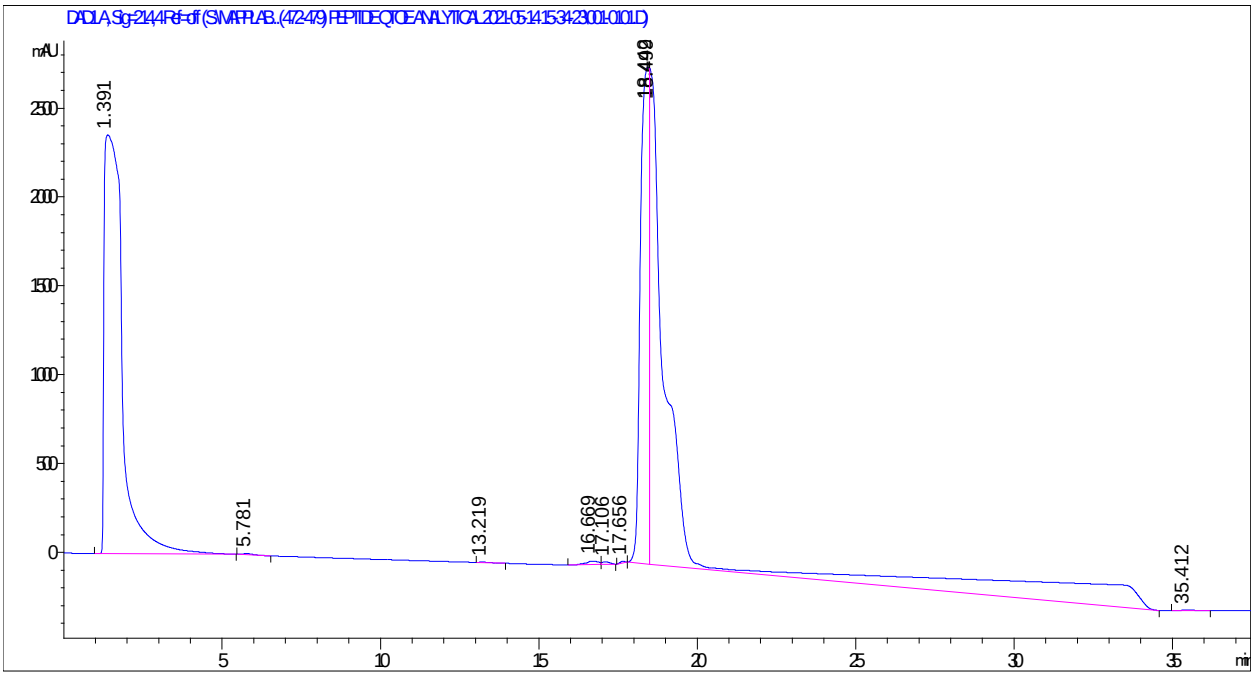

Sig=280

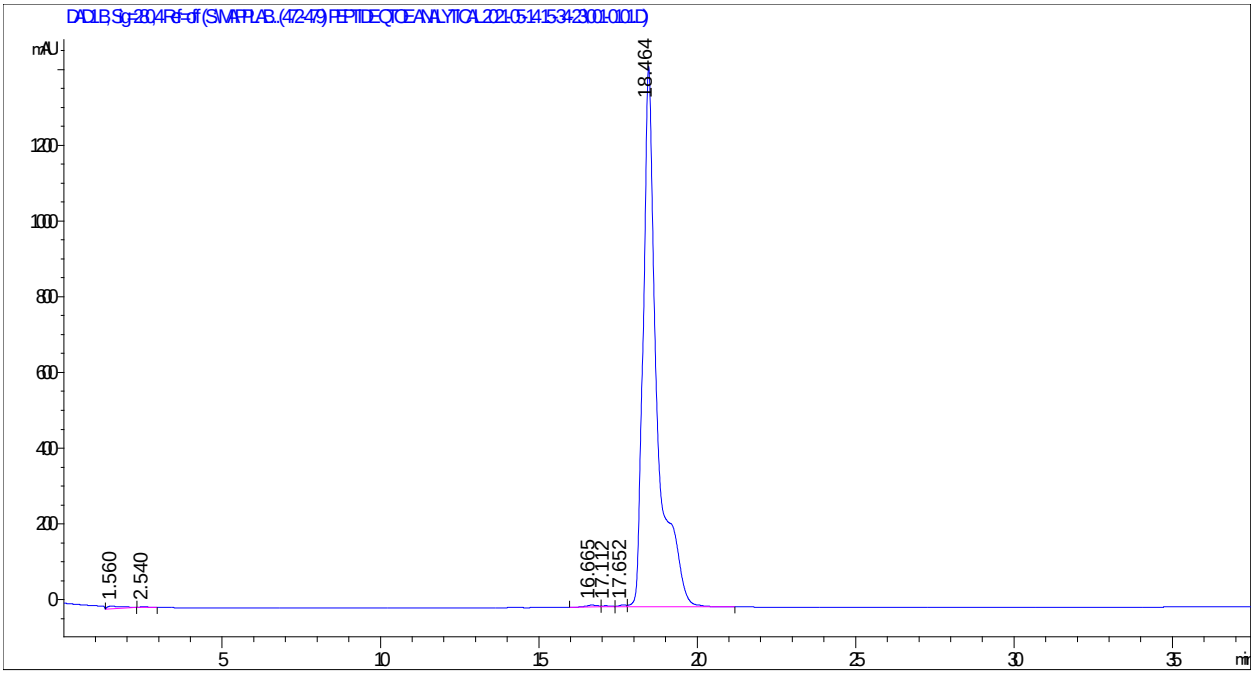

Sig=495

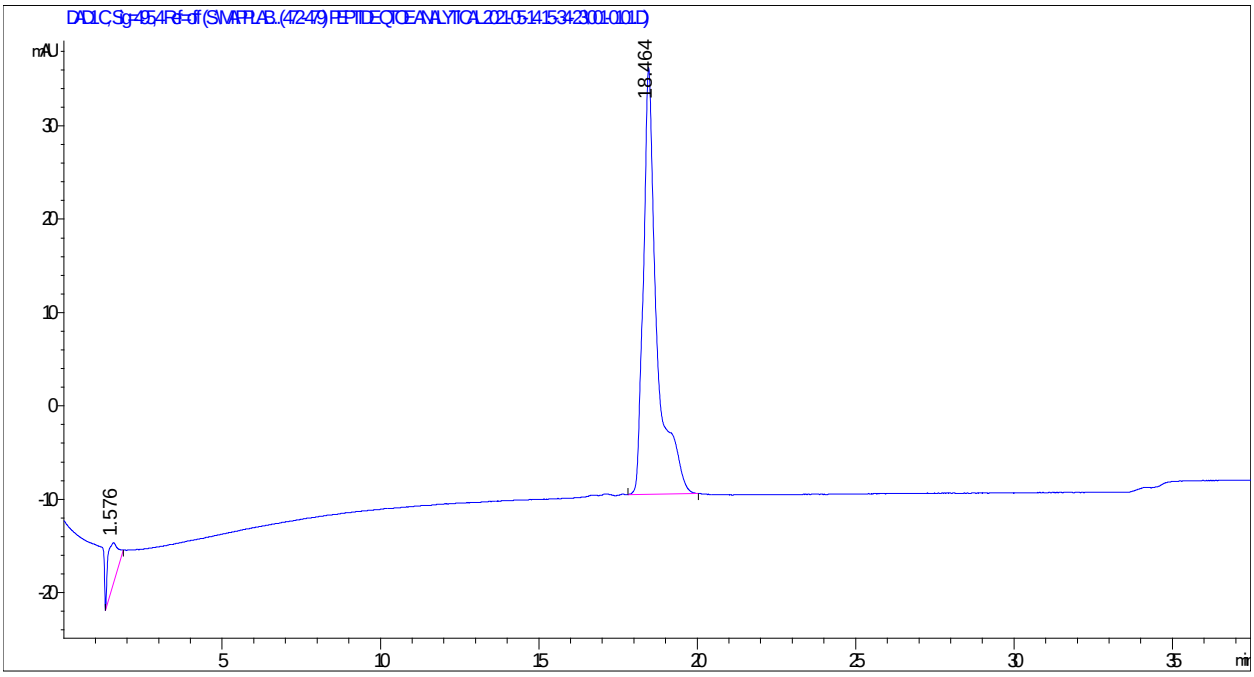

Peptoid 1

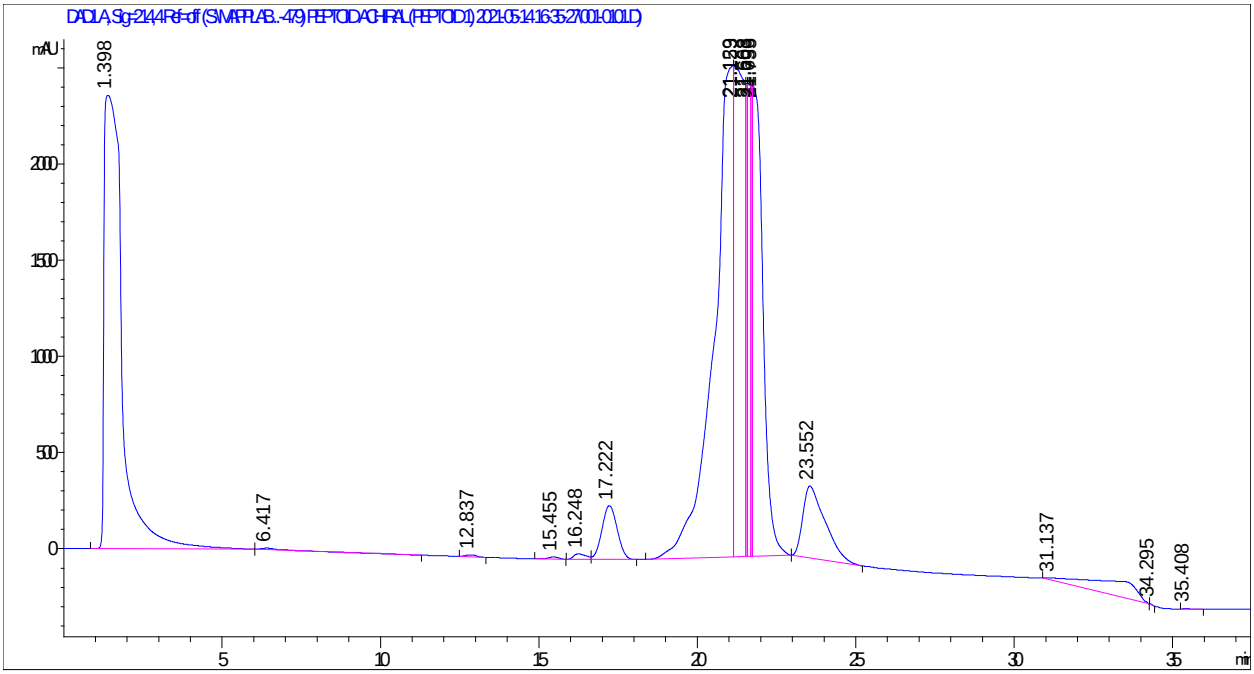

Sig=280

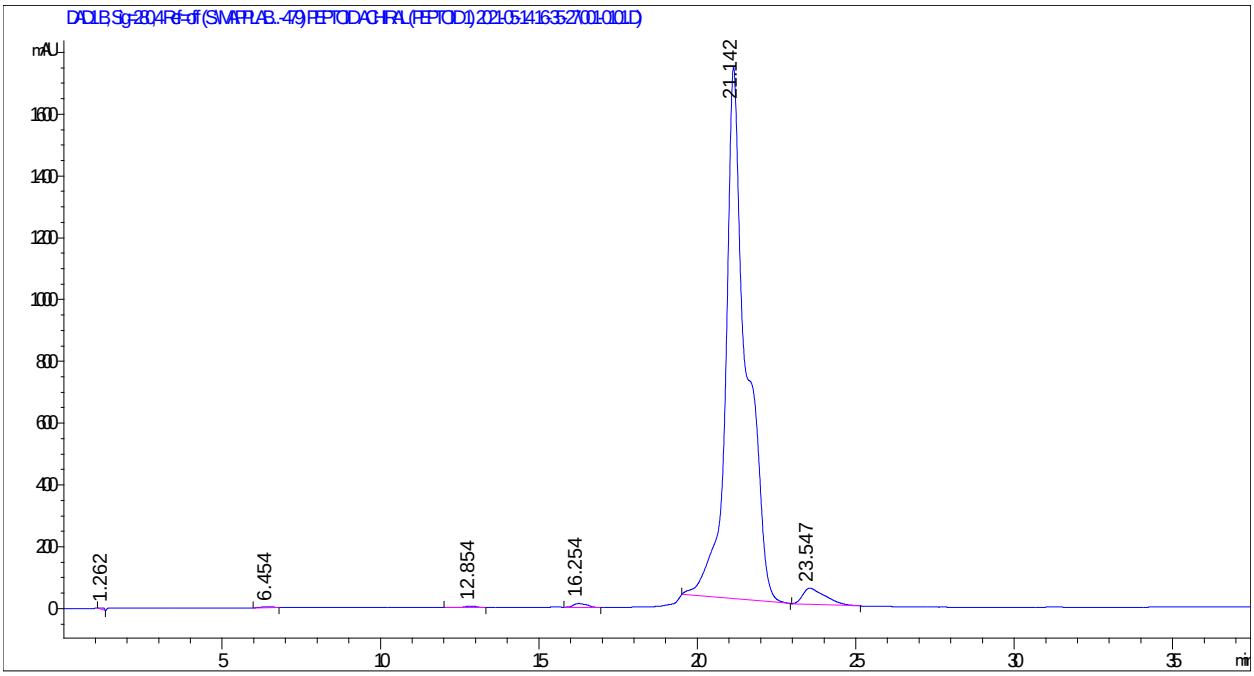

Sig=495

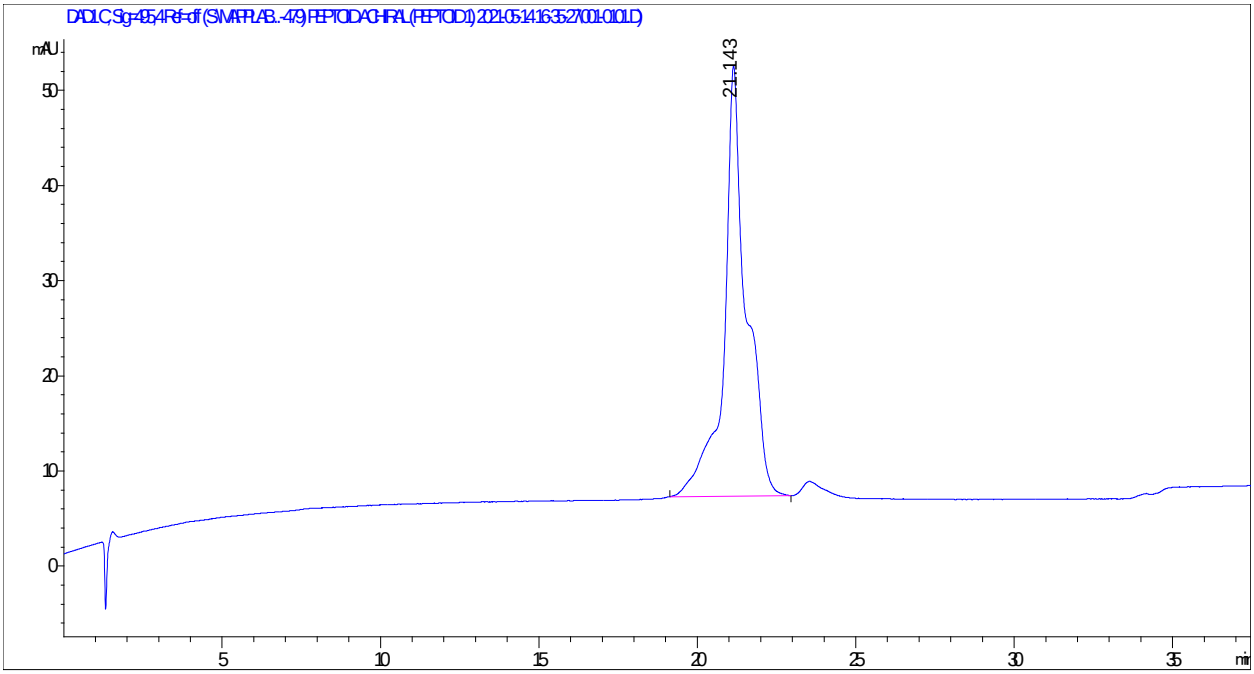

Peptoid 2A

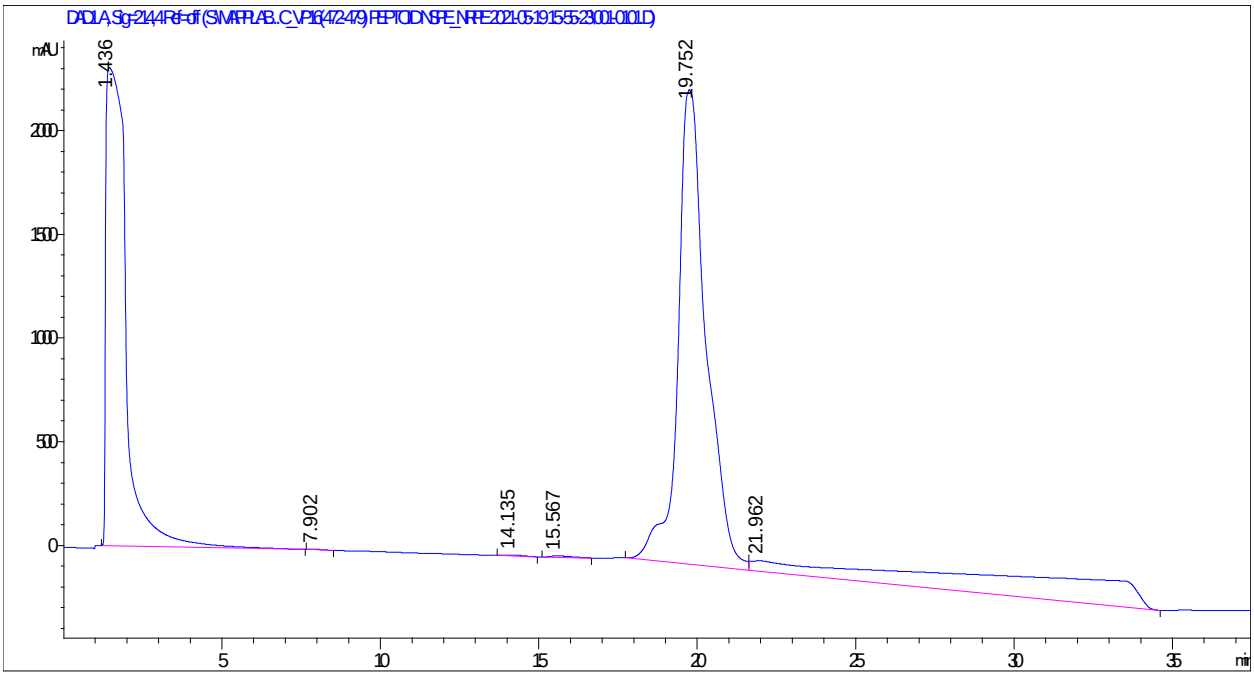

Sig=280

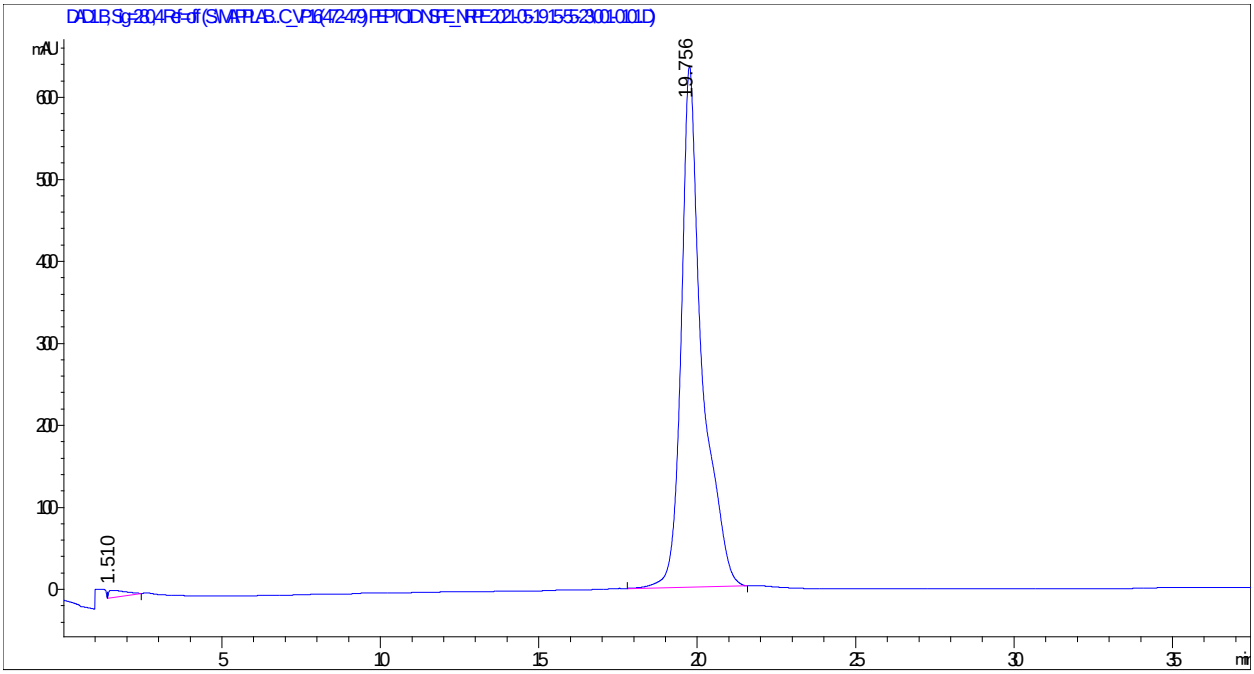

Sig = 495

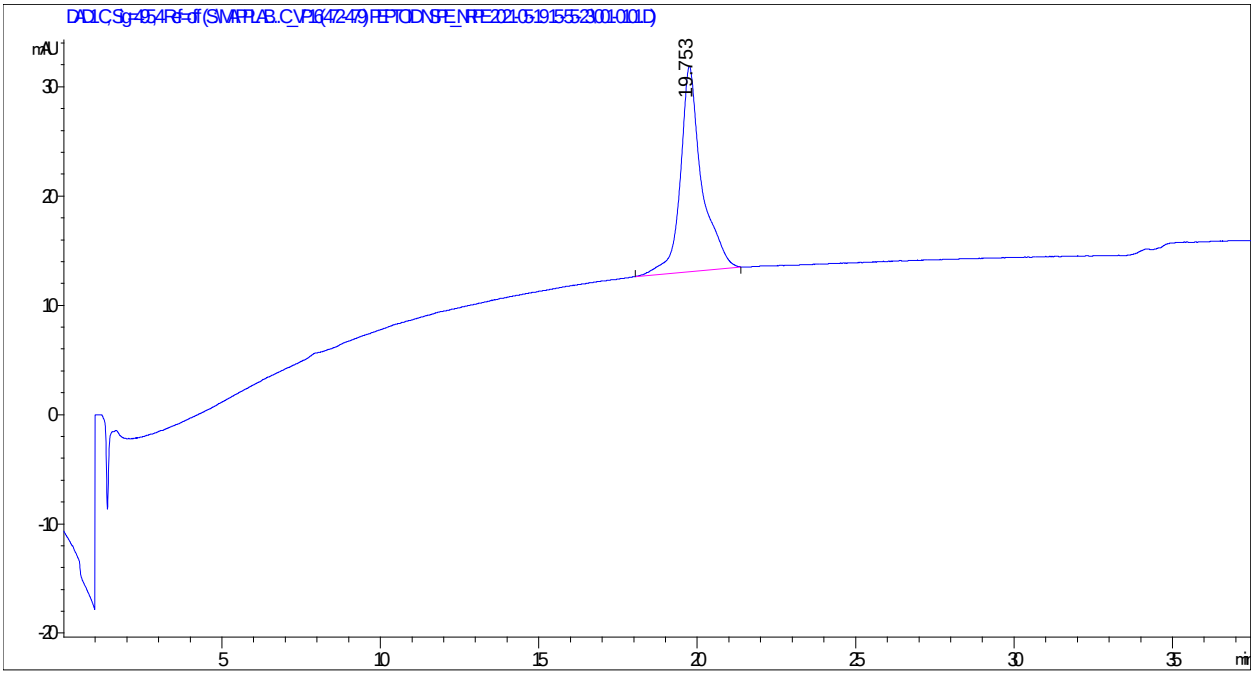

Peptoid 2B

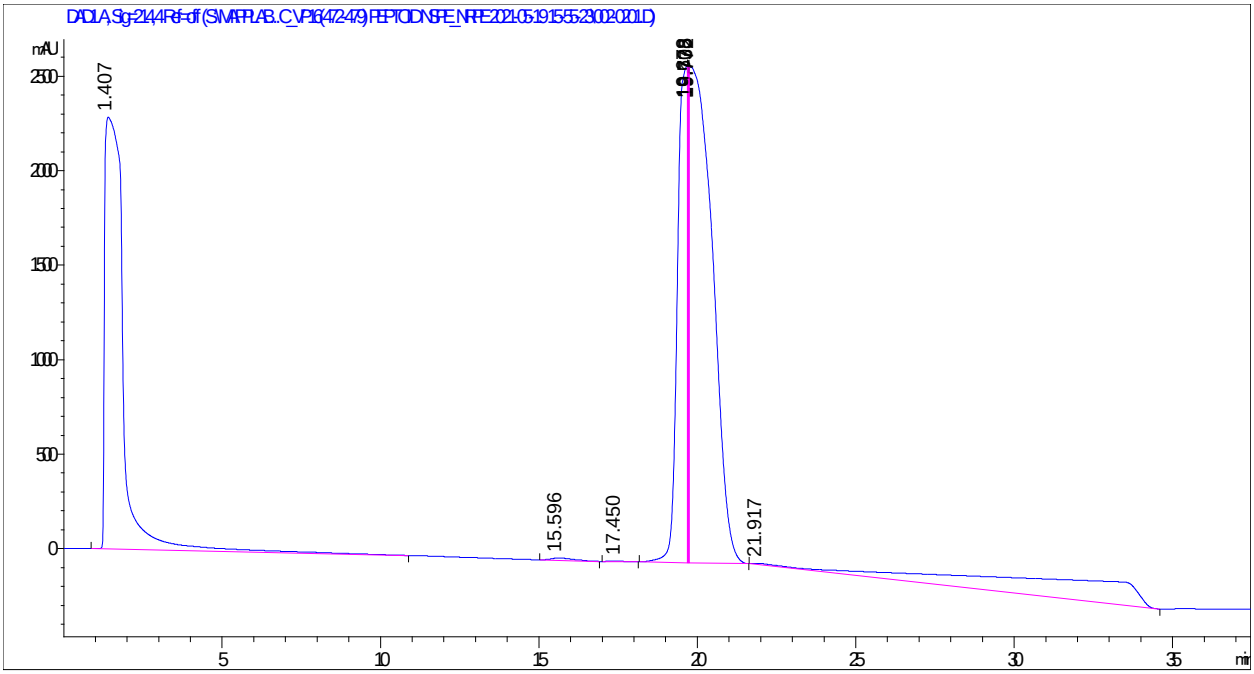

Sig=280

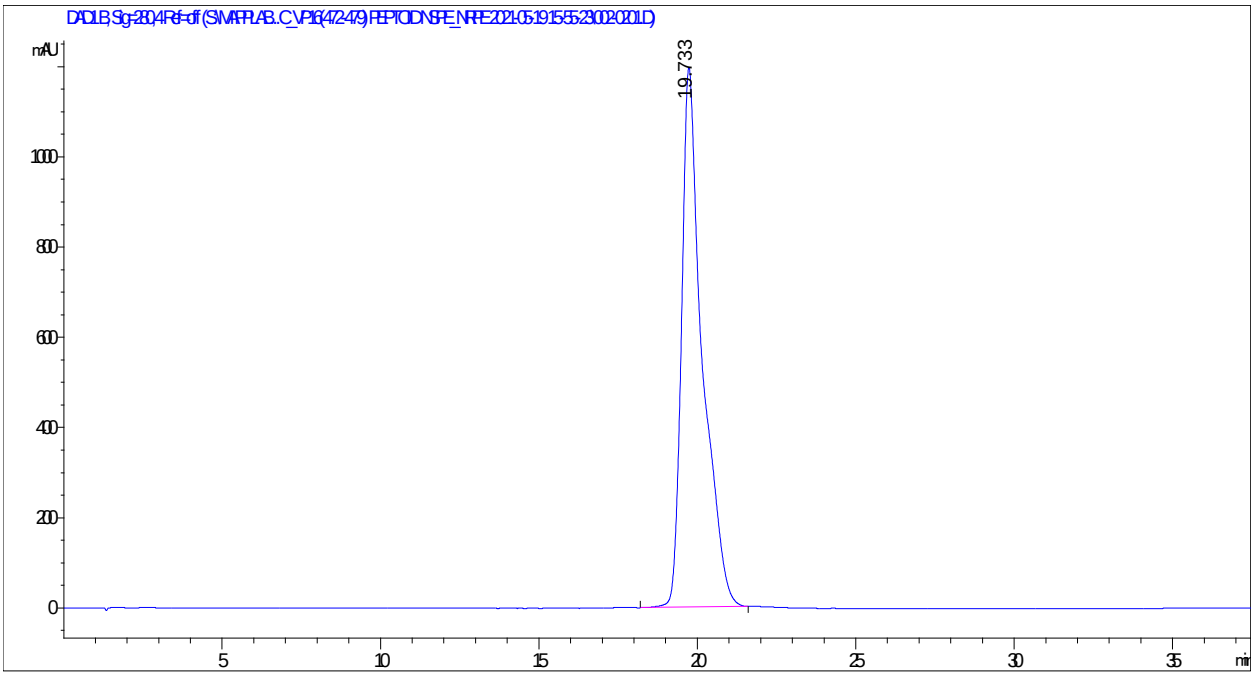

Sig = 495

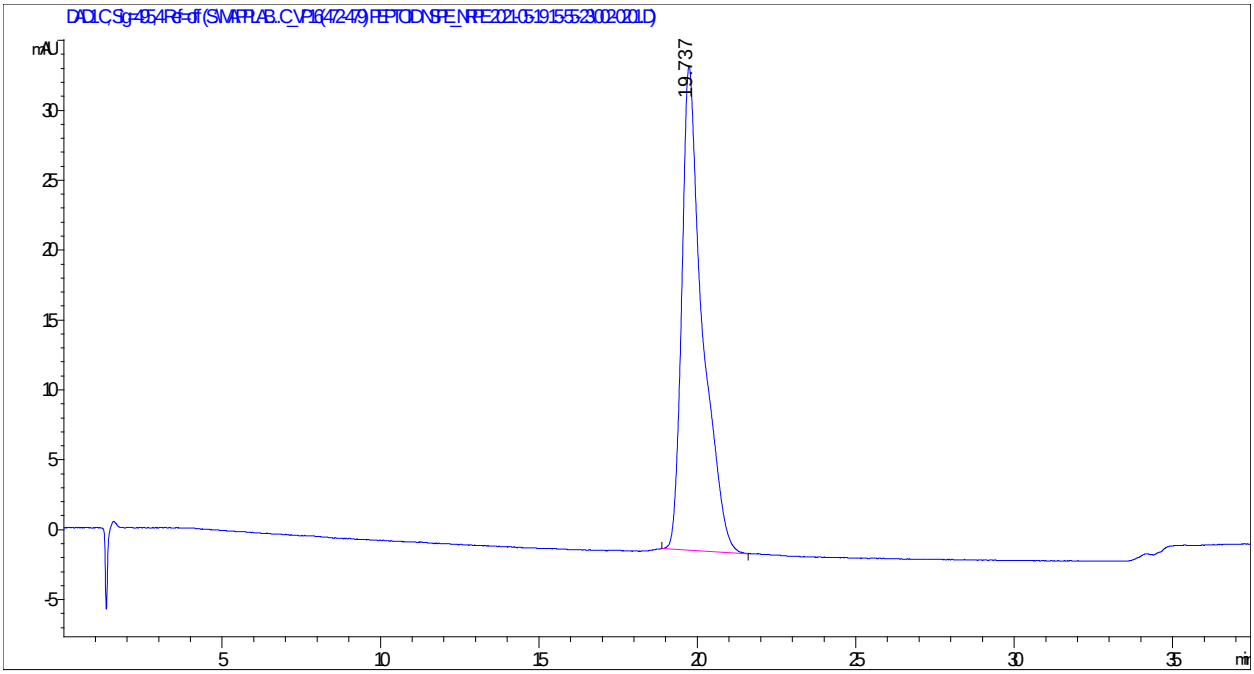

Atf6α VN8 Peptide

Sig=214

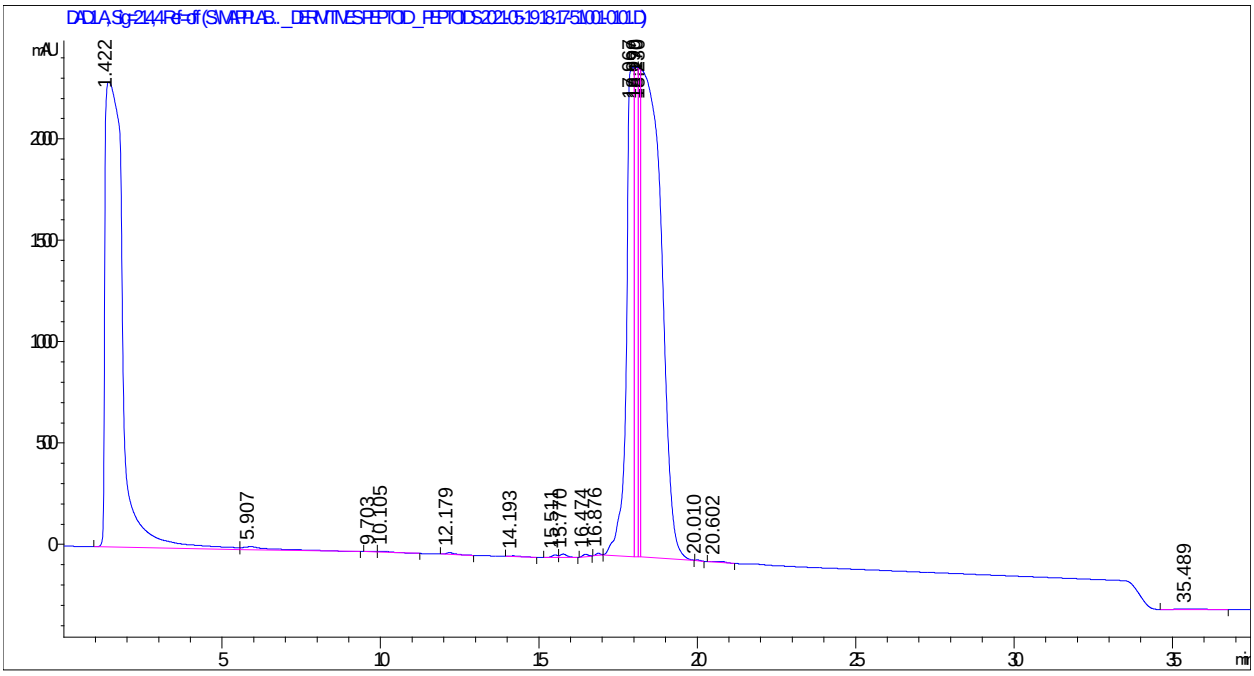

Sig=280

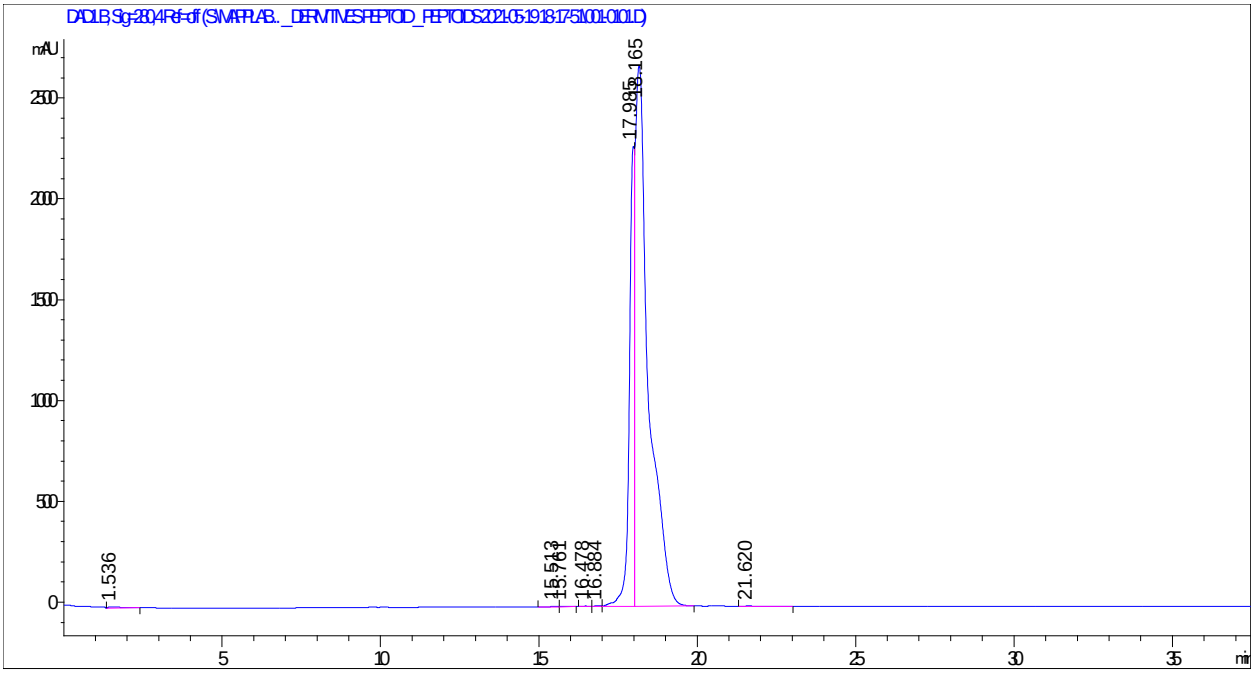

Sig=495

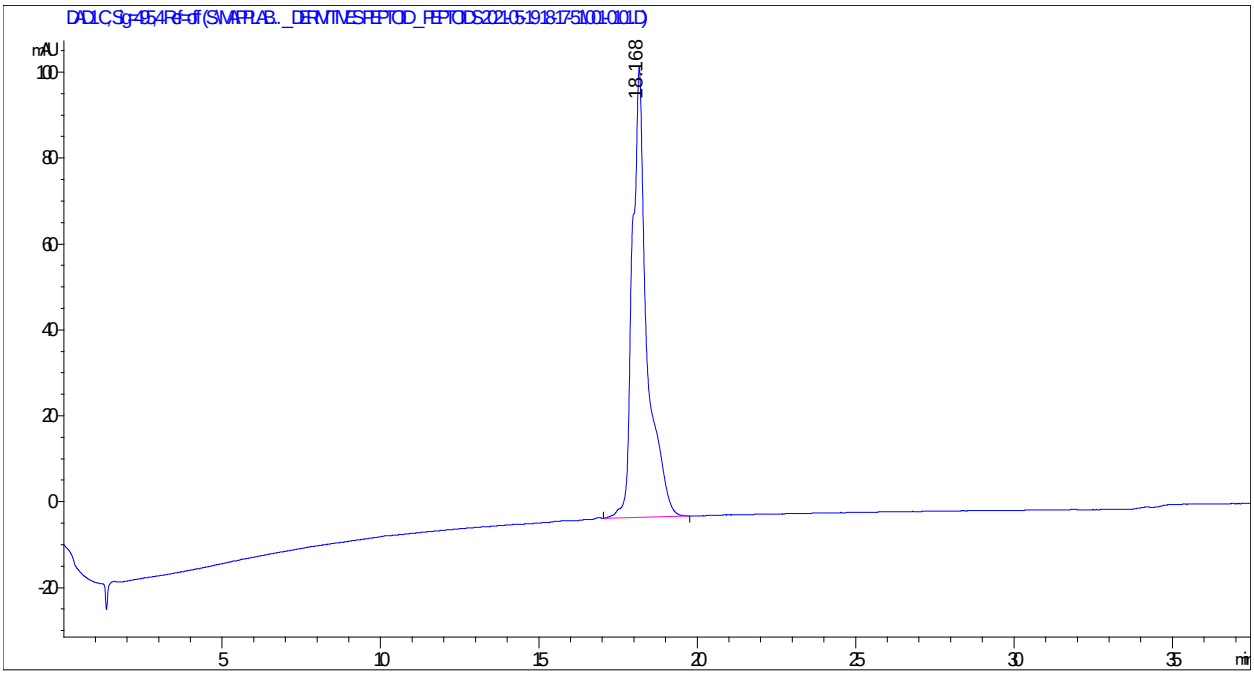

Atf6α VN8 Peptide P→F

Sig=214

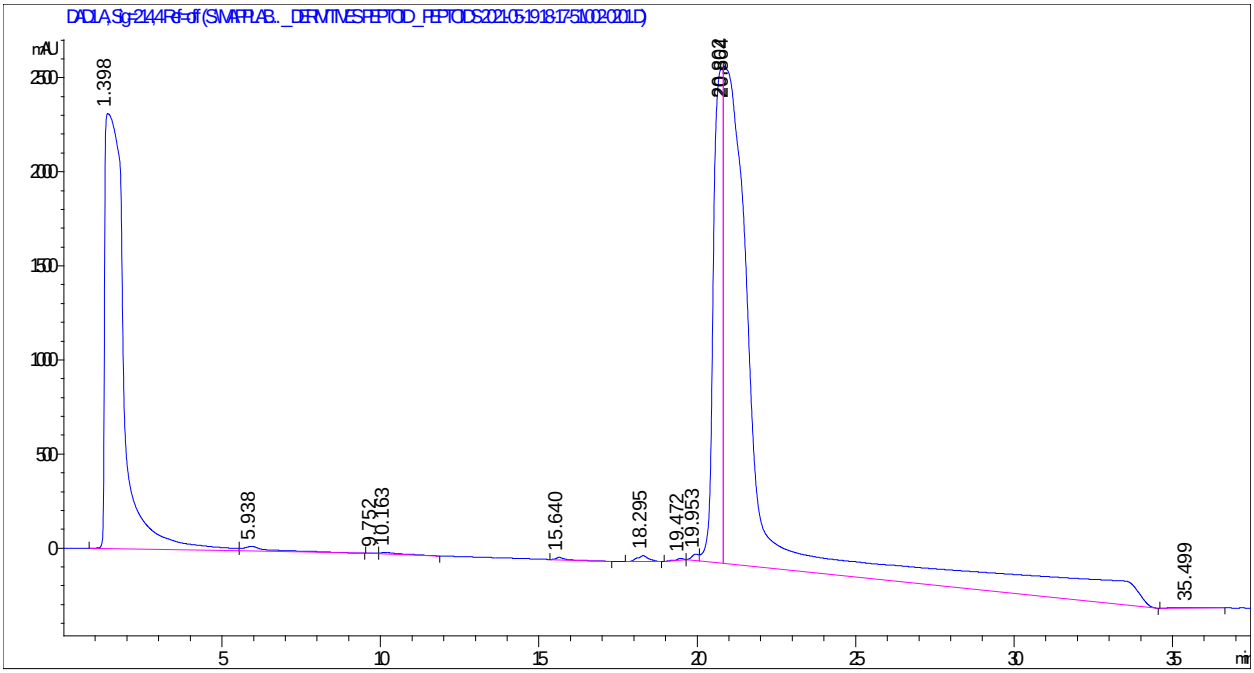

Sig=280

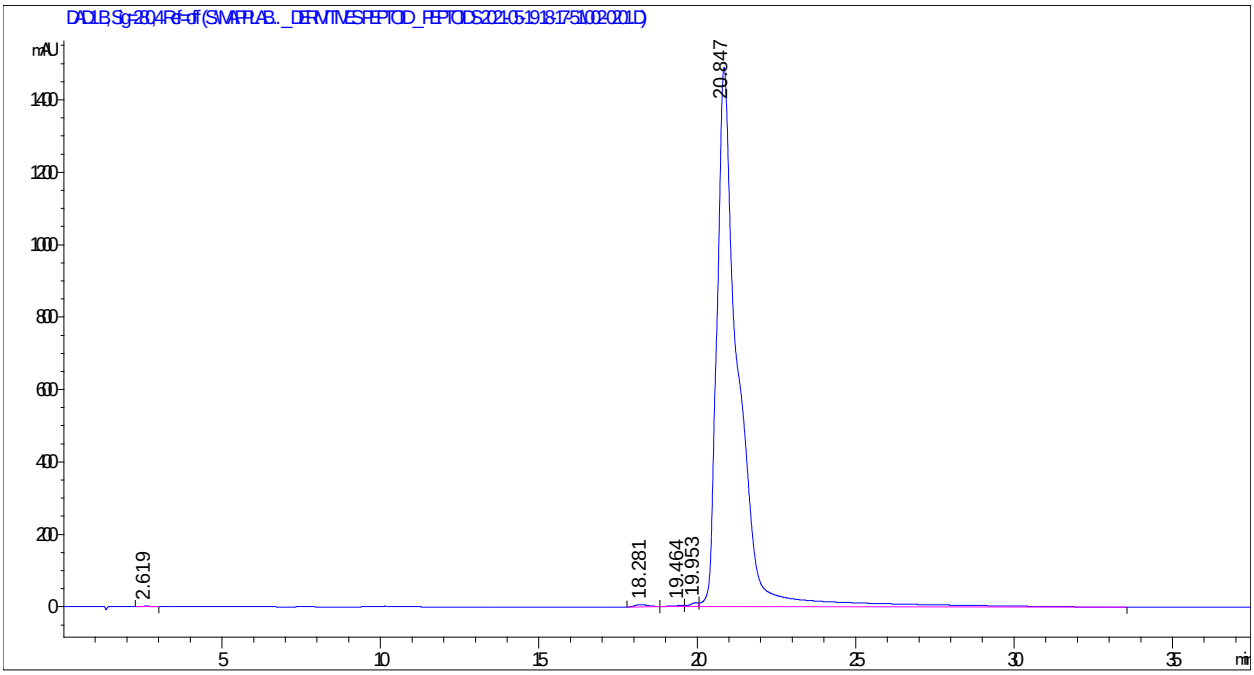

Sig=495

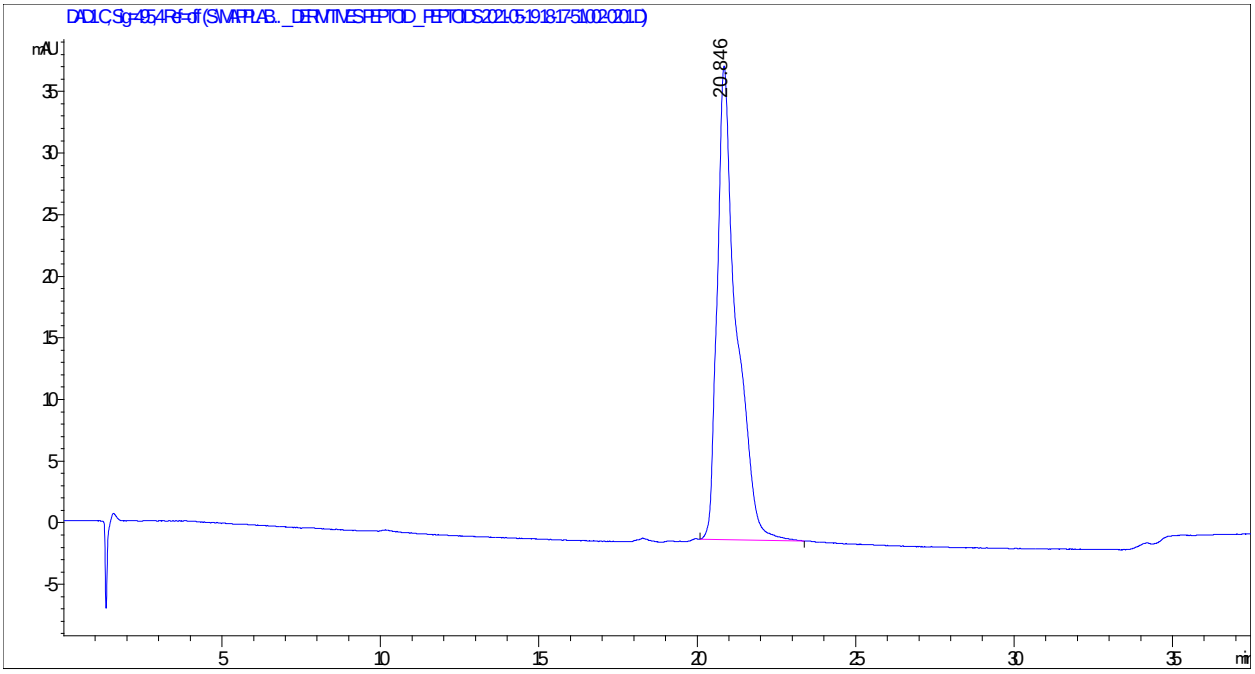

Peptoid 3

Sig=214

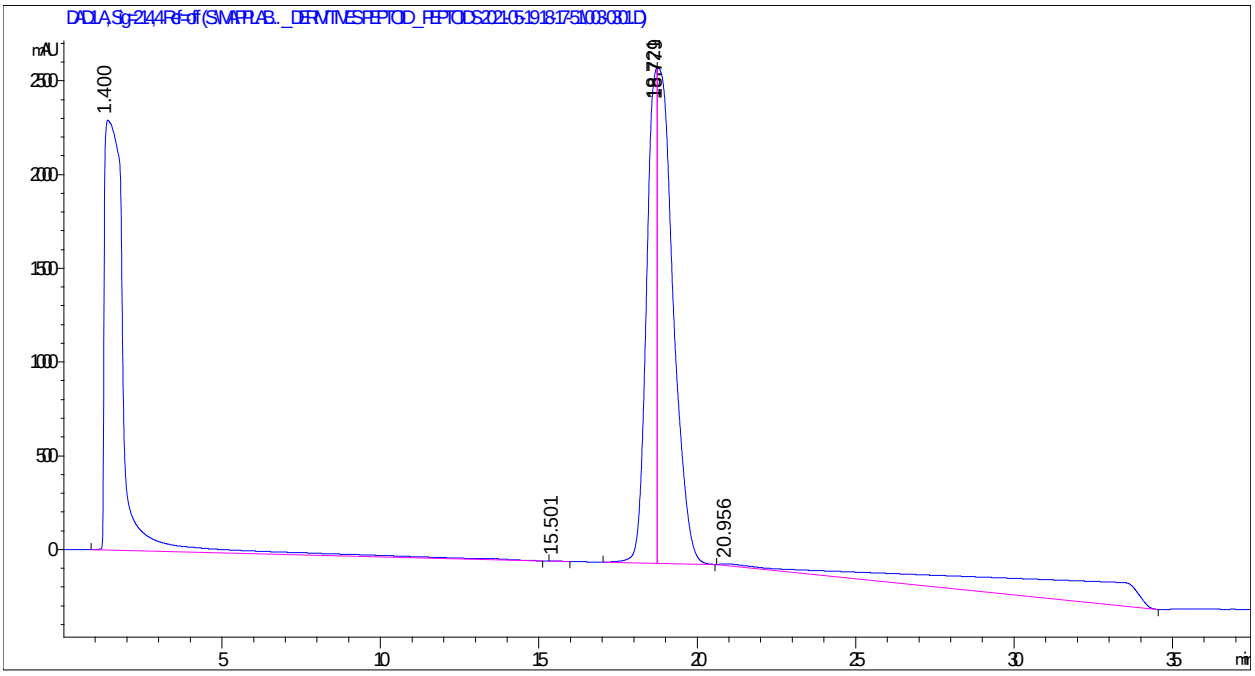

Sig=280

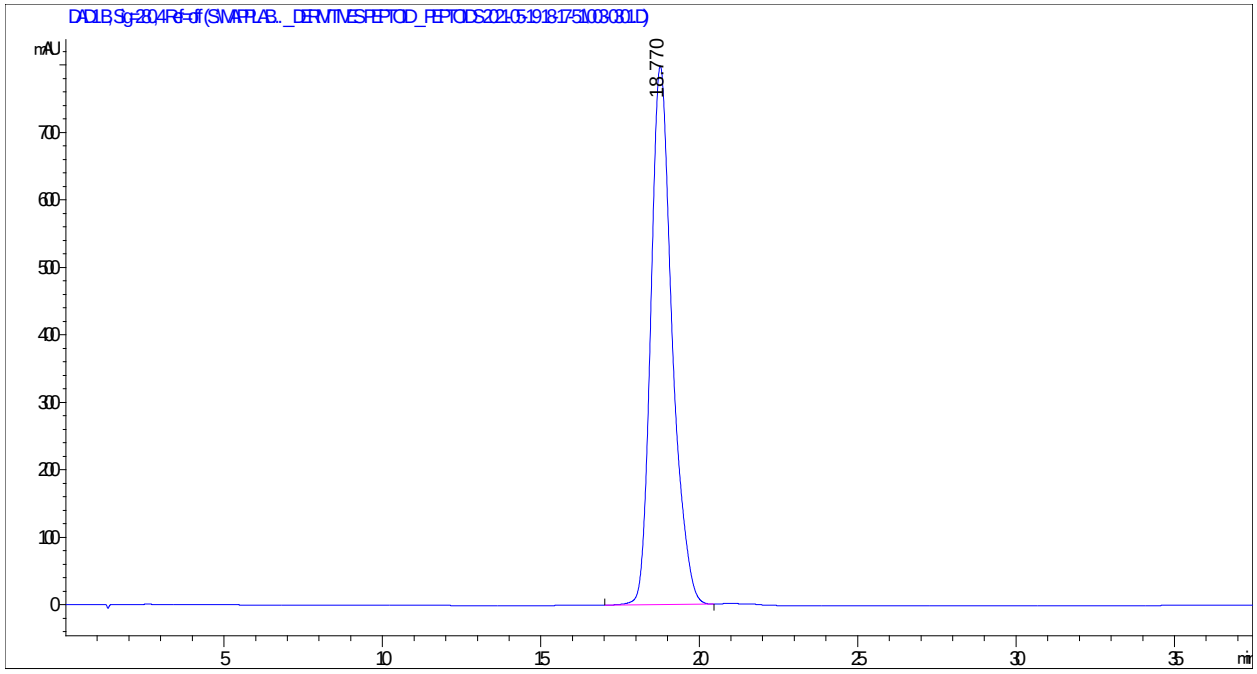

Sig=495

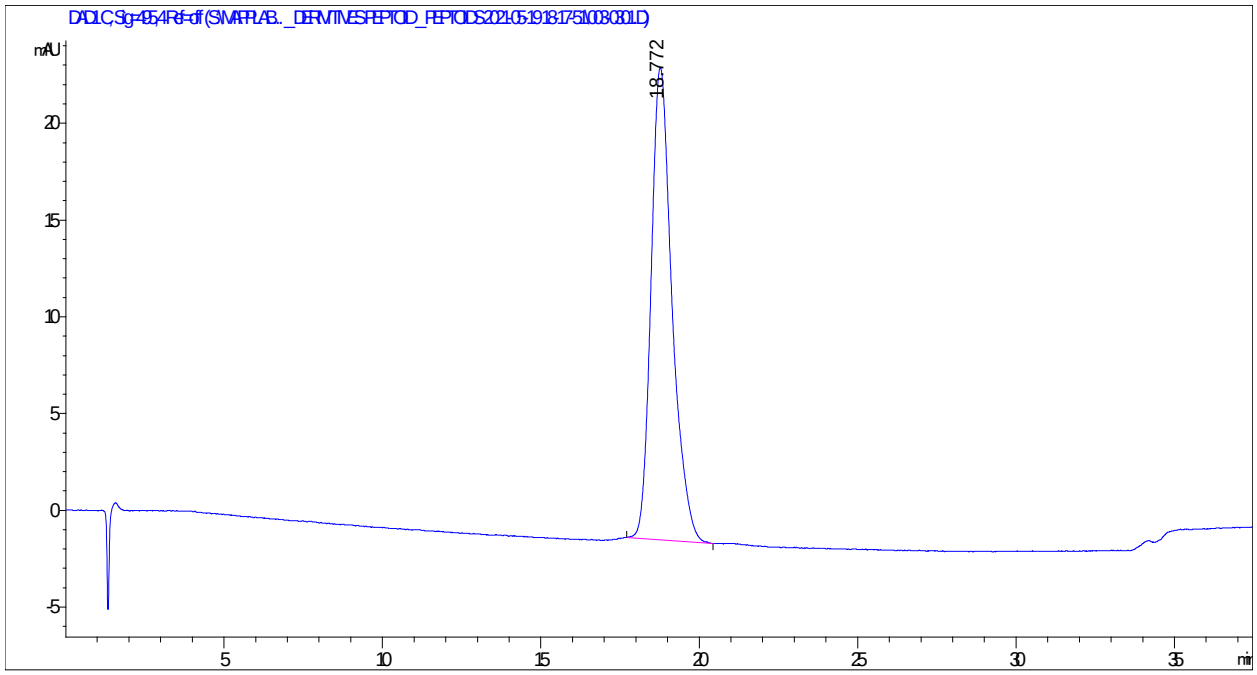

Peptoid 4

Sig= 214

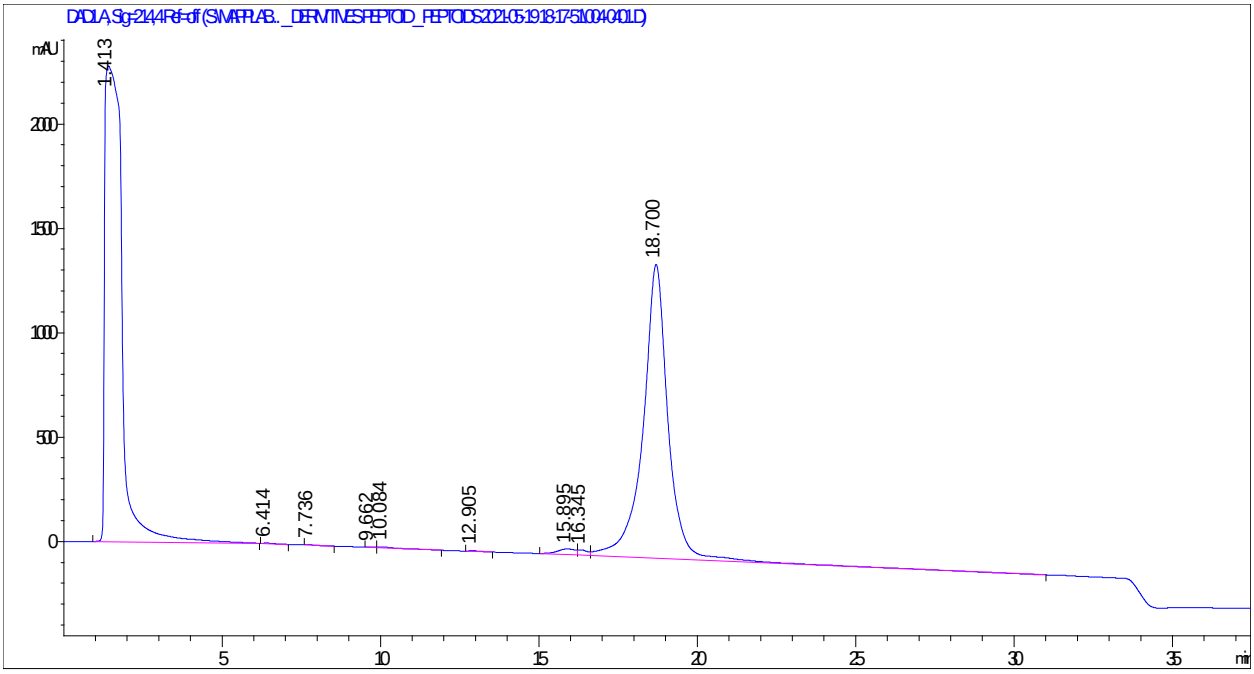

Sig=280

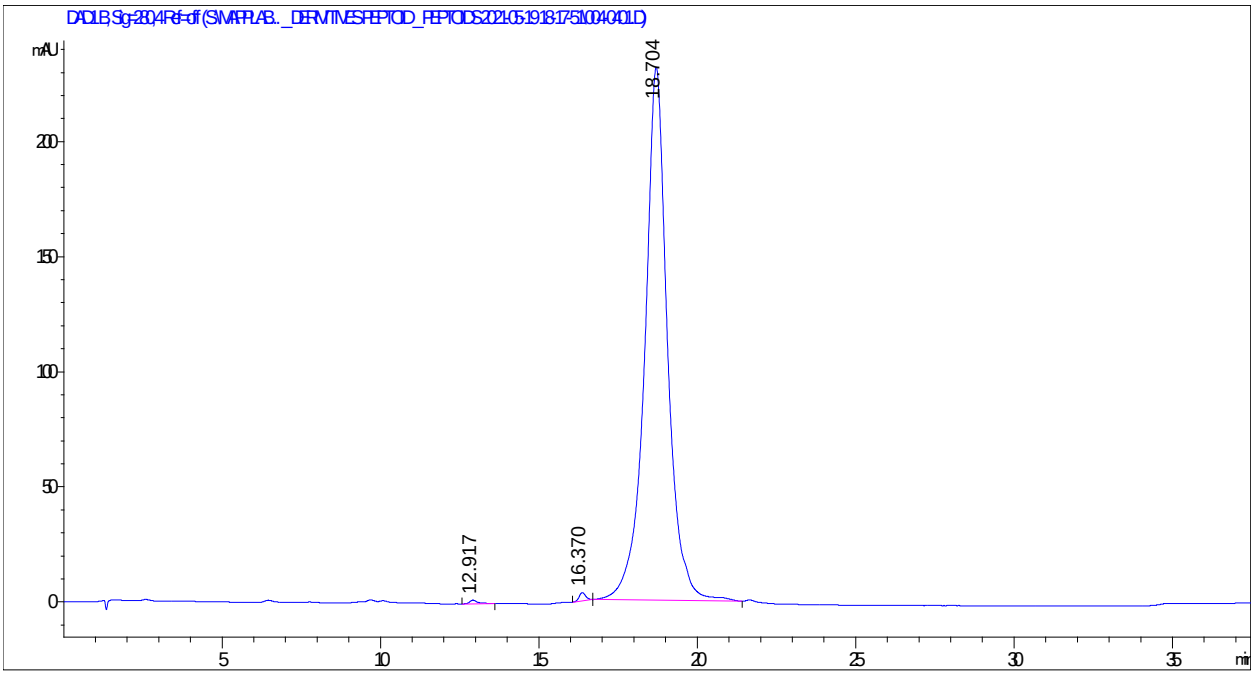

Sig =495

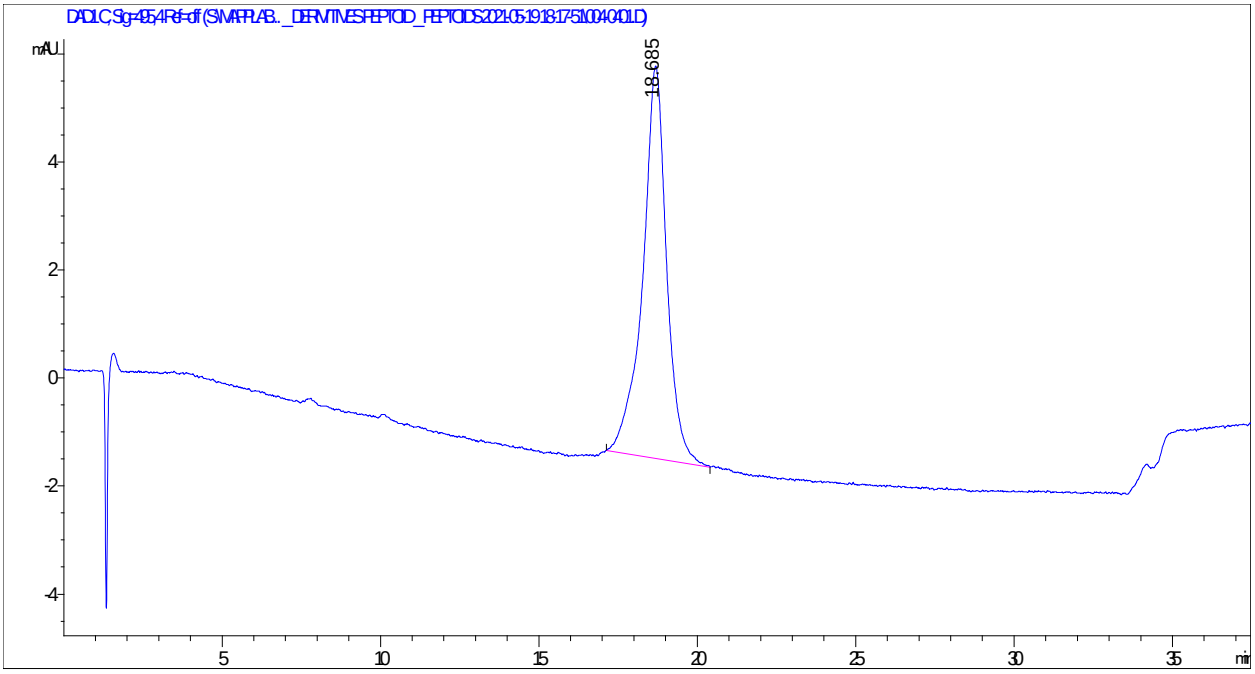

ATF6a 50-60*

Sig=214

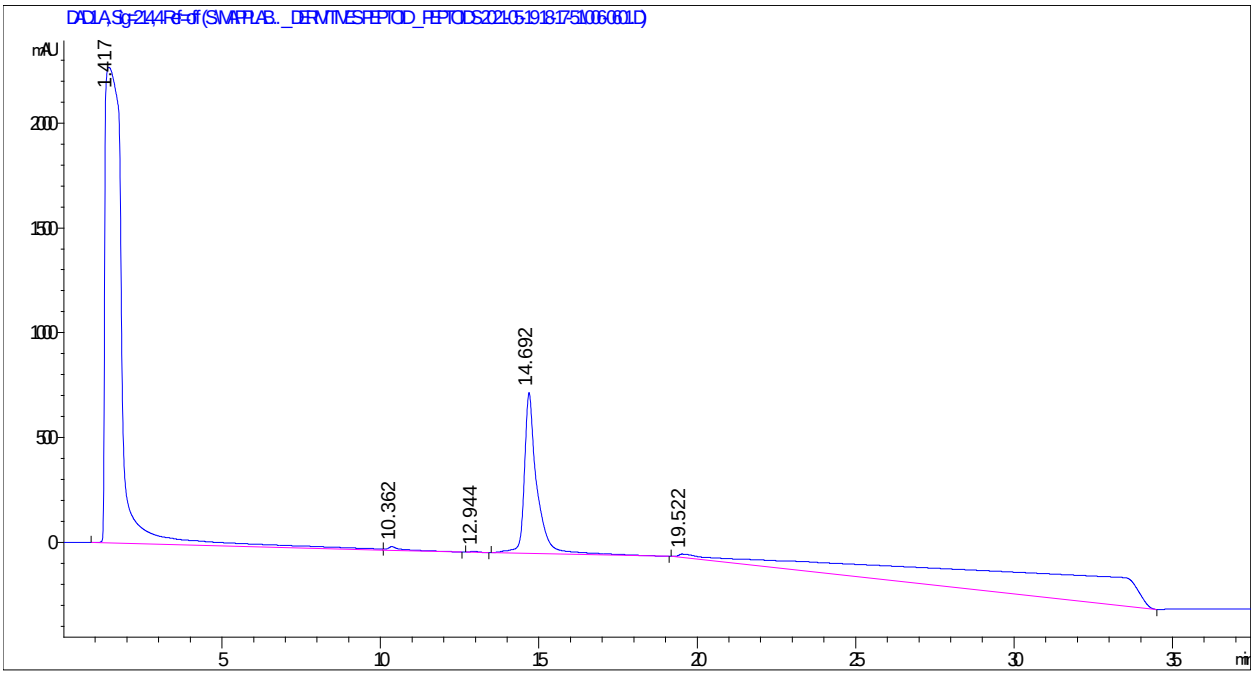

Sig=280

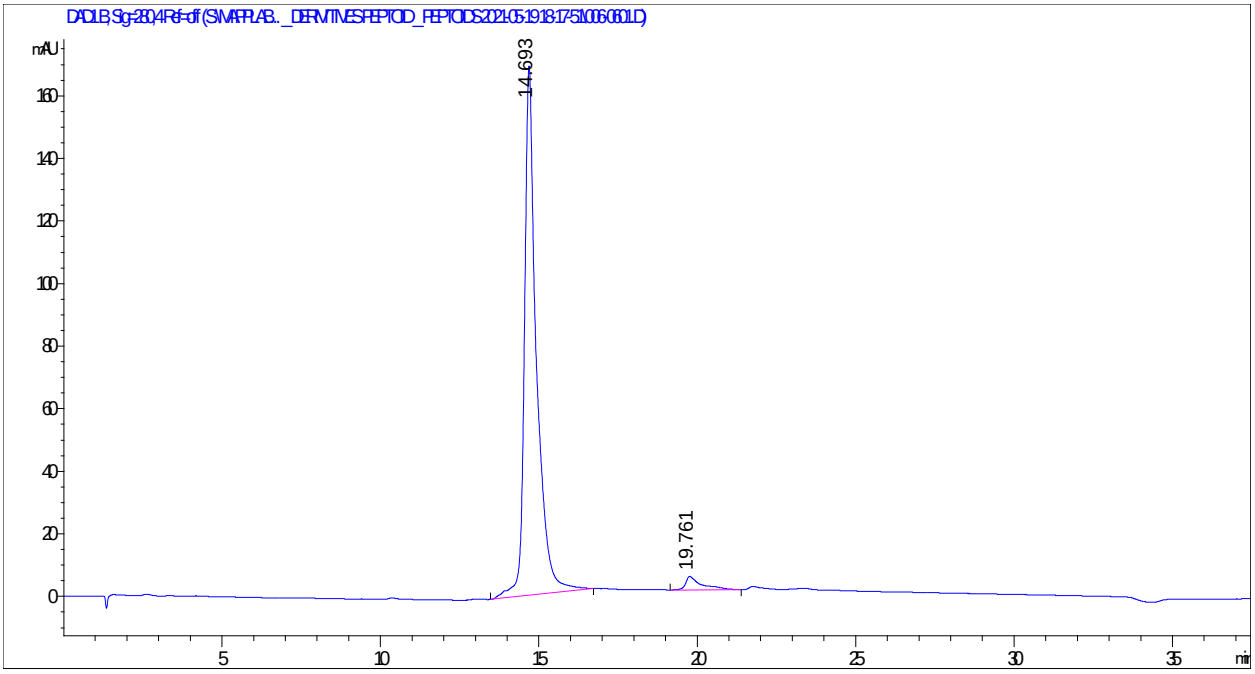

Sig=495

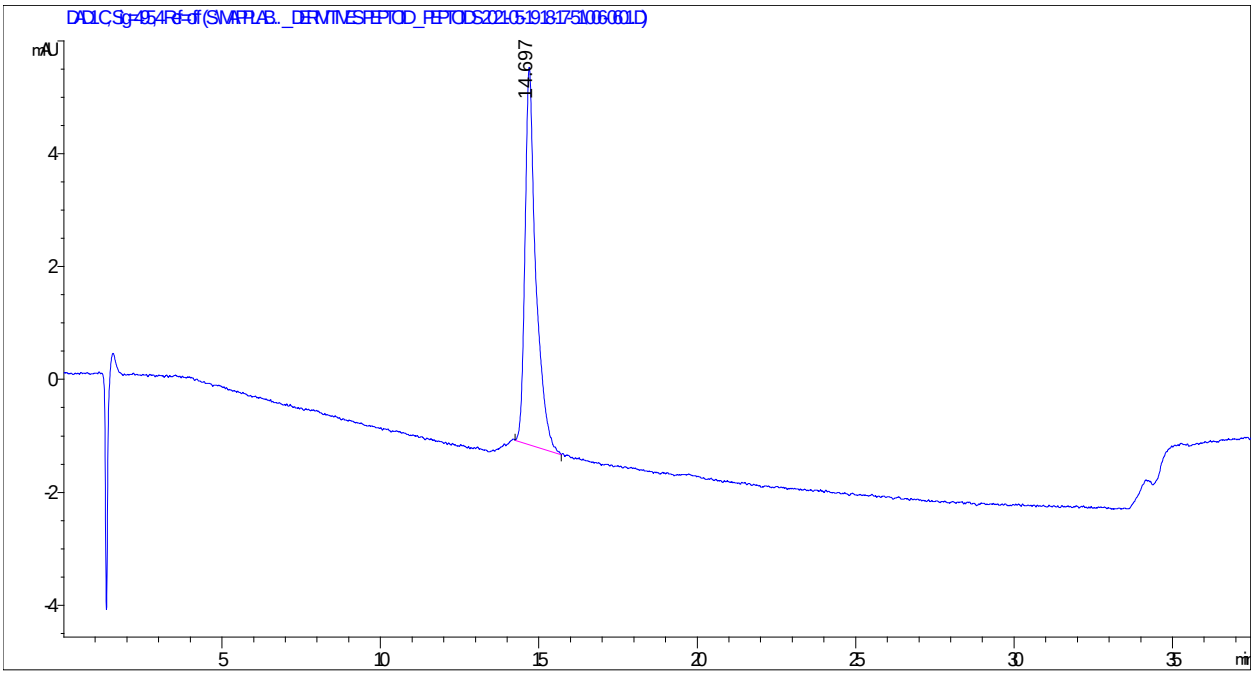

Peptoid 4

Sig=214

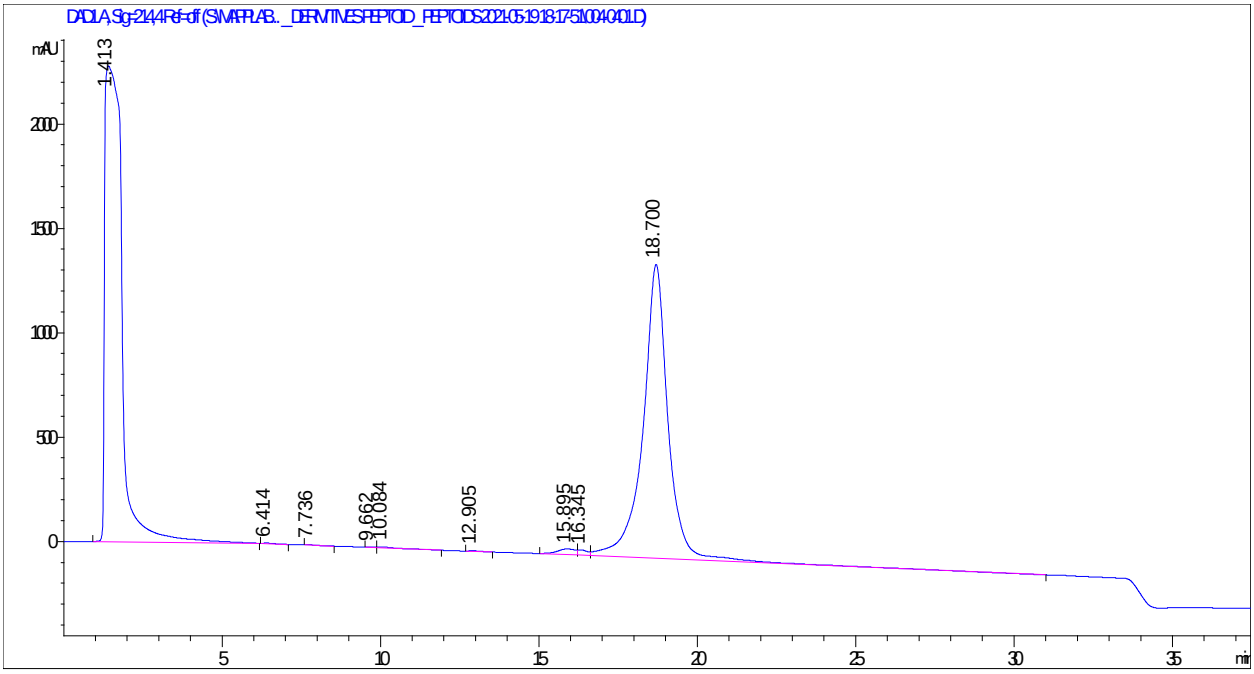

Sig=280

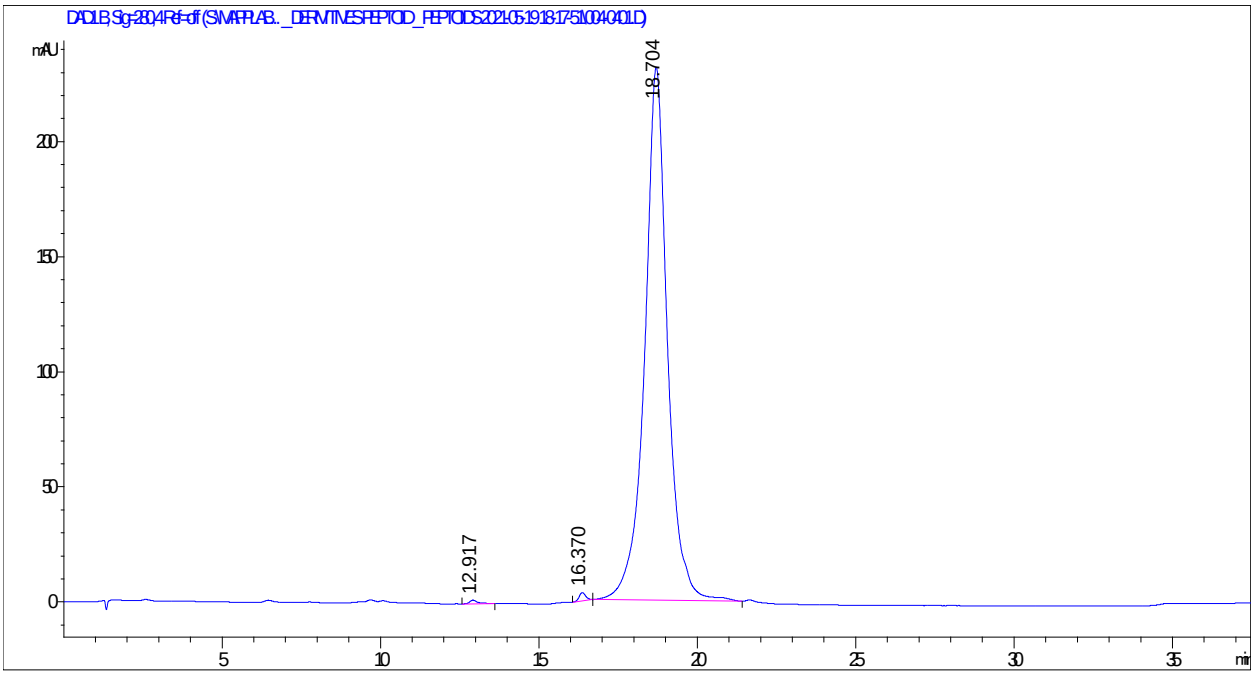

Sig=495

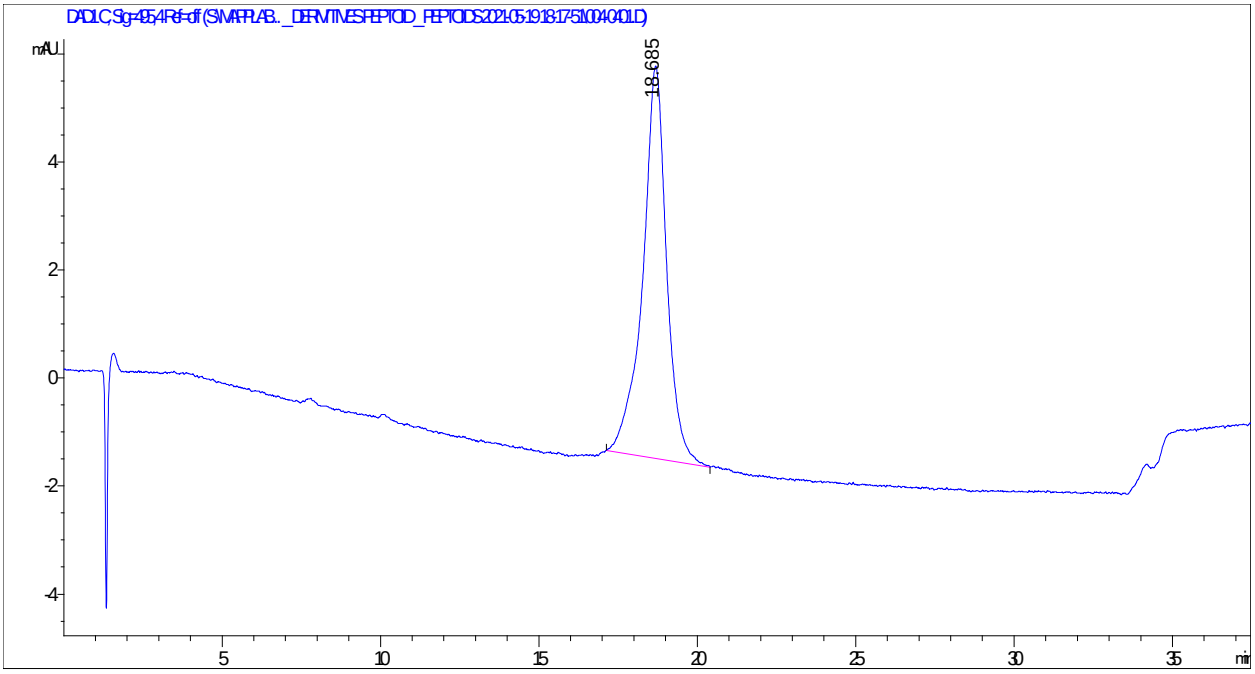
DAD1C,Sig=495,4 Ref=off (SMARPLAB..._DERIVITIVESPEPTIDE_PEPTIDES 2021-05-19 18-17-51 004-001.D)
mAU
18.685
4
2
0
-2
-4
5
10
15
20
25
30
35
min

Peptoid 5

Sig=214

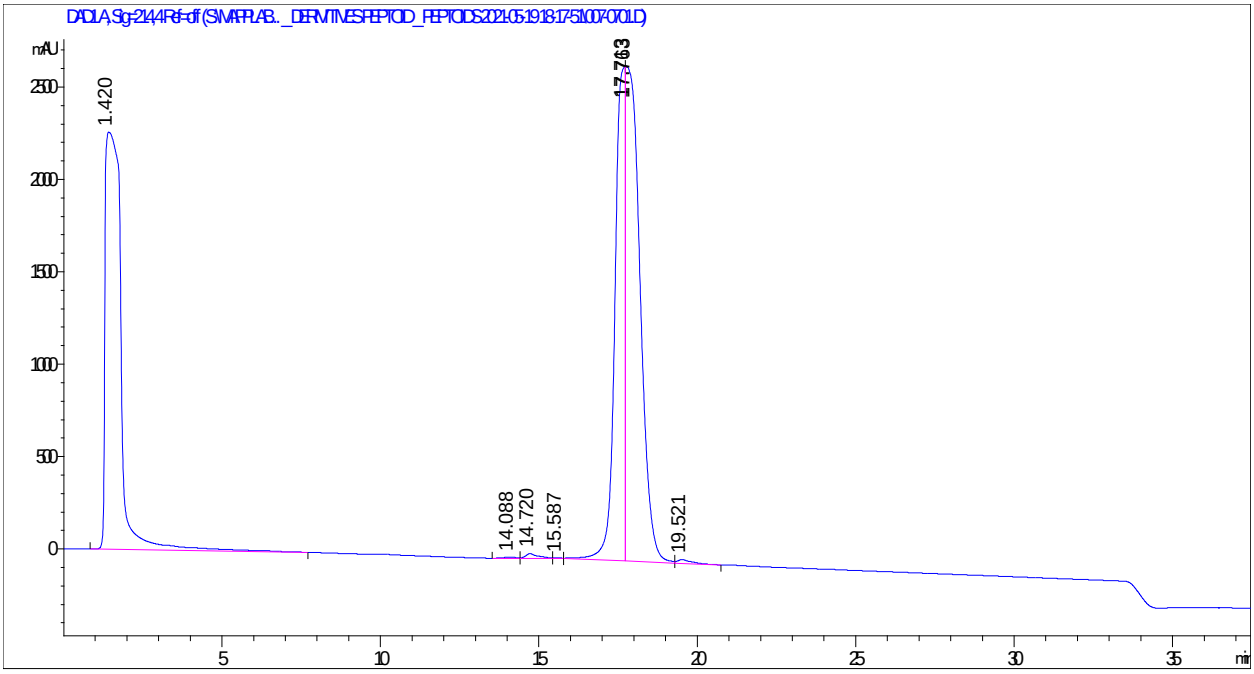

Sig=280

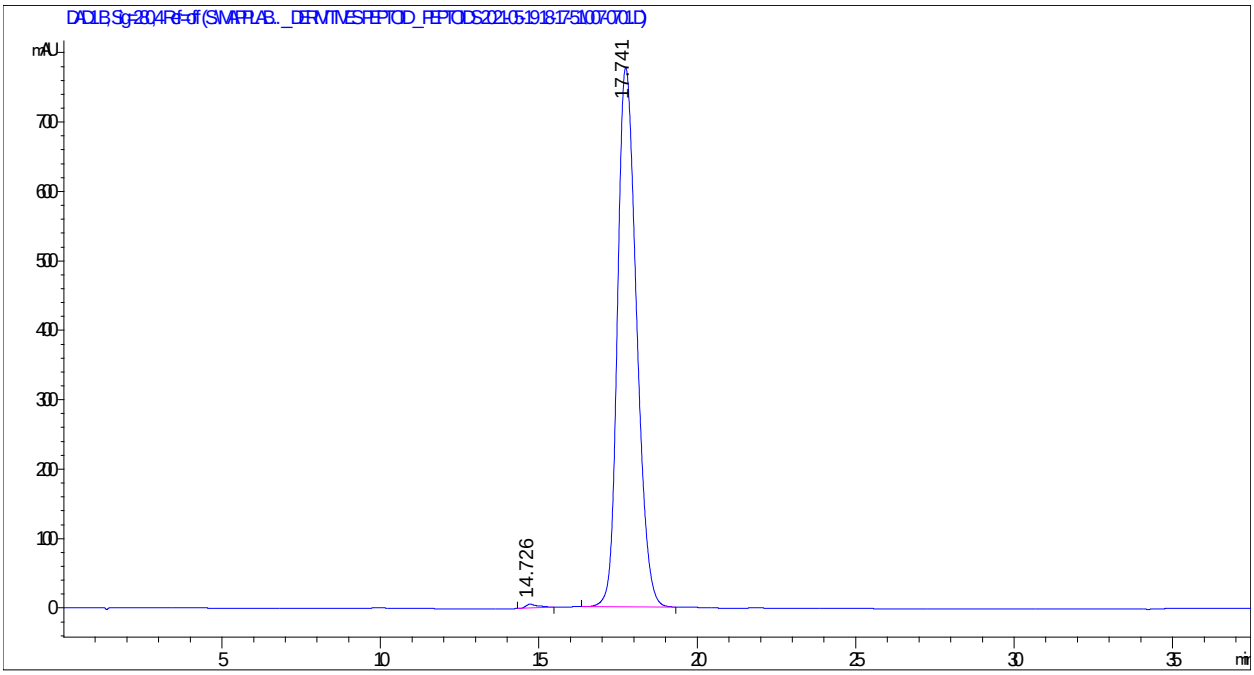

Sig=495

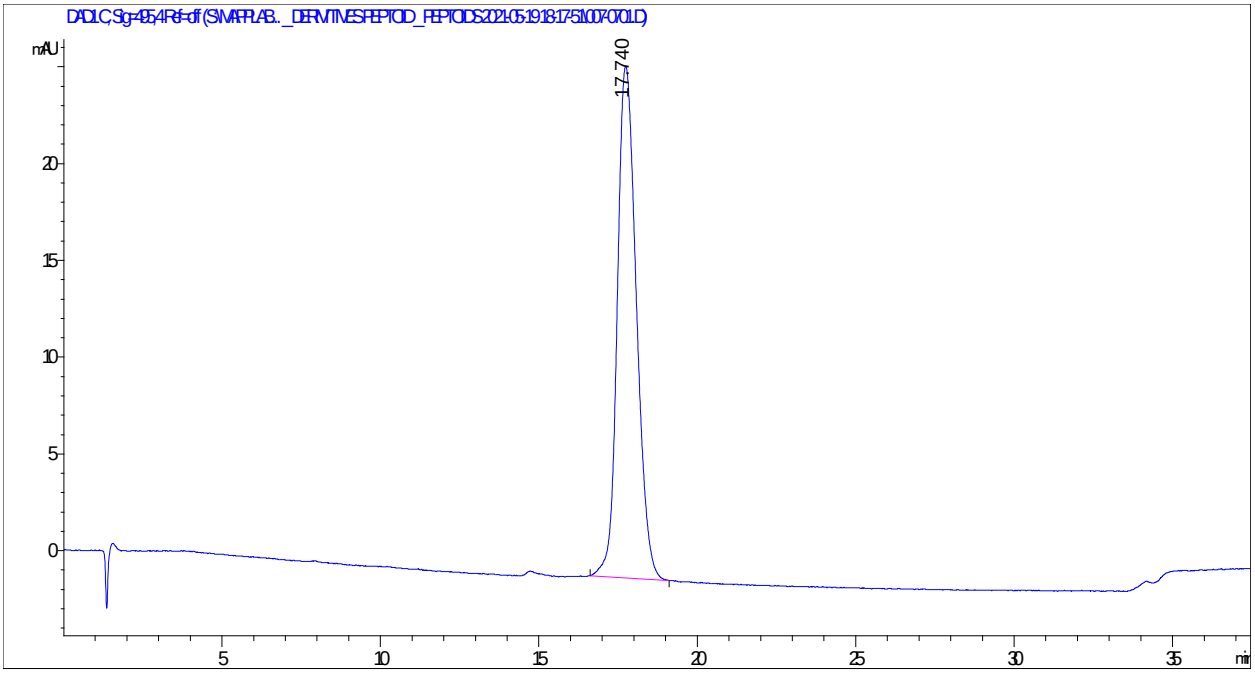
DAD1C,Sig=495,4,Ref=off (SMARPLAB..._DERIVITIVESPEPTIOD_PEPTIDES 2021-05-19 18-17-51 007-0701.D)
mAU
17.740
20
15
10
5
0
5
10
15
20
25
30
35
min

Peptoid 6

Sig=214

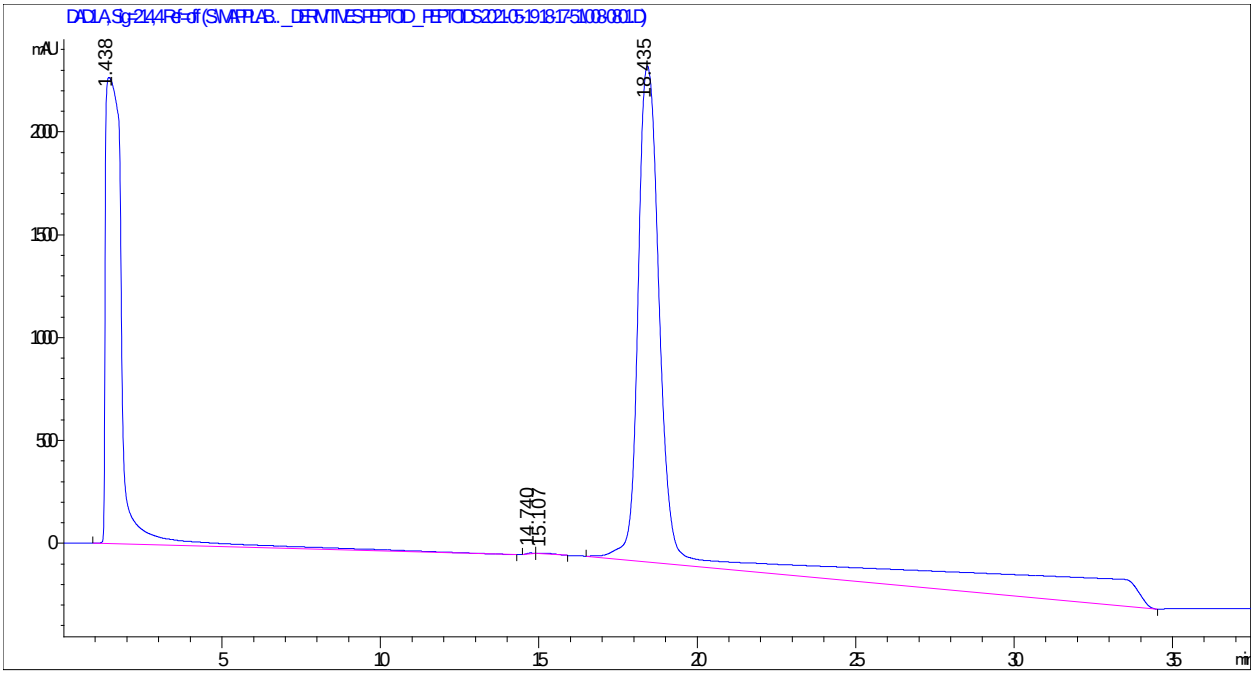

Sig=280

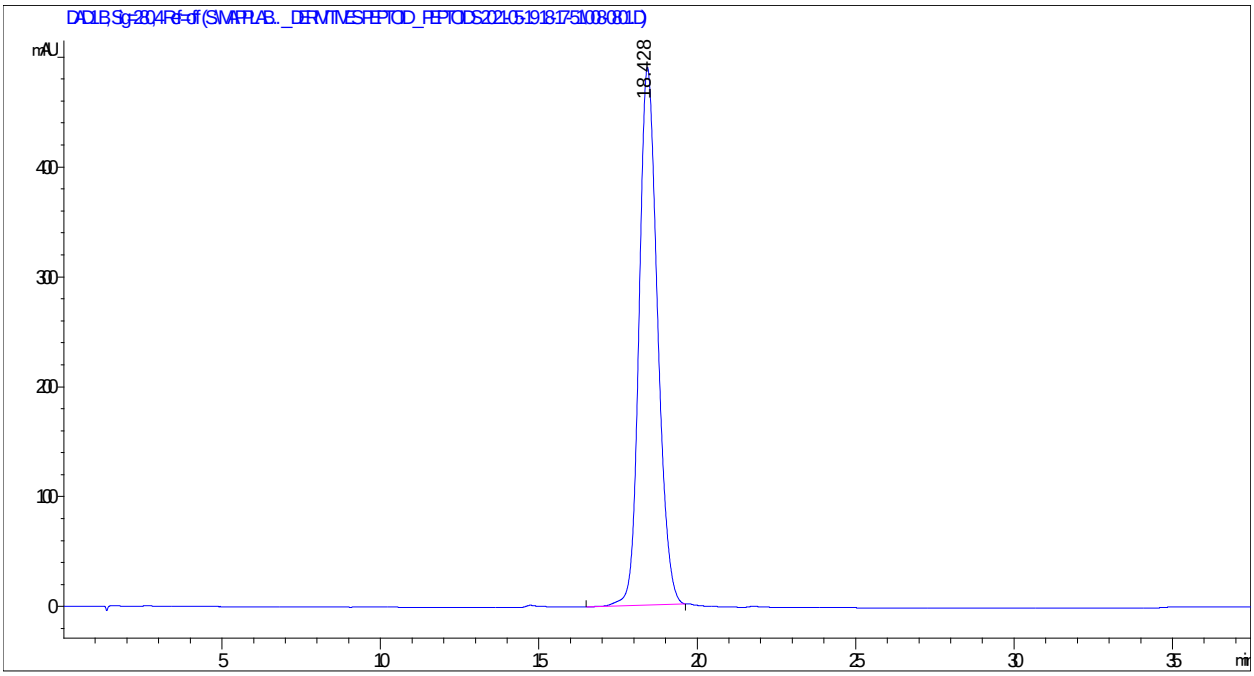

Sig=495

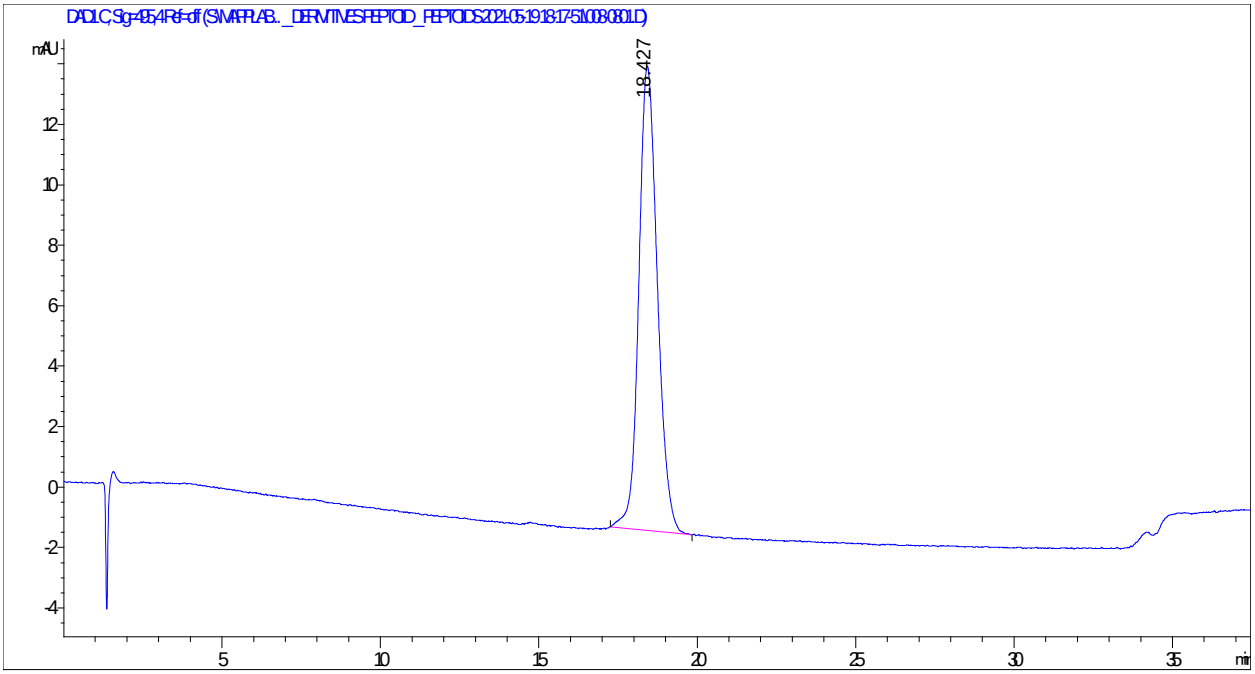
DAD1C,Sig=495,4,Ref=off (SMARPLAB..._DERIVITIVESPEPTIDE_PEPTIDES 2021-05-19 18-17-51 003.801.D)
mAU
18.427
12
10
8
6
4
2
0
-2
-4
5
10
15
20
25
30
35
min

Peptide 60-70 P→F

Sig=214

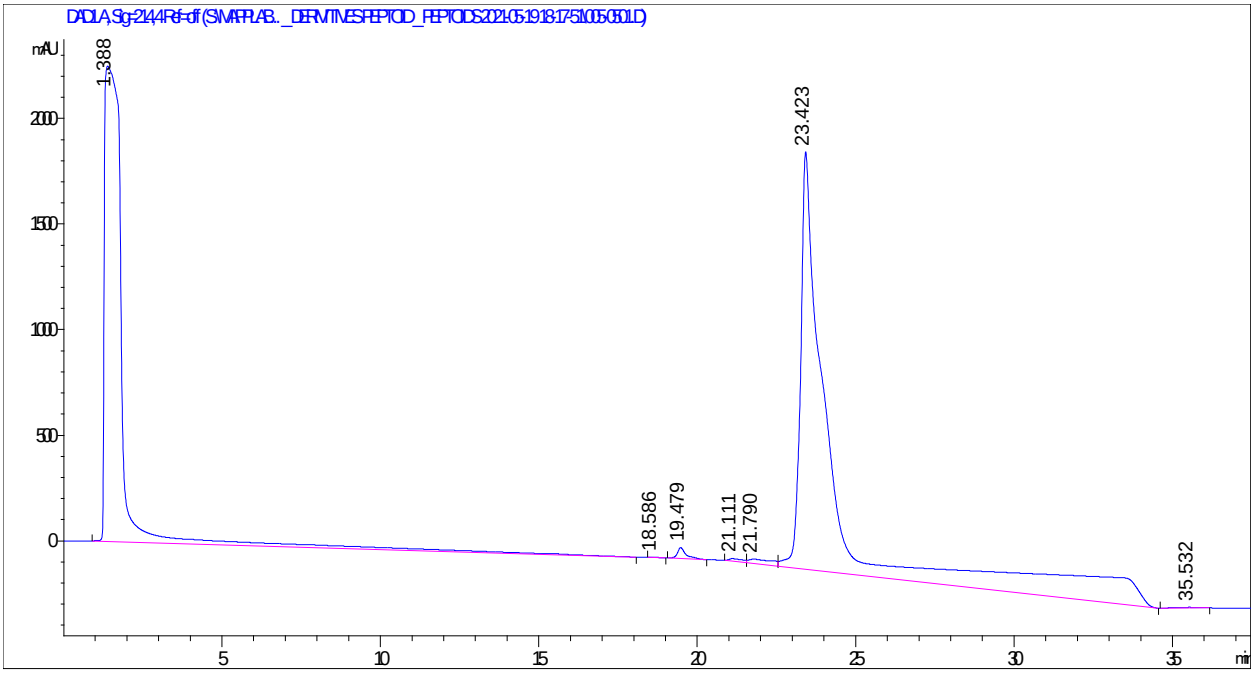

Sig=280

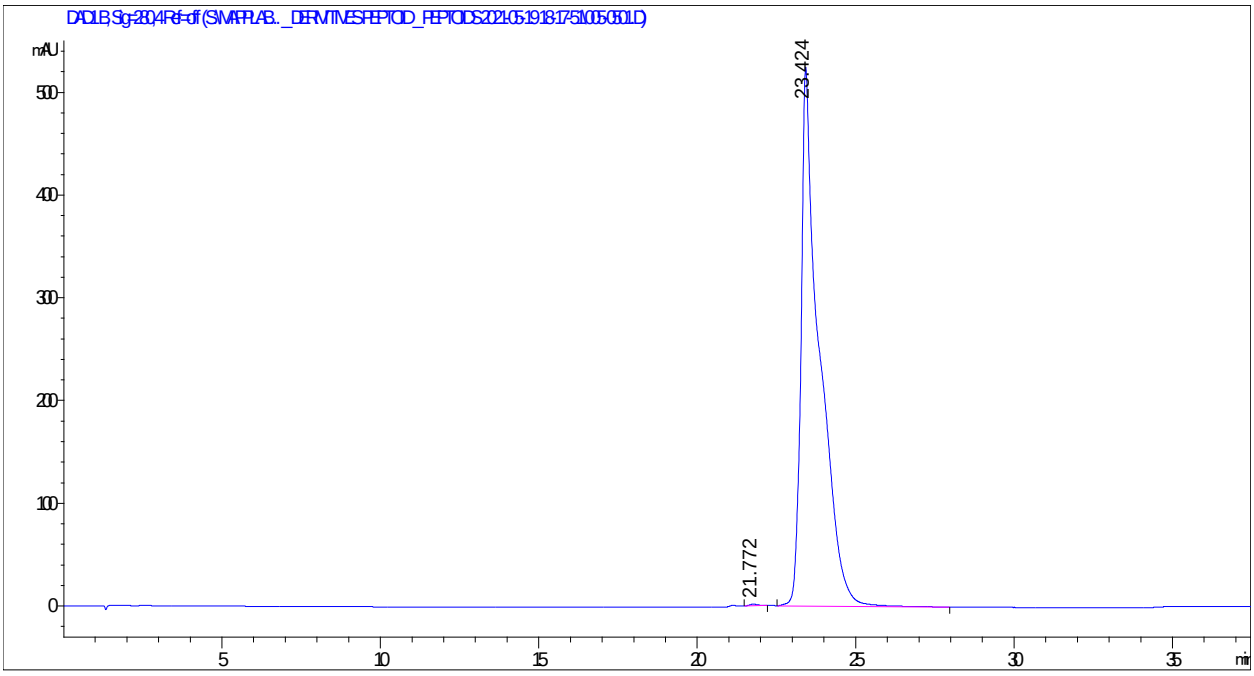

Sig=495

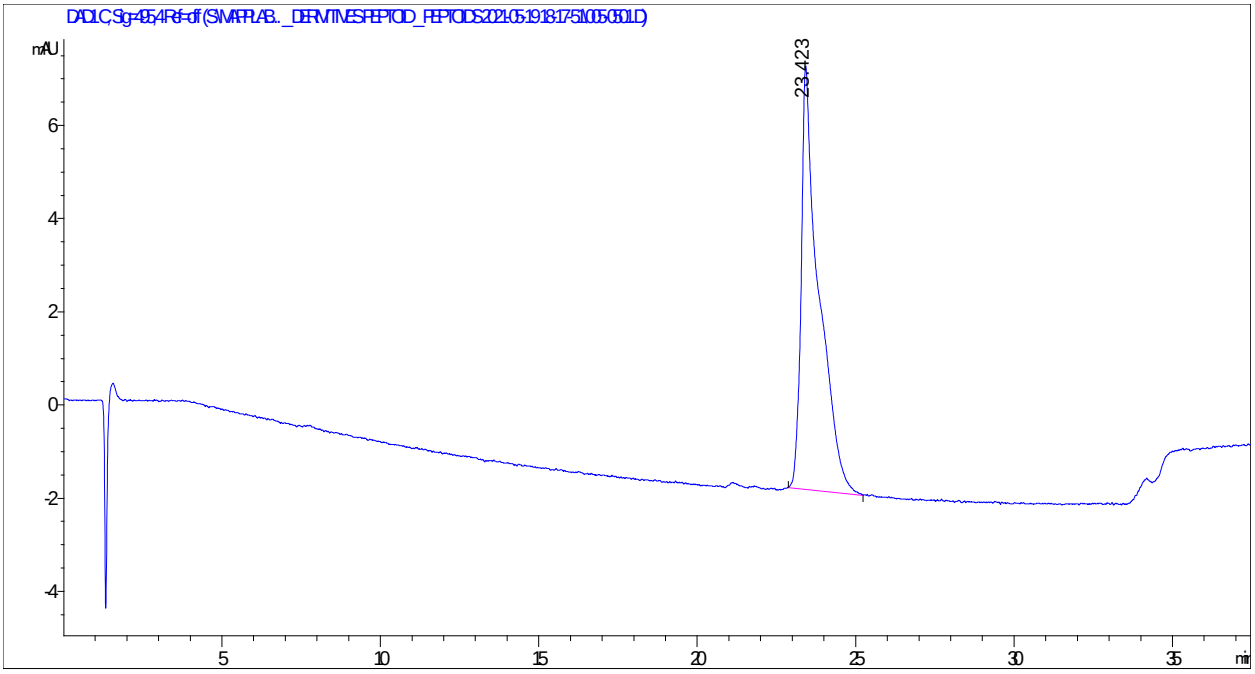
DAD1C,Sig=495,4 Ref=off (SMARPLAB_DERIVITIVESPEPTIOD_PEPTIDES 2021-05-19 18-17-51 005-0501.D)
mAU
6
4
2
0
-2
-4
23.423
5
10
15
20
25
30
35
min

Peptoid 8

Sig=214

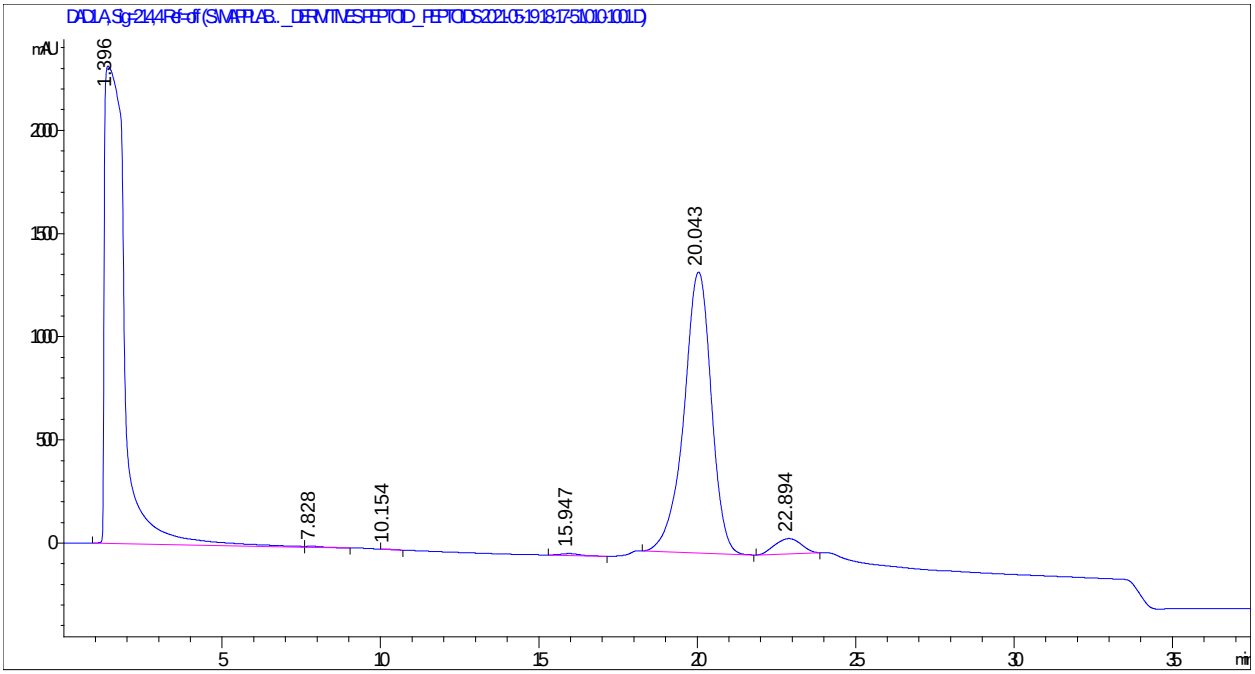

Sig=280

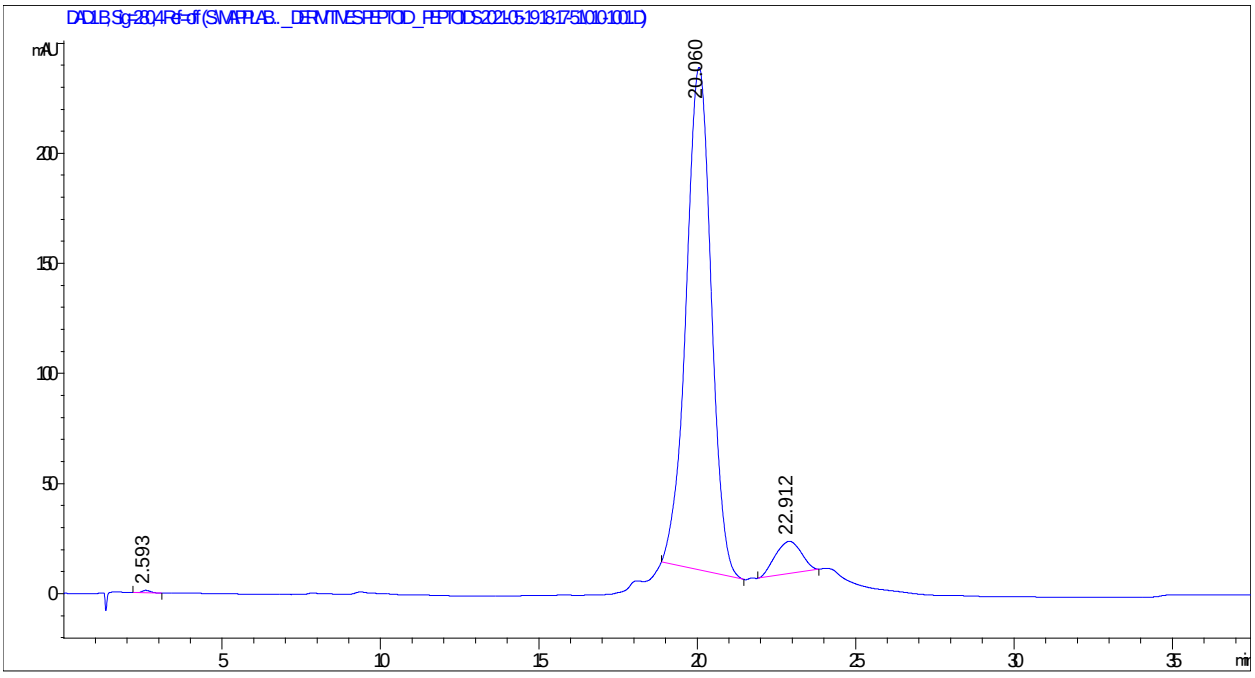

Sig=495

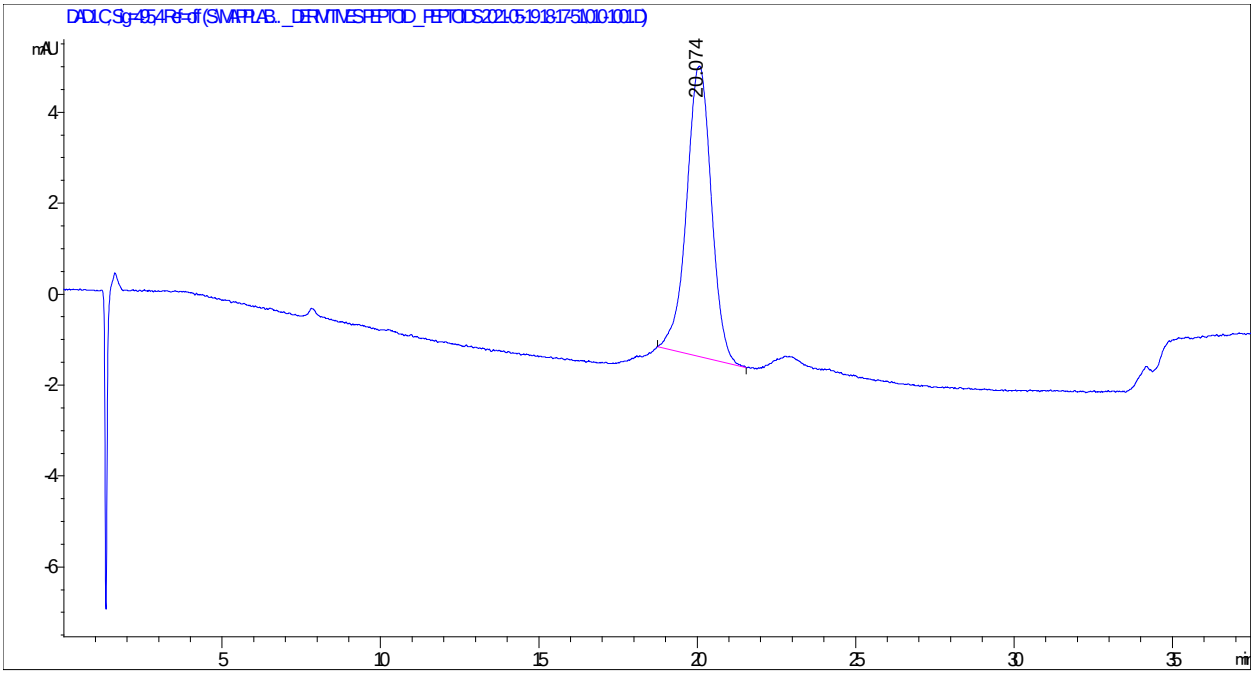

Peptoid 9 (TAMRA + ester)

Sig=214

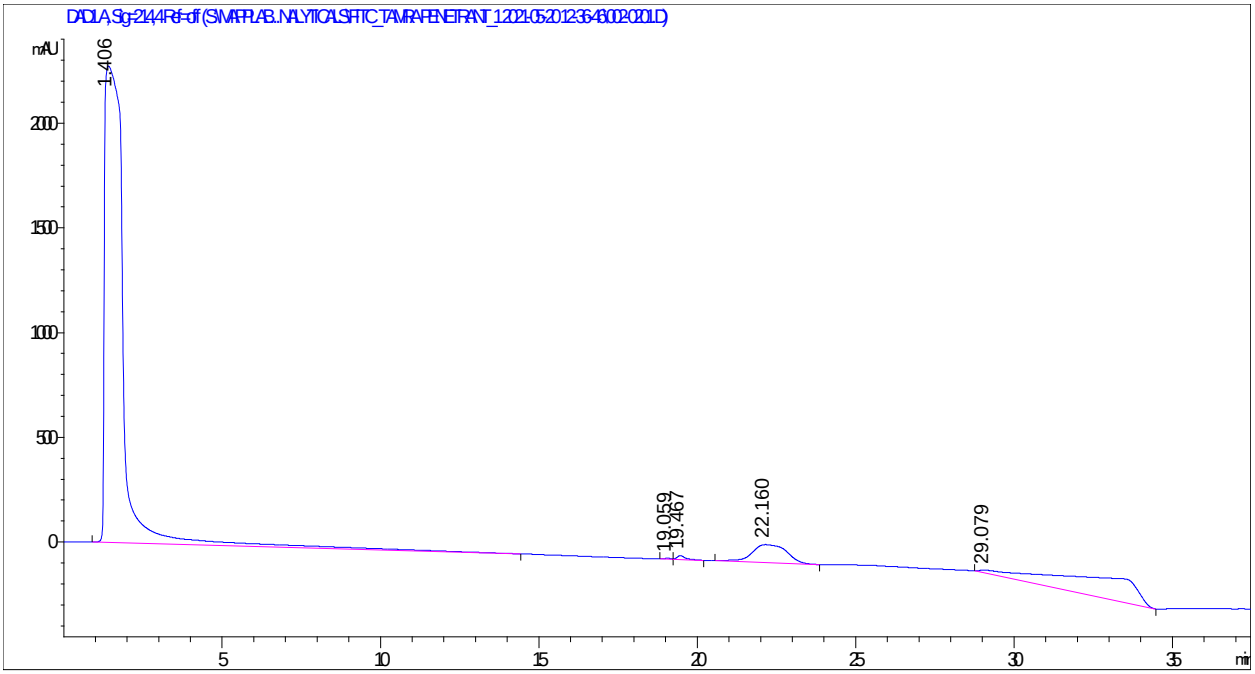

Sig=280

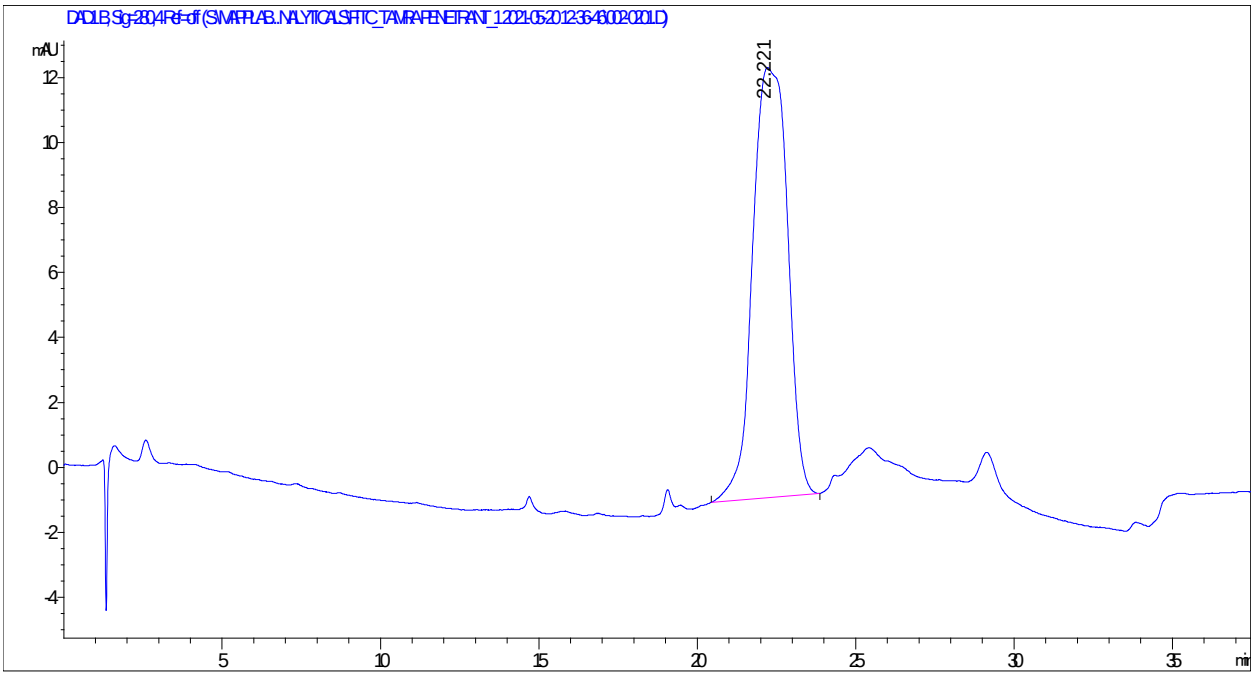

Sig=553

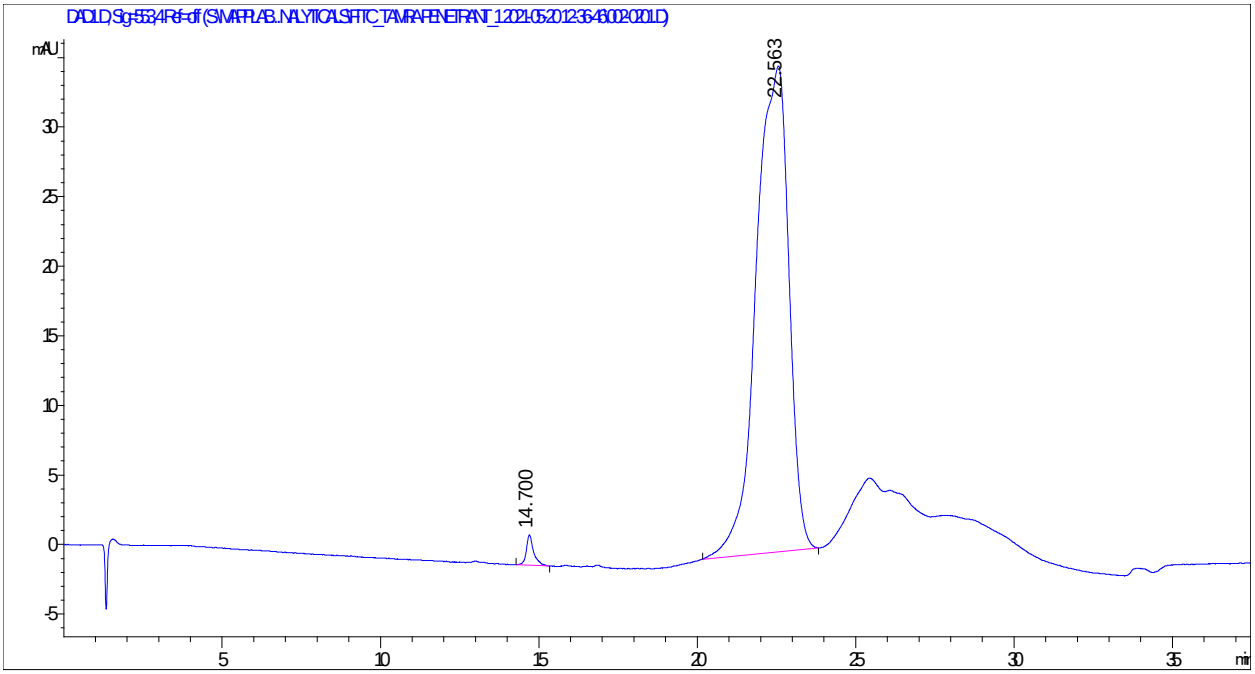

Peptoid 10 (FITC-TAT)

Sig=214

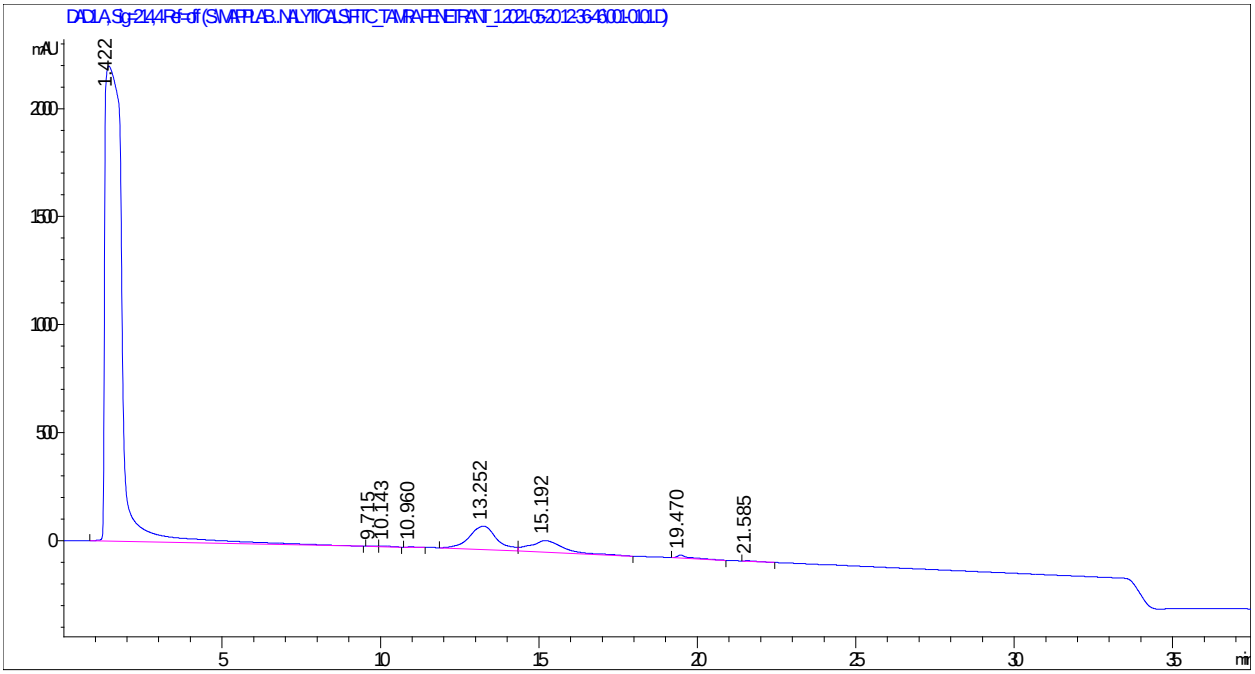

Sig=280

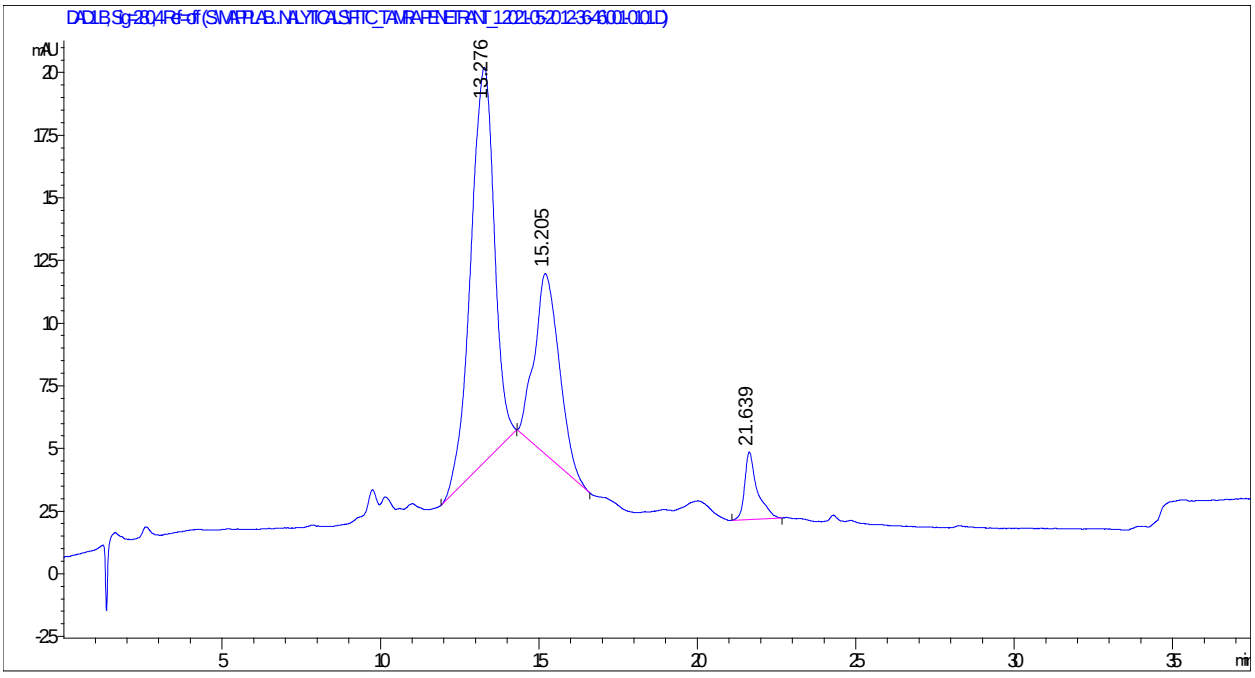

Sig=495

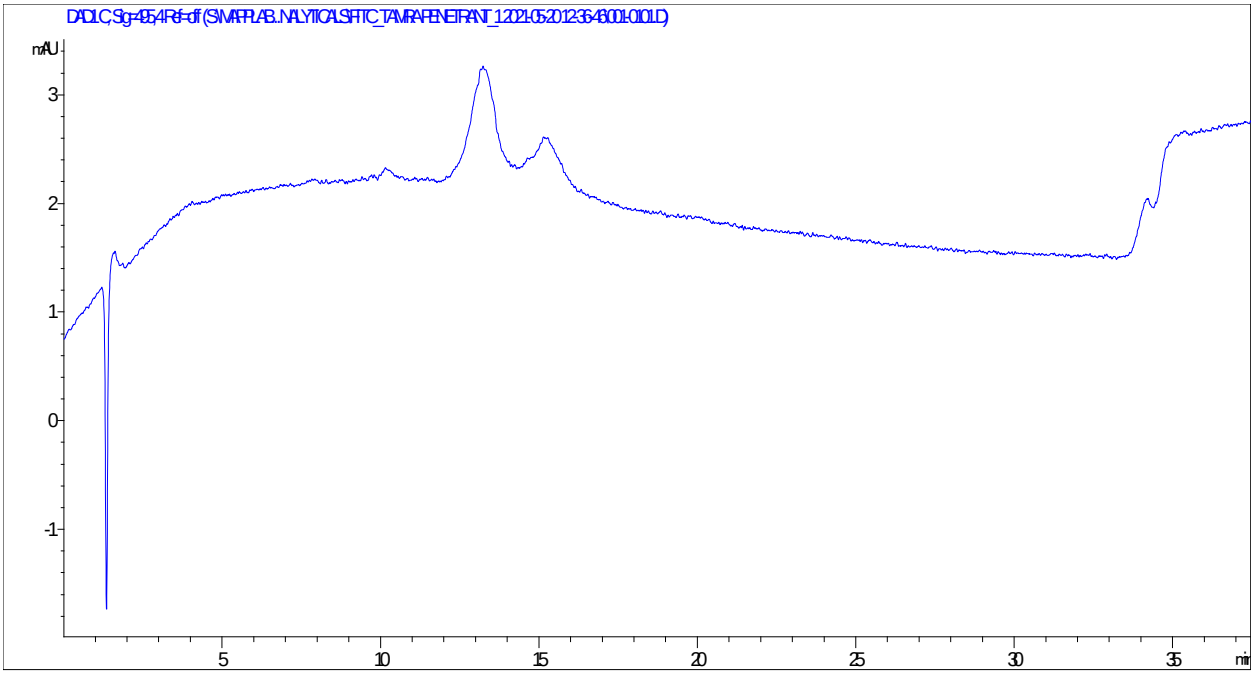

Mass spectrometry of peptides and peptoids used throughout this thesis.

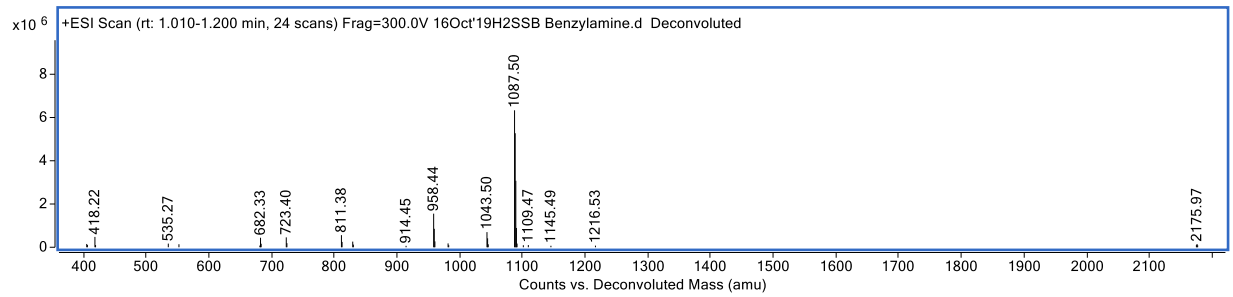

Peptoid 1 (m/z = 1087.50)

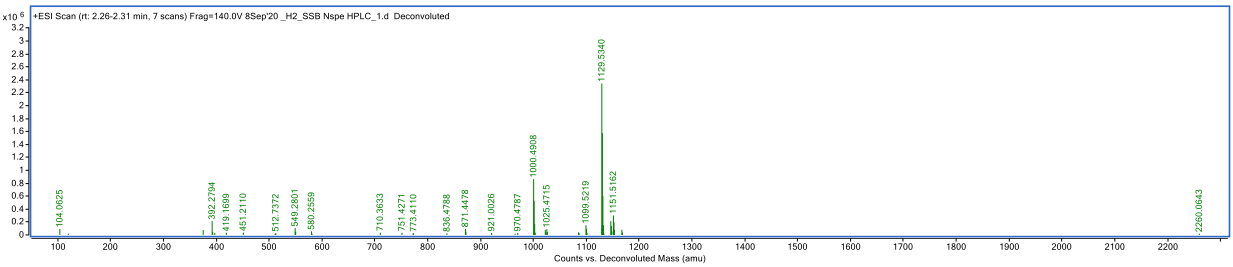

Peptoid 2 (m/z = 1129.53)

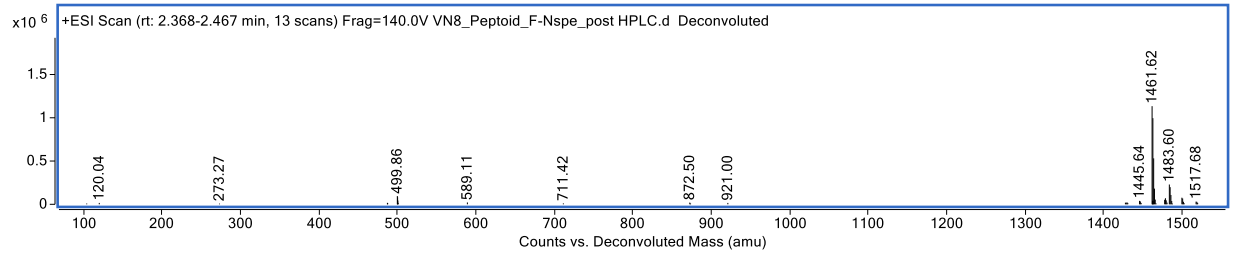

Peptoid 3 (m/z = 1461.62)

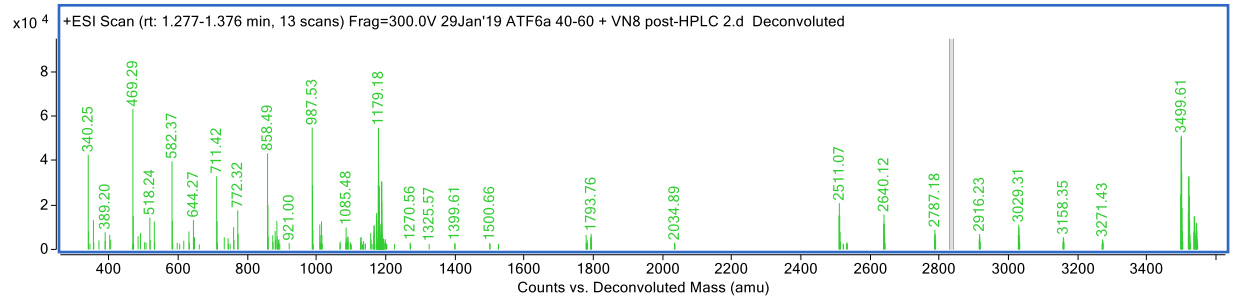

Peptoid 4 (m/z = 3499.61)

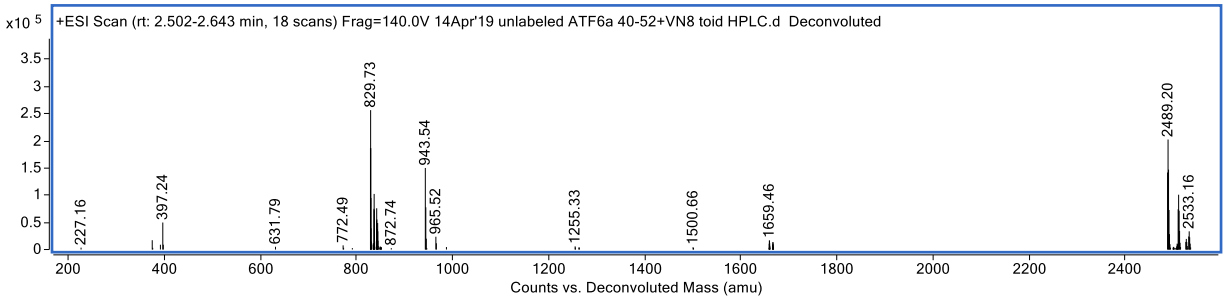

Peptoid 5 (m/z = 2489.20)

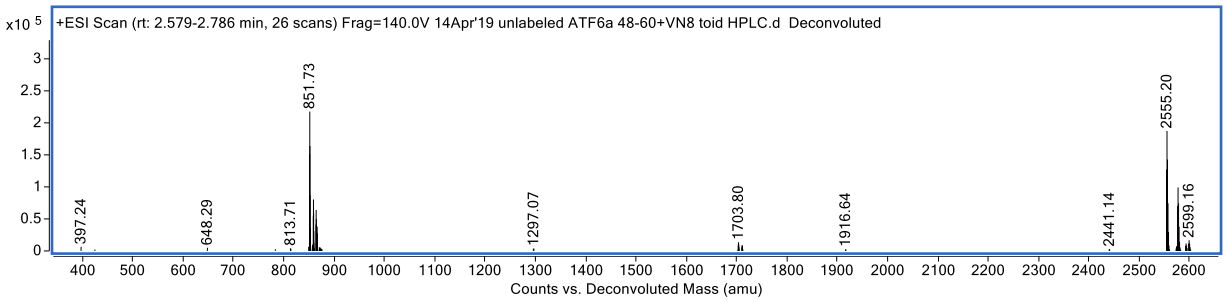

Peptoid 6 (m/z = 2555.20)

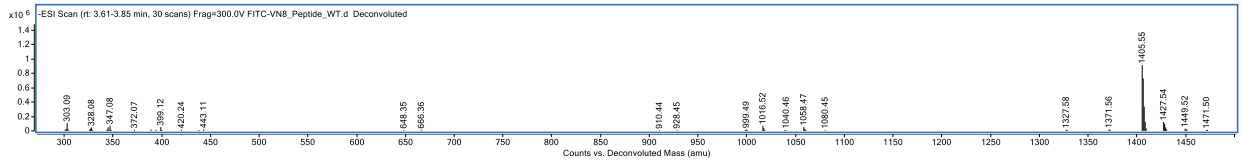

ATF6α VN8 Peptide (m/z = 1405.55)

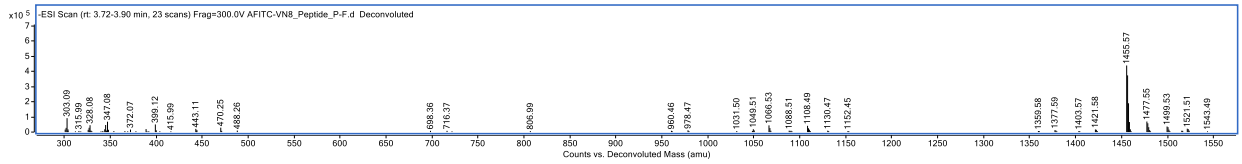

ATF6α VN8 Peptide P→F (m/z = 1455.57)

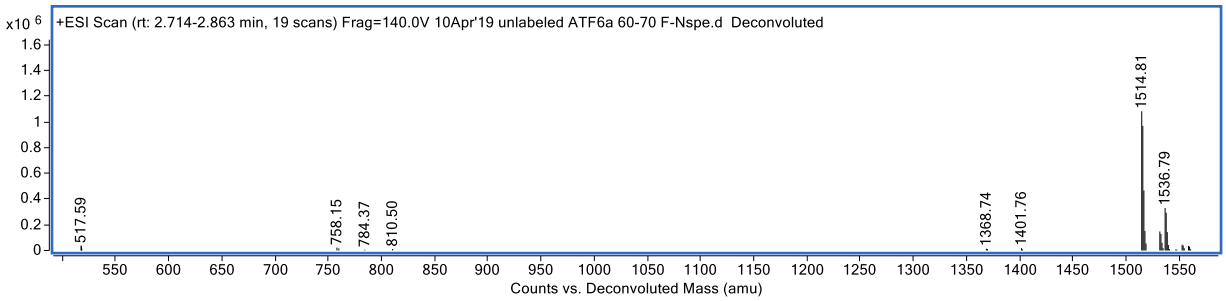

Peptoid 7 (m/z = 1514.81)

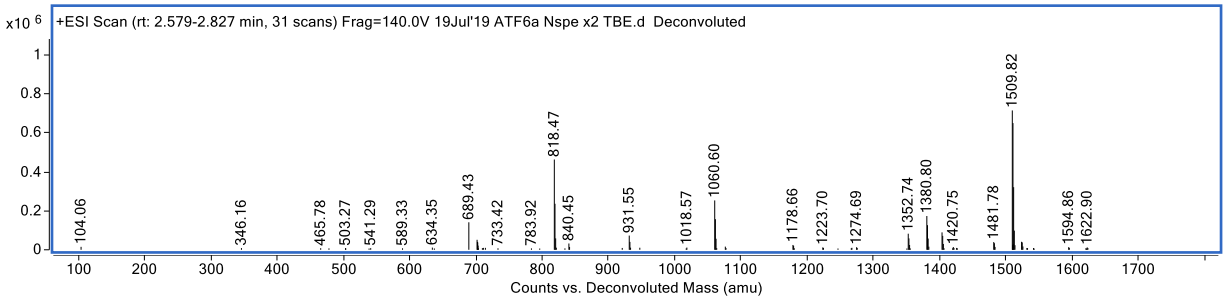

Peptoid 8 (m/z = 1509.82)

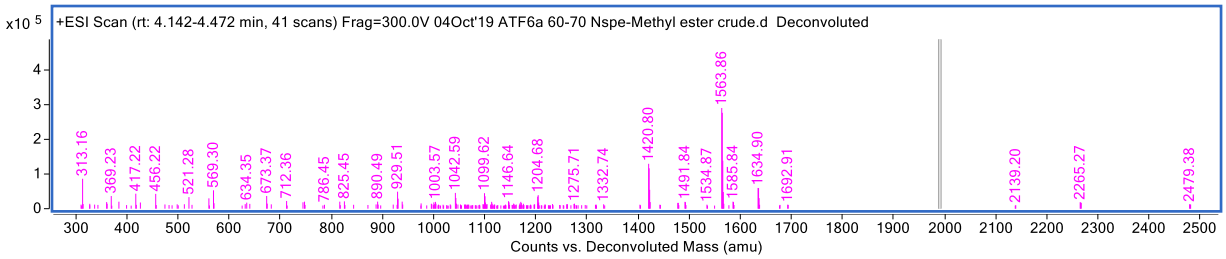

Peptoid 9 (m/z= 1563.86)

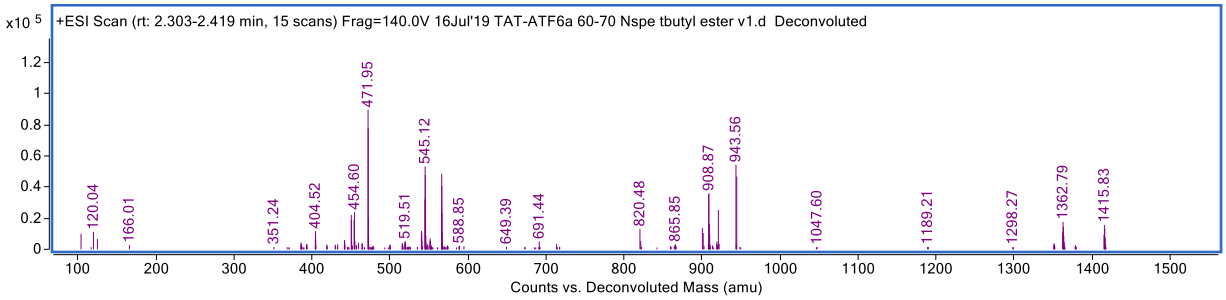

Peptoid 10 (m/2 = 1415.83)